A preliminary study for the development of Kansei value products in mobile work

感性価値製品の開発をモバイルワークで行う為の基礎的研究

August, 2022

2022 年 8 月

Masato Takahashi

高橋　雅人

Department of Imaging Sciences
Graduate School of Science and Engineering
Chiba University

千葉大学大学院　融合理工学府　創成工学専攻
イメージング科学コース

（千葉大学審査学位論文）

A preliminary study for the development of Kansei value products in mobile work

感性価値製品の開発をモバイルワークで行う為の基礎的研究

August, 2022

2022 年 8 月

Masato Takahashi

高橋　雅人

Department of Imaging Sciences
Graduate School of Science and Engineering
Chiba University

千葉大学大学院　融合理工学府　創成工学専攻
イメージング科学コース

A preliminary study for the development of Kansei value products in mobile work

Abstract

We set three development goals to develop elemental technologies necessary for the remote development of products with added Kansei value, and our study has successfully achieved them. The Kansei communication tools and telemedicine tools developed in this project are currently being tested in a field setting. Using the tools in actual situations will reveal issues and needs that need to be addressed. Based on these issues and needs, we believe that improvements and new research will bring us closer to the remote development of products with added sensitivity.

1. Tactile sense: mutual conversion of sensory and physical property information (Chapter 4)

A Kansei Communication Tool prototype (developing products with Kansei value) was displayed at an exhibition, with samples available for experiencing surface roughness changes. The prototype has the same specifications as the DIC Color Guide, and combines a tactile film to the color guide. From a questionnaire based on the Kansei communication tool 49 of 64 (77%) respondents were interested in the prototype, of which 21 (31%) wanted the prototype. Based on these results, we created the "DIC Material box," which allows users to experience systematic tactile sensations in two dimensions. This allows designers and product developers to identify their preferred sensory vectors.

2. Color Reproduction (Chapter 5, 6)

We developed a new color chart and a telemedicine tool that can use the color chart to communicate the patient's complexion and tongue color correctly. The color chart includes human tongue and skin colors that can reproduce the colors required for medical diagnosis. Telemedicine tools have been implemented on iOS. Development was performed in collaboration with Kampo medical doctors with expertise in color; since this was an urgent task under the COVID-19 epidemic, priority was given to actual use, so the tool's usability was mainly evaluated qualitatively. The results showed that corrections based on human color vision and automatic correction were more beneficial than without correction. Based on these results, we are currently continuing the evaluation with the cooperation of additional doctors.

3. Measurement of emotional state: non-contact pulse wave measurement (Chapter 6,7)

Biometric signals, such as heartbeat, reflect the movement of the emotion. We created and validated a heart rate measurement tool using an RGB camera. There are two main contributions of this study.

The first was the pulse wave detection technique utilized a technology that captures changes in the hemoglobin signal obtained by independent component analysis. Thirty-nine subjects performed accuracy validation. The results showed that the accuracy was similar to commercially available pulse oximeters. Currently, we are improving the software while considering opinions from members of the clinical field.

The second was the pulse rate measurement from the sole of rats. This study was conducted considering emotional experiments in model animals that are otherwise difficult to conduct in humans. A high-speed video camera was used to capture the pulse rate, which is about eight times higher than that of humans. To capture signals from the skin, we acquired signals from the sole. As a result, we acquired pulse waves from the sole. This method allowed for unrestrained pulse wave measurements and observations in a more normal state, since it does not require the depilation process or electrocardiogram implantation.

概要

感性を付与した製品を遠隔で開発するために必要な要素技術開発について、3 つの開発目標を掲げて研究を進め、成果を上げることができました。今回開発した感性コミュニケーションツールや遠隔医療ツールは、実際の場でテストが行われています。ツールを実際の場で使用する事により、解決すべき課題やニーズがさらに見えてきます。この課題やニーズに基づき、改良を行う事や、新たな研究を行う事で、感性を付与した製品を遠隔で開発する事に近づける事ができると考えます。以下、3 つの目標に対応する成果を記します。

1. 触覚；感覚情報と物性情報の相互変換（Chapter 4）

感性コミュニケーションツールのプロトタイプ（感性価値製品の開発）と表面粗さの変化を体験できるサンプルを用意して展示会で発表しました。プロトタイプは「DIC カラーガイド」と同じ仕様で、カラーガイドに触覚フィルムを組み合わせたものです。感性コミュニケーションツールについてのアンケートでは、64 人中 49 人が試作品に興味を持ち、そのうち 21 名（31%）は、試作品が欲しいという結果でした。この結果をもとに、系統だった触感を 2 次元で体感できる「DIC Material box」を制作しました。これにより、デザイナーや商品開発者は、自分の好みの感覚ベクトルを確認することができます。

2. 色再現 （Chapter 5, 6）

新しいカラーチャートとそのカラーチャートを利用した、患者の顔色・舌色を正しく伝送できる遠隔医療ツールを開発しました。カラーチャートには、医療診断に必要な色を再現出来る、ヒトの舌色、肌色が含まれています。遠隔医療ツールは iOS に実装しました。開発は、色彩に詳しい漢方医と共同で行いました。COVID-19 流行下での緊急課題であったため、実際の使用を優先し、ツールの使用感を主に定性的に評価しました。その結果、人間の色覚に基づく補正と自動補正は、補正を行わない場合よりも有益であることがわかりました。この結果を踏まえ、現在、さらに医師の協力を得て、評価を継続しています。

3. 感情の状態の計測；非接触脈波計測（Chapter 6, 7）

心拍などの生体信号は、感情の動きを反映します。我々は、RGB カメラを用いた心拍測定ツールを作成し、検証を行いました。本研究の貢献は 2 つあります。

1 つ目は、独立成分分析により得られたヘモグロビン信号の変化を捉えて脈波を得る技術を活用し、39 人の被験者で精度検証を行ったことです。その結果、市販のパルスオキシメーターと同様の精度である事が確認されました。現在は、臨床現場からの意見も取り入れながら、ソフトの改良を進めています。

2 つ目は、ラットの足裏からの脈拍測定です。この研究は、人間では難しい感情実験を動物で行うことを考慮して行いました。ヒトの約 8 倍程度のラットの脈波を捉える為に、高速ビデオカメラを用いました。皮膚からの信号を捉える為に、足裏から撮影しました。その結果、足裏から脈波を取得することができました。この方法は、脱毛処理や心電図の埋め込みを必要としないため、より通常な状態での観察が可能であることが示されました。

Contents

A preliminary study for the development of Kansei value products in mobile work

Chapter 1: Introduction

1.1 Motivation

In this thesis, I describe the development of a preliminary study for the development of Kansei (sensitivity) value products in mobile work. My future vision is product development in a virtual space such as the Metaverse. My image is to develop Kansei value products in the "Star Trek" holodeck [1]. Star Trek is an American science fiction media created by Gene Roddenberry that began as a television series in the 1960s and continues to be disseminated through television and movies. The holodeck can create an imaginary world in which the boundary between reality and fiction becomes indistinguishable. The holodeck is not possible with today's science and technology. However, we would like to get as close as possible to such concept. Considering feasibility, I set the theme to create a product with Kansei value in mobile work. Three steps would be necessary for the making of Kansei value products in mobile work:

- The product concept is decided by remote communication.
- Detailed specifications are decided in a virtual space.
- Manufacturing is done by on-demand modeling.

The process will be up to the pre-manufacturing stage in the virtual space.

Figure 1-1 shows the Kansei value product development procedure. First, the product concept is determined based on market needs or technological seeds. Next, development takes place to bring the concept to fruition. Next, materials and processing methods are determined, and prototypes are made to realize the product concept. After that, a sensory evaluation is conducted on the product, and improvements are made based on the sensory evaluation results to complete the product.

Currently, we cannot do all our development in a virtual space. However, some developments of products that partially use mobile work have been established. For example, meetings to determine product concepts can be held via remote communication (such as through ZOOM) while viewing 3D models. As an industrial manufacturing method for small-quantity, high-mix production, 3D printers can be used in modeling and on-demand printing can be used to add patterns to apparel products.

However, when deciding on a concept for a product with Kansei value, participants must discuss their sensibilities with the idea and value, but this part is difficult with the current tools. In addition, although 3D modeling exists, tactile sensors and displays are still under development. As for modeling, current 3D

printers cannot keep up with human perception, which can sense at the micron level, and post-processing is still in development.

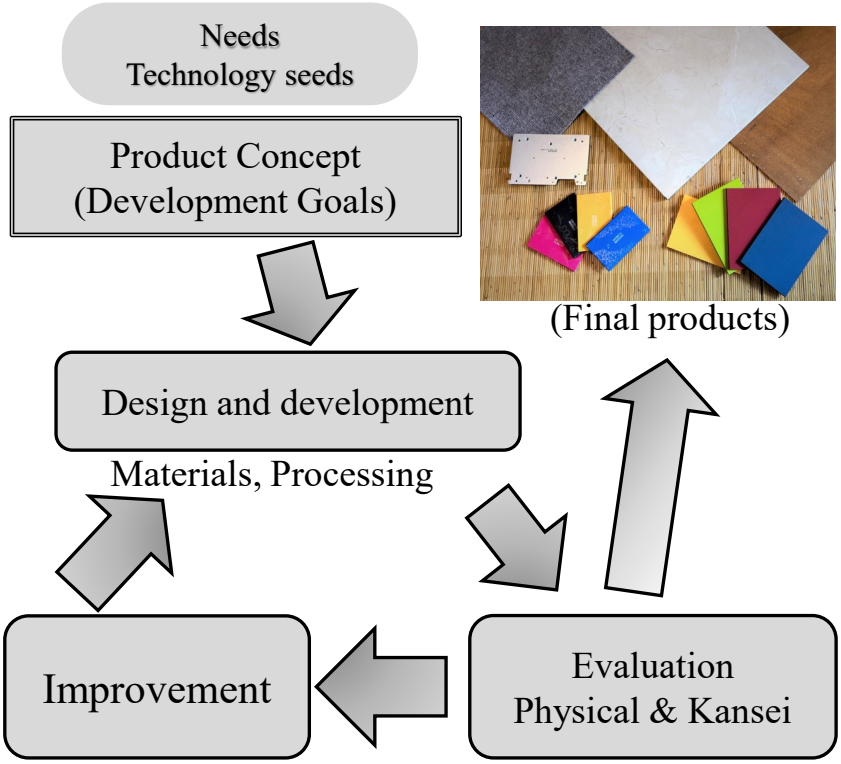

Fig. 1-1. Kansei value product development procedure.

Therefore, I thought about addressing these issues and increasing the number of items that can be developed in virtual space. Specifically, I wanted to construct a world in which participants' sensibilities can be conveyed, and their sense of touch can be transmitted.

With the advent of the SDGs and the need for emotional enrichment, we are entering an era in which manufacturing that appeals not only to function but also to Kansei value is necessary. Chemical manufacturers can provide new materials through compounding and synthesis technologies. The idea is that, if these technologies for modification and adaptation could be directly provided to creators, designers, and others who face consumers, differentiated products with Kansei value could be offered to the world.

Chemical manufacturers' conventional development of products is based on physical properties that match the target product's function. To develop products based on sensibility, it is necessary to quantify the sensibility information considered by the creator and build an interface that allows the material manufacturer to understand it as physical properties.

In the current product development process in the supply chain, creators work with processing manufacturers to create products with Kansei value, while chemical manufacturers provide materials to

processing manufacturers. In the future, it will be necessary for material manufacturers, processing manufacturers, and creators to work together in the development process.

In the manufacturing process where the three parties cooperate, we considered it necessary to have a common platform for discussion since the fields of each party are different. An excellent way to achieve a common understanding is to have discussions in the presence of actual objects, although this requires many samples and involves trial and error. Virtual reality (VR) technology is also improving. Various types of IT-based concepts, such as augmented reality and virtual reality, have been proposed [2]. The use of virtual space is also being promoted in various fields, and chemical [3] and VR training platforms [4] have been proposed. However, the level of image reproduction required by designers may be still some way far off. As for tactile displays, various methods are still being studied in laboratories. By focusing on this untapped field of haptics, we decided to create a platform where material manufacturers, processing manufacturers, and creators can have a joint discussion.

Conventional sample sets are composed of distinctive products. Samples for sensibility evaluation are also composed of different materials such as wood, stone, plastic, ceramic, glass. However, in these sample sets, a correlation between physical properties and sensitivity has not been found. Therefore, we devised a kind of sample set in which mechanical properties are controlled. If we can make many of these sets, it will be possible to remotely discuss about materials. The initial idea was to distribute these sets to the overseas subsidiaries of DIC Corporation, to which I belonged to, and use them as a basis for material discussions.

Subjective evaluation is necessary for the development of Kansei value products. If the subject to be evaluated is limited, the number of times required for sensitivity evaluation is not so large. However, in a systematic sample set, many evaluations are required. When a subjective evaluation is conducted on actual samples, it is necessary to evaluate many parameters, such as hardness and softness, warmth and coldness, and surface roughness. Actual products are even more complicated, with multi-layered structures and coatings on the surface; moreover, the thickness of the coating changes the evaluation. Therefore, we aimed to implement a measurement method using biometrics and other methods that are not subjective.

For a sense of the diversity of textures and materials, **Fig. 1-2** shows diversity in texture of wine cork stoppers (a) and various materials with diverse texture such as, carpet, stone, plywood, aluminum sheet, and paper packaging (b).

(a) Cork stoppers with a variety of textures

(b) Samples of a variety of materials

Fig. 1- 2 Diversity of samples.

1.2 Overview of goals

The ultimate goal of my study would be the development of Kansei value products with tactile sensation through collaboration remotely among material manufacturers, processors, and creators. Since this goal involves many developmental elements, we considered following a blueprint. In addition, we also considered the possibility of improving the performance of remote conferencing using cameras, which are currently available (**Fig. 1-3**).

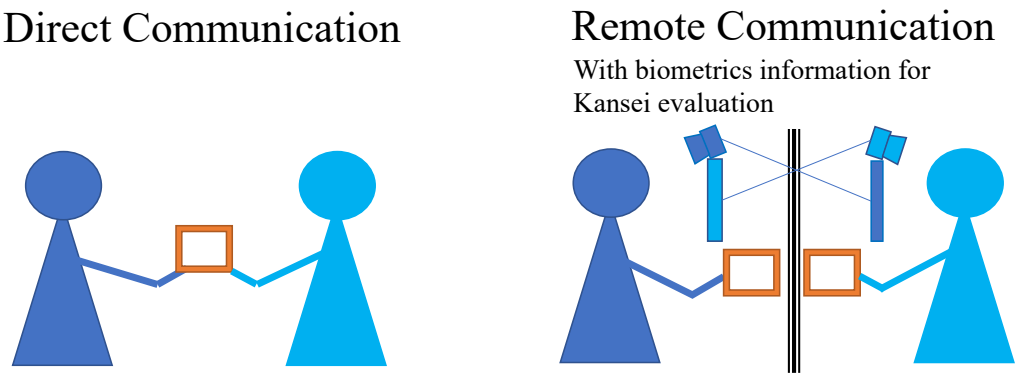

Fig. 1- 3 Remote development of Kansei value materials and sensory evaluation

Fig. 1-4. lists the technologies required to develop products with Kansei value in a remote environment and the research conducted in this thesis.

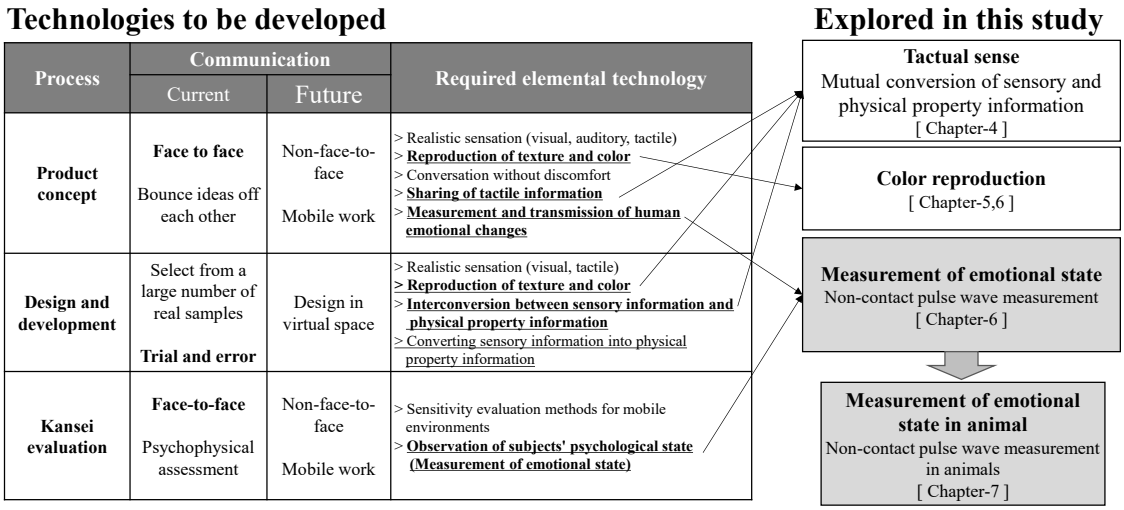

Fig. 1- 4 Technologies to be developed and explored in this study

Product concepts are developed in a face-to-face meeting, exchanging ideas and sensory images with each other.

Material selection and processing corresponding to the design are discussed during design and development. In the design process, the image is developed by looking at and touching various materials. The elemental technologies required for mobile work are the reproduction of texture, color matching, and the ability to communicate emotion to each other. After that, concrete objects are created. While technologies for creating visual images of objects in virtual space have advanced, tactile displays are still in the research stage. Therefore, another technology for sharing tactile information is required.

Two types of product evaluation are necessary: physical property evaluation and sensory evaluation. Physical property evaluation involves calculations based on 3D models and information on the physical properties of materials. Since sensitivity evaluation is usually performed in person, developing a sensitivity evaluation method suitable for mobile environments is necessary. Since there is a wide range of technical issues to be developed, we have set three goals in this study.

The initial plan of my research was to focus on technology for color reproduction and sensory evaluation for development of Kansei value products. While engineering is a technology that provides valuable things to the world, the priority of issues to be solved has changed with the prevalence of COVID-19. Since the elemental technologies for development are similar, I shifted my research focus to using the same base technology (i.e., color reproduction, biometrics) for observing and evaluating humans in telemedicine.

1. Tactile sense

We will create a system that enables mutual conversion between sensory information and physical property information regarding tactile sensation. This system converts the sensory information that designers and product developers consider into physical property information that material developers can understand. If the information can be appropriately converted, physical property information that should be given to the actual material can be obtained from tactile information, such as *shittori* feel, and can be used for designing.

2. Color reproduction

We will develop a simple color reproduction technology for remote environments. While VR technology is advancing and high-definition monitors are being developed, color reproduction is not widespread. Therefore, we have developed a new method for color reproduction in remote environments. In this study, we aim to achieve simple color reproduction in remote environments. Since color reproduction technology is a common issue in product development and telemedicine, we approached this issue from the telemedicine

3. Measurement of emotional state

Current remote work tools are not sufficient for communicating emotional information. If human emotional changes, which cannot be obtained with current tools, can be captured and transmitted simply, the missing information can be supplemented. In this study, we will develop a method to measure heart rate, which is the basis of emotional measurement, using a remote RGB camera. Biometric measurements in mobile work and telemedicine have to be performed in a non-contact manner, which is another common issue. Furthermore, animal experiments are also being conducted to elucidate human emotions. Therefore, we have also developed a remote non-contact heart rate measurement adapted for animals.

1.3 Thesis Outline

The structure of this thesis is shown in **Fig. 1-5**, where I describe the Chapters of my research corresponding to the three goals established in the previous chapter.

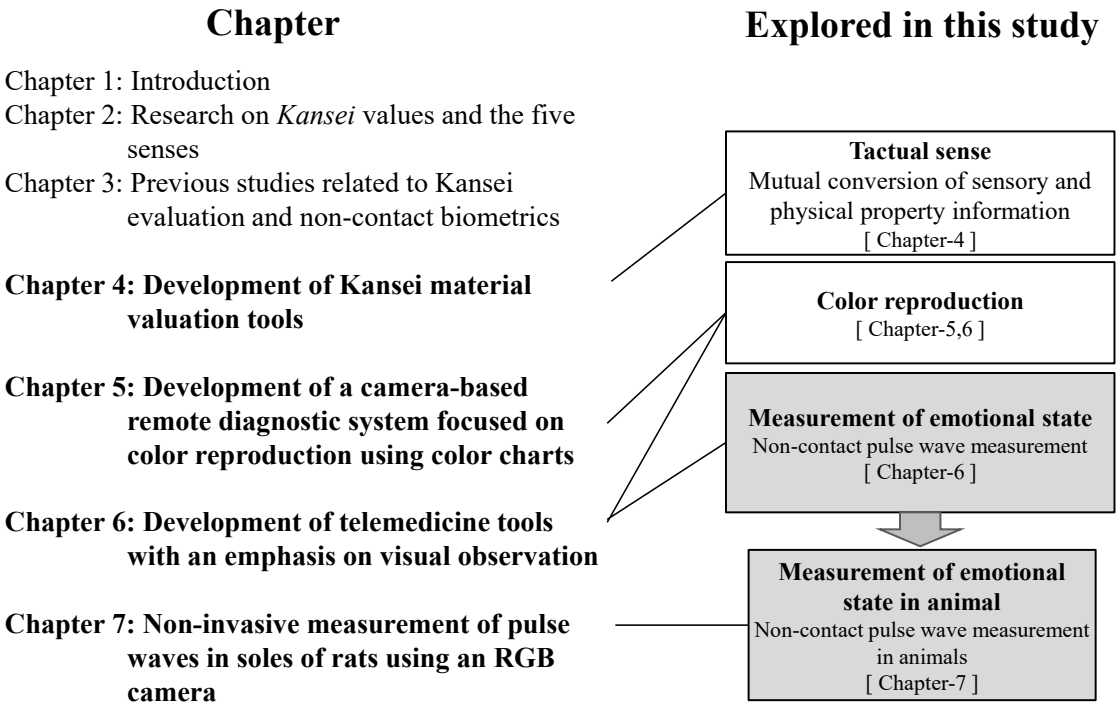

Fig. 1- 5 Structure of this thesis.

Chapter 2: Research on Kansei value and the five senses

In this chapter, I introduce the previous studies related to Kansei value and sensory evaluation. These are the basic concepts related to the development of value-added products that we aim to create.

2.1 Kansei value

In 2007, the Ministry of Economy, Trade, and Industry (METI) positioned “Kansei value” as the fourth value axis after function, reliability, and price. They proposed the “Kansei value initiative” [5] as a national policy as one of the ways to differentiate and add value to products in the shift from mass production to small-lot, high-mix production. The competitiveness of Japanese industrial products has been based on functional value.

With the increasing generalization of highly functional products, differentiation based on functional value is becoming more complex. Nobeoka noted that focusing on premium value is important to differentiate products [6]. According to Nobeoka, the definition of product price is functional value plus premium value. Functional value refers to the numerical specifications listed in the catalog, whereas premium value refers to values that are difficult to express with numerical specifications, such as brand and luxury (**Fig. 2-1**). The products of Apple Inc. and Dyson Ltd. are examples of products that add premium value. From the perspective of business economics, product design brings functional aspects and emotional satisfaction to consumers [7], [8]. With the realization of high added value, it is necessary to design and manage attractive product designs deliberately. This development requires the integration of three elements: design, engineering, and marketing. Furthermore, design management, which naturally bridges the engineering and marketing worlds, can provide a more comprehensive vantage point to examine the development of emotional product characteristics and consumer response to the designed items [9]. Regarding Kansei research in the academic research field, the Ministry of Education, Culture, Sports, Science and Technology (MEXT) has been conducting cross-sectional projects called “Texture Brain and Informatics” [10] since 2010 and “Innovative Science and Technology of Texture” [11] since 2015. For social implementation, MEXT has been implementing the “Kansei Innovation Center for Fostering Spiritual Richness through the “Center of Innovation (COI) Program” project [12]. In this way, Kansei values are becoming increasingly important.

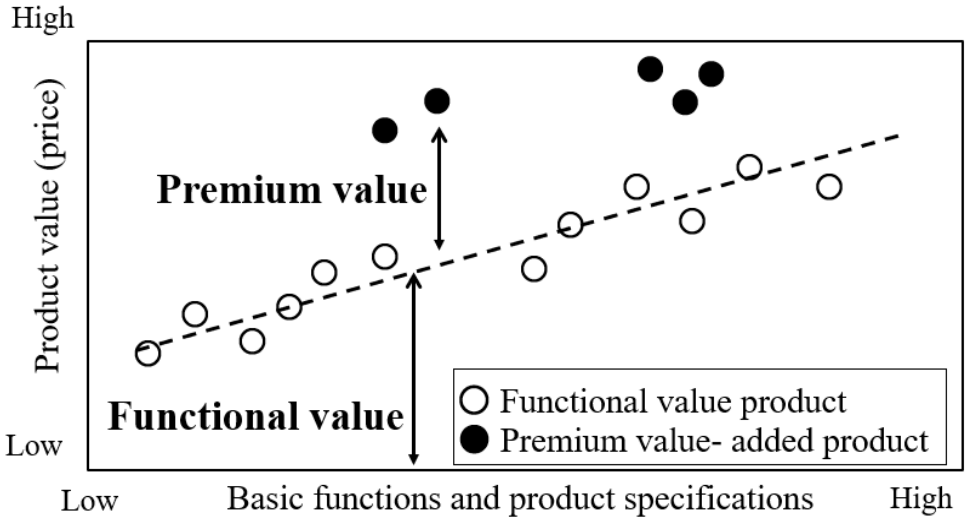

Fig. 2-1. Functional and semantic values (virtual example) **[6].**

2.2 Methods of adding Kansei value to industrial products and the supply chain

The development of industrial products with premium value-added has become a process involving many companies. The actual supply chain is complex. A simplified supply chain consists of materials produced by a chemical manufacturer, processed by a processor (converter), provided to a manufacturer (brand owner) who sells the product directly to the consumer, assembled, and delivered to the consumer as the final product (**Fig. 2-2**).

Material manufacturer (Chemical)	→	Converter (Processing Industry)	→	Brand owner (Consumer electronics, automobile)	→	Consumer

Fig. 2-2. Supply chain of premium value products.

The following is a general description of the sensory product development process. First, the product image is created by the designers and creators of the brand owner. The product parts used to convert the designed image into a concrete product are made by the converter. Converters manufacture products by combining materials, molding, and surface processing according to the brand owner's specifications. The converter then orders the materials needed to create the product parts from the material manufacturer. The components of the process that require evaluation of human sensitivity are evaluated by people using multiple samples called limit samples. To date, material manufacturers and brand owners have rarely collaborated to establish a directory of Kansei value product development.

2.3 Proposals for collaboration between chemical manufacturers and brand owners in the development of highly Kansei valued products

Chemical manufacturers can synthesize materials with a variety of physical properties. Furthermore, they can provide materials with various physical properties by compounding the synthesized materials. Chemical manufacturers also understand the molding and processing, as they develop materials in consideration of the molding and processing that converter perform. However, designers and creators do not have the opportunity to collaborate with chemical manufacturers, so they are unaware of the possibilities and developmental potential of the technologies possessed by chemical companies.

For the development of products with higher premium value and competitiveness, it would be ideal for material manufacturers, processing manufacturers, and brand owners to cooperate in the manufacturing process. The problem is that material manufacturers develop products based on physical properties, whereas designers and creators develop products based on sensibility, so they cannot discuss on the same basis.

2.4 Focusing on Kansei value in manufacturing

To manufacture Kansei value products, the manufacturer needs to convert the sensory information of the designer into product manufacturing information. At Dyson Ltd., engineers learn design based on the idea that technology and design are inseparable in manufacturing [6]. Takram, a design innovation firm with offices in Japan, the U.S., and the U.K., utilizes pendulum thinking (a way of thinking that moves between design and engineering, individuals, and teams, and thinking and making). Additionally, they promote collaboration between design and manufacturing [13].

Chemical manufacturers are also attempting to appeal to creators. Salone International del Mobile di Milano, the world's largest international furniture fair, is held simultaneously with FUORI SALONE, a design exhibition held at various locations in Milan. Japanese consumer electronics and automobile manufacturers exhibit their products at FUORI SALONE. In 2018, several Japanese material manufacturers participated in the exhibition, including Mitsui Chemicals, Inc. and AGC Corporation. Mitsui Chemicals, Inc. started the Material Oriented Laboratory (Molp: MITSUI CHEMICALS) [14] as an open laboratory activity to rediscover the functional value and sensory appeal that lie dormant in various materials by making full use of all the senses and to sharing ideas for the future. DIC Color Design Corporation, a subsidiary of DIC Corporation, has been publishing the “Asia Color Trend Book” with added material samples since 2008 [15]. DIC Corporation is also conducting the “Colorial Project” in 2018 [16], an event for creators to help them understand the value of tactile materials.

Captor 3: Related works of Sensory evaluation and non-contact biometrics.

This chapter will introduce prior research on the tactile sense that we have focused on in our study. We also introduce previous research on color reproduction, which is necessary for remote human observation, and previous research on non-contact biometric heart rate measurement.

3.1 Recognition of materials with tactile properties

In manufacturing with tactile sensation, material design involves investigating the relationship between the physical quantity that causes tactile sensation and the tactile sensation perceived by humans. In designing a haptic material, if the relationship between the physical quantity used to induce tactile sensation and the tactile sensation felt by humans is known, the design is easy. Since the mechanism of tactile sensation is still being determined, in designing, several samples can be built to get closer to the target, considering the past results. Humans recognize the external world through the information that is perceived through their sense organs. Therefore, humans can recognize the external world by inputting information within the range that their sense organs perceive. The Japan VR Society defines the range of visual perception as 380-780 nm electromagnetic waves and auditory perception as 20-20000 Hz air vibrations [17].

In the human perception of color, color can be evaluated by a physical parameter, the light spectrum entering the human eye. In a more simplified model, humans perceive colors based on the tristimulus value of a color stimulus X, Y, Z, which are the three primary colors of color used in the CIE which created by the International Commission on Illumination (CIE) color system (X Y Z color system). The color display makes use of this principle. When the tristimulus values are input to the eyes, which are the receptors for human light, the human brain processes the information and reconstructs the information input from the eyes. **Figure 3-1** shows an overview of human visual perception of things.

However, humans may perceive the same color even if the input spectrum is different. This case is called color adaptation, and it is a phenomenon whereby a person perceives the same color even when the same object is viewed under different lighting. This phenomenon is due to the brain's perception of color and the brain's ability to perform color correction.

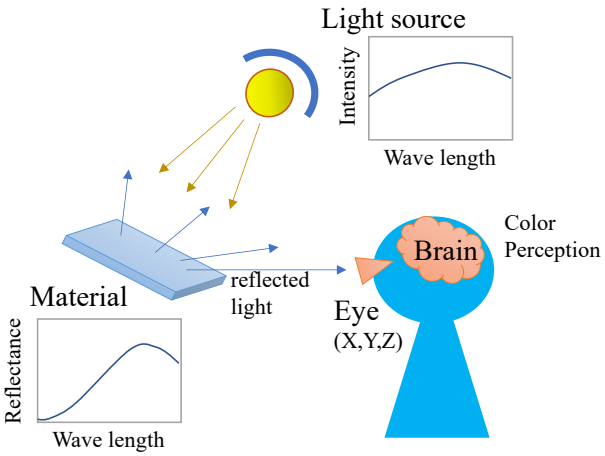

Fig. 3-1. Human visual perception of things.

Tactile sensation in a broader sense belongs to somatic and visceral sensation and is defined as any sense other than vision, hearing, taste, and vestibular sensation. The receptors related to touch include mechanoreceptors that respond to mechanical stimuli, thermoreceptors that respond to thermal stimuli, chemoreceptors that respond to chemical stimuli, and nociceptors that respond to stimuli that cause injury.

Four types of mechanoreceptors exist in the finger abdomen, with different types of responses to mechanical stimuli (**Fig. 3-2**) [18].

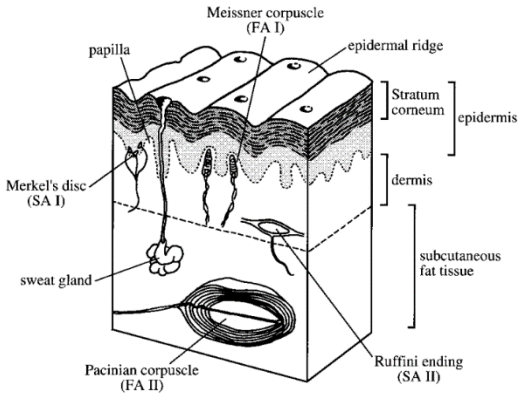

Fig. 3-2. Tissue and tactile receptors of glabrous **[18].**

Shirado et al. proposed a model of the material cognition mechanism based on receptors (**Fig. 3-3**) [19].

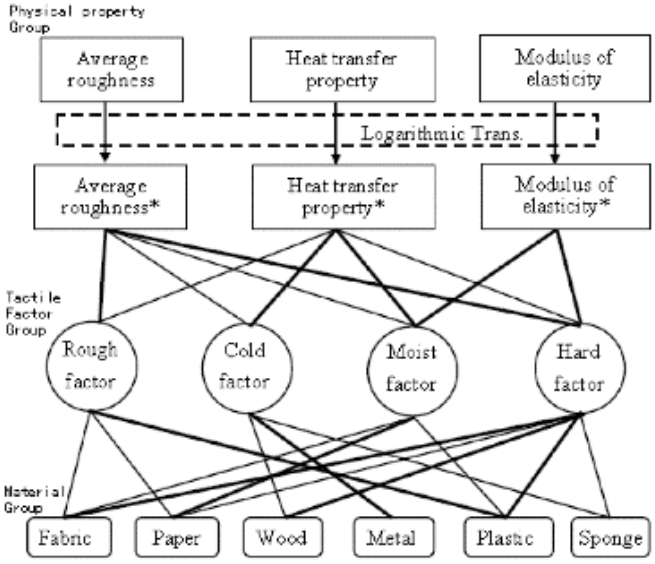

Fig. 3-3. Texture perception model **[19]**.

Okamoto proposed that tactile perception of materials is composed of five dimensions, namely, macro and fine roughness, warmness (warm/cold), hardness (hard/soft), and friction (moist/dry and sticky/slippery), as shown in **Fig. 3-3** and further studies on the perceptual mechanisms of each tactile dimension will confirm the classification [20].

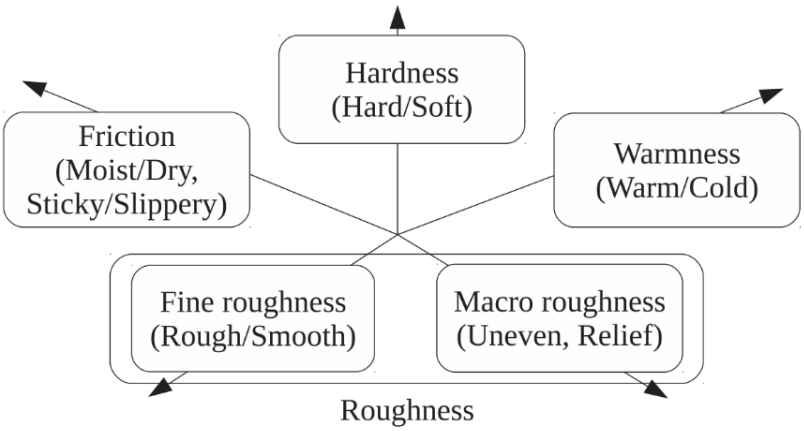

Fig. 3-4. Five psychophysical dimensions of tactile perception for materials/textures **[20].**

In material design with sensitivity, research on dimensional texture composition is necessary, and research trends are reviewed by Nagano et al. [21]. This review shows that research on texture dimensions includes examples of constructing inter-material dimensions from a group of materials selected from a wide range of categories and designing the material feel of materials in a specific field of products. The proposed dimension was between three and five. As an example of product research in a specific field, Picard et al. have identified four dimensions for 24 car seat materials: Soft / Harsh, Thin / Thick, Relief (Uneven), and Hard [22]. Okamoto et al. have proposed a hierarchy of dimensions for cognitive mechanisms [23]. Multiple proposals have been made for tactile perception, but no definitive model such as RGB has been developed. On the other hand, a sensory language method has been proposed instead of directly linking perception to physical properties. Sakamoto et al. have attempted to use onomatopoeia to map the materials of industrial products [24]. Kawabata et al. [21] developed a Kawabata evaluation system (KES) to evaluate textile sensibility. Shitara et al. [25], [26] reported that in evaluating the tactile sensation of wood, the touching behavior differs depending on the type of adjective being evaluated. This research shows that the signals to the receptors change depending on the way a person touches the object, which means that people receive different sensations depending on how they touch the same object. From the viewpoint of sensory perception, when a person judges the hardness or softness of an object, he pushes it, and when he judges the surface roughness, he traces the surface. In the actual field, to confirm the identity of the material, the judges use a set method of touching. Okamoto et al. conducted a study in which they visually evaluated and categorized material texture [27].

Hence, research on tactile sensation in texture has been conducted with human cognition, such as research-based on tactile receptors, hierarchical models that consider tactile perception, and verbalization of tactile sensation using onomatopoeia. However, few examples of systematic material research on material design add sensitivity to industrial products. Because many sensitized products are available in the market, they are made based on the experience and intuition of artisans who have accumulated know-how within each company rather than systematic research.

From the above, heat conduction, contact area, surface topography, mechanical strength, and rheological properties related to heat sensing and oscillation are considered necessary to develop material samples.

3.2 Remote tactile evaluation (tactile sensors and tactile displays in VR)

To evaluate the sensibility of materials with tactile sensation under remote conditions, measurement at the sending side and display at the receiving side are required. With the advancement of VR technology, there are some cases of remote evaluation of sensibility. In the case of remote evaluation, three requirements are necessary: sensing, transmission, and display. For sensing, various methods have been proposed, partly due to advances in Micro Electro Mechanical Systems (MEMS).

However, if the characteristics of the human skin do not match those of the sensor, it is not easy to obtain accurate values. The quantification of heat transfer is detected by the heat transfer between the sensor and the object. However, if the sensor does not have the same thermal conductivity as the human skin, techniques such as correcting the detected value to that of the human skin are required. Some examples of tactile communication have been proposed, but they are still in the laboratory stage, and further development is expected.

The principle of tactile perception is that tactile sensation is perceived when the tactile receptors in the skin are stimulated. To stimulate the mechanoreceptors in the skin, it is necessary to vibrate and deform the skin. Therefore, there have been proposals to use ultrasound to vibrate the skin [28], [29].

Considering the three elements of tactile perception as force, vibration, and temperature, an attempt to transmit them is also being considered [30]. Based on the correspondence between the four receptors in the

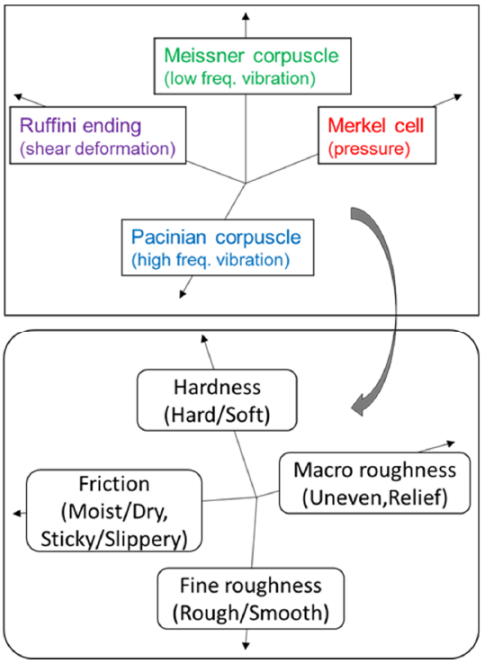

Fig. 3-5. Dimension transformation of four-mode stimulation (top) to four psychological dimensions of tactile perception (bottom) **[31]**.

skin for force and vibration and the sense of touch in **Fig. 3-4**, a device that makes us feel touch has also been proposed [31]. However, haptic VR is far from the practical level. Therefore, in our research, we intend to develop a method to create a product by touching several industrially produced samples that each person can hold.

3.3 Color reproduction

Color reproduction technology is well-established, and theoretically, color information can be reproduced with the tristimulus values shown in **Fig. 3-1**. The camera's performance for input and the monitor for output has been improved, and in regular use, we do not feel any discomfort even without calibration. Color recognition explains this phenomenon in the human brain. Calibration technology is also advancing, and recent advances in color management technology have created a system that allows the colors of imaging devices and display equipment to be calibrated using device profiles [ICC 1998, IEC 1999]. In industrial use, color reproduction is essential, and calibration is performed. However, due to the labor and cost involved, it is used in a limited number of fields. In addition, when sending images to others using a camera mounted on a smartphone, people want to make the images look good, so they are converted into beautiful images. In the case of remote evaluation of sensibility and telemedicine, color reproduction to the extent that changes in human complexion can be understood is necessary because it is essential to convey human facial expressions and complexion.

This system assumes that the image will be displayed on a monitor and viewed by a human. However, it can also be a valuable means to quantify and communicate changes in human skin color.

The goal of color reproduction is to match the actual object being viewed with the object viewed remotely via the device (**Fig. 3-6**) [32]. Color reproduction must match calorimetrically and visually as close as possible. Because we use our brains to see things, we may not see the same colors even if they are the same calorimetrically due to color adaptation and memory. On the other hand, when the lighting environment is different, the colors are different calorimetrically, but they look the same visually.

Hunt's model [33] is famous for its color

a) Spectral color reproduction

b) Colorimetric color reproduction

c) Exact color reproduction

d) Equivalent color reproduction

e) Corresponding color reproduction

f) Preferred color reproduction

While a-c is to match physical colorimetry, d-f considers human appearance. The model used in smartphones is f, where the captured image is adjusted so that humans would prefer adding a reddish tint to the skin color. In telemedicine, color changes in the human face cannot be observed if the preferred color transformation is used. For telemedicine, d and e are required for color reproduction when observing

humans. For color reproduction, there is the method of using color charts, which is also used in academic research [34]. Usually, to use the color chart is to photograph the color chart and the object simultaneously when shooting; DIC Corporation also provides calibration charts for digital color guides. The achromatic portion of the color chat helps measure the luminance of the area. The colored portion is used to reproduce the color. Many color patches increase the accuracy, but since the accuracy is based on the color of the patches in the color chart, the burden of quality control increases in response to many colors.

In this study, we use a color chart-based method for calibration.

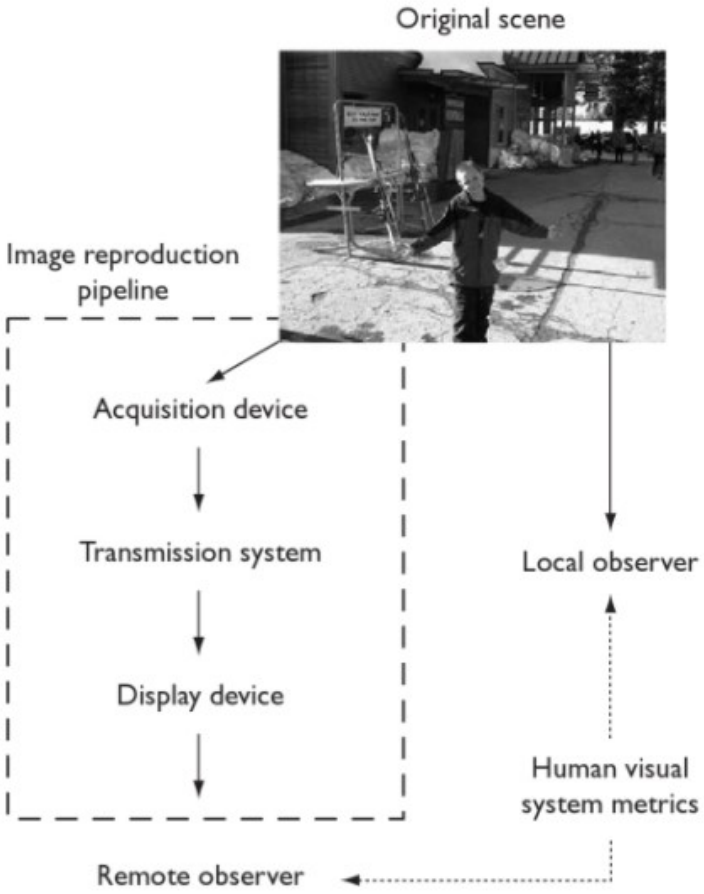

Fig. 3- 6. color reproduction pipeline.

3.4 Non-contact biometric evaluation

Psychological evaluation, which is observing a human being, is similar to observing a patient in medical practice. The heart rate fluctuates due to changes in the mind and body. In medicine, measuring the heart rate using a stethoscope is a common practice. The heart rate variability, R-R wave interval changes of the

pulse have also been used to measure emotion. The heart rate variability R-R affects the sympathetic and parasympathetic nerves, so it is used to capture changes in human emotions, and there are many research examples.

Human heart rate measurement requires accuracy and reduced impact on patients and subjects. The ECG is usually used in medicine because it can measure the heart rate with high accuracy. The electrocardiogram measures the electrical signals of the heart. Since the pulse wave is generated due to the heart contracting with electrical signals, the pulse rate obtained from the ECG and that from the pulse wave coincide. Therefore, when measuring the reliability of the heart rate, the difference between the ECG and the pulse rate is compared.

In the case of arrhythmia, a condition such as blood not flowing due to a blockage in a blood vessel occurs, the heart rate on the electrocardiogram may not match the heart rate obtained from the pulse. In addition, since the body condition in which blood flows and the arteries themselves have rheological properties, the pulse wave fluctuates even with exercise, arteriosclerosis, and other diseases. Because of this, the nature of the signal obtained from the ECG and the pulse wave signal differs, the pulse wave provides different information from the ECG. For example, pulse wave velocity can be determined, and arterial stiffness can be judged by measuring pulse waves from the ECG and the extremities. Along with electrocardiography, pulse oximetry is another method that is considered effective in measuring heart rate.

The principle of the pulse oximeter is to use infrared light to detect changes in the amount of hemoglobin caused by the beating of arterial blood [35]. For example, pulse oximeters measure heart rate (HR) in the first few minutes after birth because it is difficult to wear an electrocardiogram [36]. There is also a proposal to use electromagnetic waves to indirectly measure the contraction of blood vessels for heart rate measurement. The microwave-based method detects body surface movement by microwaves and captures the heartbeat and lung movement to detect vitals. However, this requires special equipment [37], [38] . The proposed camera-based methods for measuring vitals include RGB cameras, infrared cameras, and time-of-flight (TOF) cameras. An RGB camera-based method has been proposed to measure rats and wild animals' HR and respiration rate (RR) by capturing their skin movements with a camera [39], [40], [41], [42], [43]. There has been much research in recent years on the use of RGB cameras.

There are two main methods: one is to capture the change in hemoglobin level based on the contraction of blood vessels, and the other is to use the change in luminance obtained from the change in body surface based on the contraction of blood vessels. The method that captures body motion requires the removal of noise from motion other than that of the heart and breathing. The method that captures the change in hemoglobin amount based on the contraction of blood vessels is robust against noise because it is not affected by luminance if only the amount of hemoglobin is separated by independent component analysis. Wang et al. have proposed a method for noise reduction [44]. Independent component analysis (ICA) and wavelets have been proposed as signal processing methods to capture weak signals. Fukunishi et al. [45]

have also developed a signal separation technique using ICA. Another advantage of using an RGB camera is that if it can observe the flow of blood, it can observe blood flow. Kamshilin et al. [46], [47], [48] is researching to understand the flow of blood by breaking down the photographed areas in detail. In general, pulse waves can be detected using the method shown in the **Fig. 3-7**.

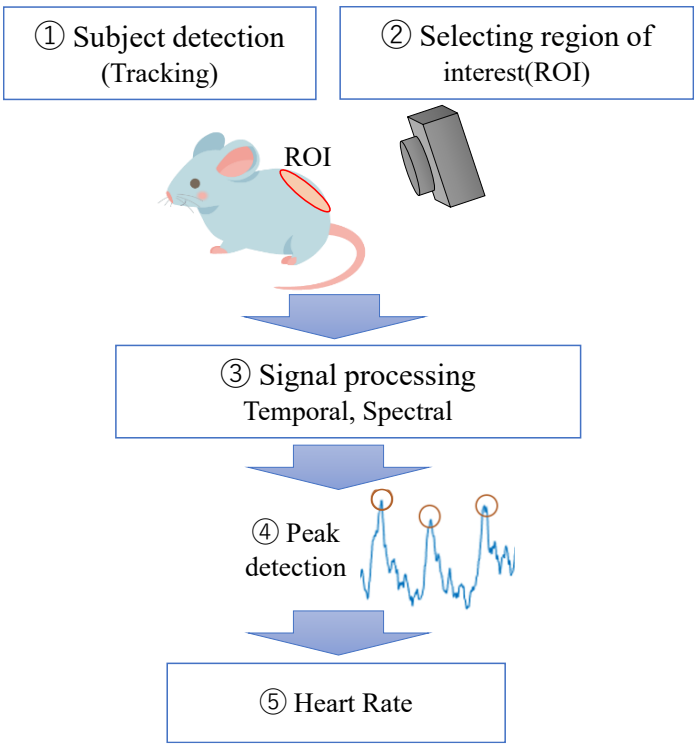

Fig. 3-7. Pulse wave detection flow.

Chapter 4: Development of Texture Communication Tools

In this chapter, we describe the development of a tactile communication tool. When sharing tactile material information, a new method of presenting tactile samples was considered because of the difficulty of transmitting tactile information in a mobile work environment. Therefore, we have developed a tool for tactile sensation.

4.1 Introduction

With the shift from mass production to small-lot, high-mix production, one of the ways to create differentiation and high added value for products is by adding Kansei value such as tactile sensation. In 2007, in Japan, the Ministry of Economy, Trade and Industry (METI) proposed the Kansei value Initiative [5] as a national policy, positioning Kansei value as the fourth value axis beyond function, reliability, and price. In the field of academic research, the Ministry of Education, Culture, Sports, Science and Technology (MEXT) has been conducting a cross-sectional project called “Brain and information science on *SHITSUKAN* (material perception) [10]“ since 2010, and “Innovative *SHITSUKAN* science and technology [11]“ since 2015. Based on these projects, exchange of information has also been established to deepen the scientific understanding of texture and promote texture-related technologies. As for social implementation, MEXT is implementing the “Center of KANSEI Innovation Nurturing Mental Wealth in the Center of Innovation (COI) Program [12]“ project. In this way, Kansei value is becoming increasingly important. However, in actual product development, when reflecting a designer's Kansei words in a product, such as “good texture,” many prototypes are created and selected through trial and error. Among the five senses, color sense has been the subject of much research. In practical use, color reproduction in e.g., monitors and printed materials is performed using the three primary colors. Tactile perception, which is the subject of this paper, is even more complicated, and attempts have been made to define it using various parameters [49]. We have been creating color guides, developing various tactile materials, and developing quantification technologies. To develop tactile products efficiently and quantitatively, we attempted to apply these technologies to develop a tool to clarify what kind of tactile sensations designers and others are demanding. In this paper, we describe the background of the base technology for quantifying tactile sensation, develop a “Texture Guide” tool, and then evaluate the Texture Guide.

4.2 Development of quantification technology for tactile sensation

4.2.1 Quantification of tactile sensation using dynamic friction coefficient

We focused on *Shittori* feel as an expression of tactile sensation and attempted to measure it using conventional physical measurement methods such as dynamic coefficient of friction and surface roughness. However, we could not find a suitable conventional method that correlates with *Shittori* feelings. We focused on how people move their fingers on an object to confirm their sense of tactile sensation. Based on the hypothesis that there is some correlation between finger movement speed and the coefficient of kinetic friction, we measured the coefficient of kinetic friction at several different measurement speeds. The measurements were conducted using a texture analyzer manufactured by Stable Micro Systems. The contact surface of the friction device was 63.5 mm x 63.5 mm, the weight was 200 g, and the surface was covered with felt. Measurements were performed at three different speeds: 2 mm/s, 20 mm/s, and 40 mm/s.

We used three types of paper for the evaluation: plain, matte, and paper with a “peachy-feel” finish that provides a *Shittori* feel. The results showed that the coefficient of kinetic friction of the regular and matte papers did not change with measurement speed. In contrast, the coefficient of kinetic friction of the paper with the “peachy feel” increased with measurement speed (**Fig. 4-1**). In preliminary experiments, the coefficient of friction decreased with increasing measurement speed on paper that was considered to have a “dry” feel. These results suggest that when people feel tactile sensations with their fingers, they recall a wet or dry feeling by sensing a change in the coefficient of kinetic friction that is different from what they expected [50].

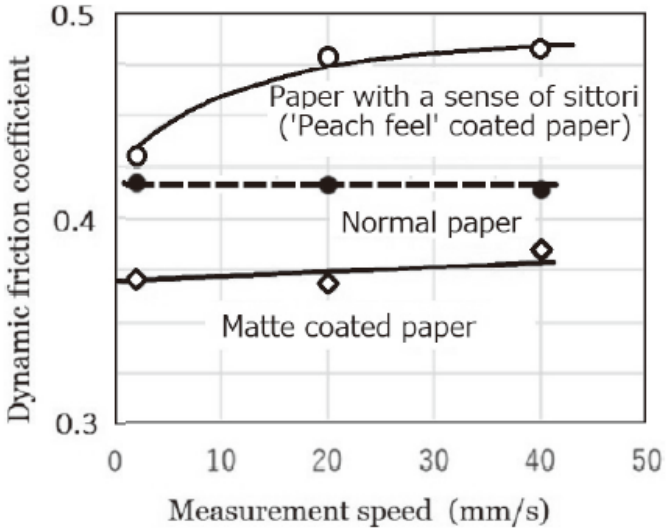

Fig. 4-1. Dynamic friction coefficent.

4.2.2 Psychological evaluation of tactile samples

Metal beverage cans are designed in a variety of ways to make them attractive to consumers. While many designs appeal to the sense of sight, few designs appeal to the sense of touch. We focused on designs that appeal to the sense of touch. The purpose of the survey was to examine the psychological evaluation of tactile samples with systematic physical quantities.

The three parameters varied in the sample preparation were the particle size of the polymer beads that are blended in for tactile sensation, the hardness of the beads, and the coating resin. The psychological evaluation included adjectives such as “smooth” and “rough,” which are considered to be directly related to physical properties, as well as catchphrases in beverage products such as “cute” and “wild”.

The results showed that adjectives directly related to physical properties were correlated with formulation, primarily particle size, while “cute” also showed a high value in a specific particle size range [51].

The details of the experiment are as follows. For the evaluation experiments, we used a coffee can-like container. To make this container, we first coated a metal plate with coating layer using a bar coater and cured using heat treatment, then we wrapped the plate around the container. The coating film composition used in the preliminary experiments consisted of three types of coating resins, seven types of beads with particle sizes ranging from 6 μm to 93 μm for each resin, and four types of bead hardness, and a bead content of 5% by weight. We also prepared a sample consisting only of the coating resin without beads. In addition, two different weights of containers were prepared for each sample. Sixty-six different samples were prepared, except for cases where the blended material was not dispersible enough to make a coating film. Using the 66 types of samples, we conducted a preliminary experiment to select the samples for the main experiment. After excluding samples with similar tactile sensations, a total of 26 different samples were selected for evaluation in the main experiment.

For the main experiment, the 26 samples were subjected to evaluation by 12 participants, six males and six females, aged in their 20s. Among the results, analysis of variance for bead hardness, resin material, and gender for “cute” showed that there was a significant main effect for bead hardness in tactile presentation ($p < 0.05$), and the softer the bead, the higher the rating. The results of the analysis of variance for bead particle size, resin material, and gender for “cute” were as follows. a) There was a significant main effect of bead particle size for all presentation methods ($p < 0.001$), and the smaller the particle size, the higher the rating. b) There was a significant main effect of gender for visual and tactile presentations ($p < 0.001$), with females having higher ratings than males.

Figure 4-2 shows a two-dimensional texture guide by cutting the samples used in the above evaluations into small pieces and pasting them on an A4-size paper. The horizontal axis represents the particle diameter of the beads, and the vertical axis represents the hardness of the beads. The difference in tactile sensation

due to the difference in coating resin can be achieved by using multiple sheets with different coating resins. The white squares on the sheet in **Fig. 4-2** are the samples, and the gray squares contain no sample. Not all of the samples were attached because of the problem of the dispersion state of the coating and the number of person-hours required for the experiment.

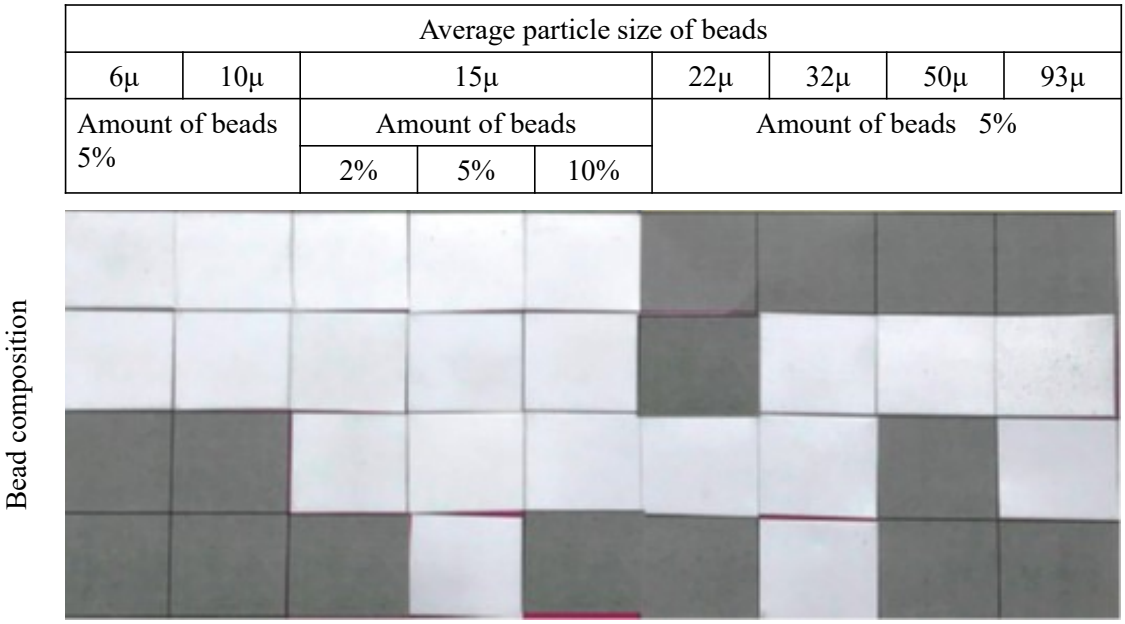

Fig. 4-2. Photograph of bead-coated resin samples.
The white patches are the sample, and the gray patches have no sample.
Photo courtesy: DIC Corporation

4.2.3 Interaction between texture and color

Commercial beverage cans emphasize designs that appeal to the visual sense. We conducted a sensory evaluation of the interaction between color and texture, with the value addition from texture [8]. Details of this experiment were as follows. A pair of adjectives were selected from among those used in previous studies to evaluate visual and tactile sensations. The visual stimuli were different hues (color types). The samples were presented in pairs, one as the reference/standard sample and the other as the target sample, and each sample was fixed with a magnet so that the samples could be touched in a stable manner (**Fig. 4-3**). The visual stimuli were provided in stereoscopic view using the Oculus Rift head-mounted display (HMD) (**Fig. 4-4**). The model right hand displayed on the HMD is shown in animation touching either standard (right) or target (left) samples. The aim of displaying the model hand in the HMD is to control for the different touching methods when humans touch the samples (**Fig. 4-5**). The results showed that differences in the color of the model affected the evaluation of all pair of adjectives. To be more specific,

the experiment was conducted with 24 participants, 12 male and 12 female students in their 20s who were normal color vison. The samples used for evaluation were the same shape as those described in the previous section, but with three different particle sizes (10, 22, and 93 μm). Seven colors types (yellow-red, yellow-green, blue-violet, red-violet, gray, black, and white) were presented in the HDM. The number of pair of adjectives pairs used was 21. A three-way analysis of variance was performed on the experimental results. a) All pair of adjectives had a main effect of color ($p < 0.01$). b) Particle size had a main effect for all pair of adjectives except "warm-cold" and "sharp-dull" ($p < 0.05$). c) Gender had a main effect on the pair of adjectives "pleasant-unpleasant," "warm-cold," and "wild-not wild" ($p < 0.05$).

These results indicate that color and particle size have a more significant effect on sensory evaluation than gender, with color having the most significant effect. As an example of the effect of particle size on color perception, reddish-purple tended to increase the evaluation of "feminine." In contrast, gray tended to increase the evaluation of "plain," "passive," "ordinary," and "inconspicuous."

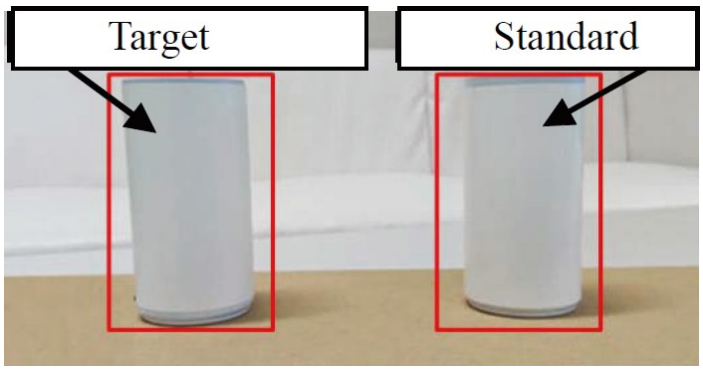

Fig. 4-3. Display of samples in real environment **[51]**.

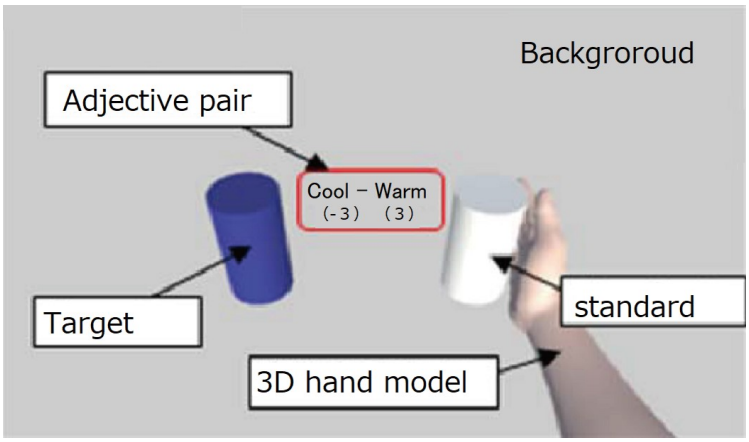

Fig. 4-4. Display of 3D models in a virtual environment **[51]**.

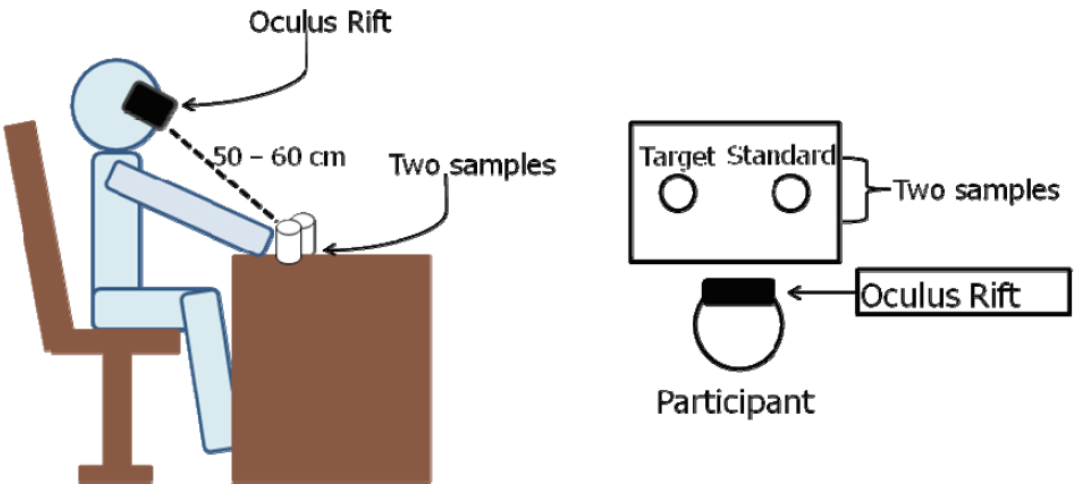

Fig. 4- 5. Experimental setup **[51]**

4.2.4 Quantification of Grasping

Quantifying tactile evaluation using beverage cans is necessary to consider universal design, such as the ease of holding. In order to quantify the ease of grasping, we considered using an index based on the relationship between the coefficient of kinetic friction and the measurement speed that we developed, which did not provide a good correlation. Next, we used the eccentricity index proposed by Kurita et al. [52] to determine whether a correlation could be identified. Details of this experiment were as follows. Eccentricity is a measure of the change in the area of the contact surface. An apparatus (**Fig. 4-6**) was used for this purpose. An infrared camera can identify the change in the area. Three texture samples were prepared by bonding polymer beads of different diameters (15 μm, 32 μm, and 93 μm) to polyethylene terephthalate (PET) film. The slider movement speeds were 2.5 mm/s and 10.0 mm/s. The eccentricity was determined by applying a 5 N force in the vertical direction. The subjects were six healthy males. To investigate the relationship between the measurement data and human sensibility, principal component analysis and multiple regression analysis were performed by combining eccentricity, physical parameters of the film, i.e., bead diameter, roughness, and coefficient of kinetic friction, with the sensibility evaluation conducted by Okura et al. As a result, we found that eccentricity at the beginning of slippage, independent of the film's physical parameters, also affects the sensitivity [53]. This method shows that the change of eccentricity E for the slider travel distance L, dE/dL, is assumed to have a higher grasping sensation than slippage, because

the smaller the value, the higher the stickiness. Based on these results, it is possible to quantify the sensitivity of grasping.

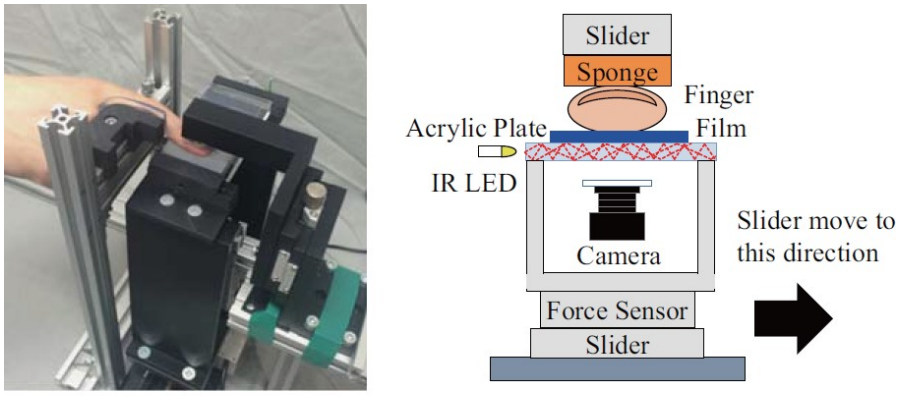

(a) Overview (b) Configration

Fig. 4-6. Experimental equipment **[53]**.

4.3 Development of texture (Kansei) communication tools

This section explains our proposed communication tool for sensibility, which emphasizes the sense of touch. Generally, in the process of developing a textured product, the first step is for the material manufacturer to propose to the user using a catalog or product catalog, and then propose several types of prototypes that meet the user's needs Kansei value and then make improvements according to the user's needs. Since there is no simple correlation between human sensibility and physical properties, commercialization is conducted using trial-and-error. For this reason, the material manufacturer often proposes texture samples that are extensions of existing products that have been quantified to some extent, even though they are products that respond to human sensitivity. The quality control agreement for the commercialization of a product cannot be limited to numbers.

The goal of the Kansei communication tool we propose is to solve the above problems:

1) By presenting texture samples, the direction of sensitivity and physical properties will be clarified and used as a guideline for development and improvement.

2) To quantify Kansei information for efficient development.

This proposal helps to ensure efficient product development. The development of a Kansei communication tool was based on a sample (**Fig. 4-2**) that showed a systematic sample in two dimensions, which was used in the experiment to quantify tactile sensation. The concept of our Kansei communication tool is shown in **Fig. 4-7**. The tool is equipped with texture information so that those in charge of materials can share the same understanding of the designers' and product developers' direction of preference. The numerical values

of the samples mounted on the tool can be used as feedback for product design. In addition, the tool can be equipped to samples with textures that go beyond the scope of current products so that designers can further expand their ideas. The arrangement of the samples in the communication tool should be based on the human perception of the material in multiple dimensions. According to Okamoto et al., tactile sensation is based on macro-roughness, micro-roughness, hardness, softness, friction, and warmth/coolness [20] .

We consider that this tool would be improved if it included samples based on this idea. Considering the perception of materials by humans, the correlation between the image that people perceive of warm/cool and hard/soft sensations and the physical properties is relatively well. In contrast, the physical property information, such as macroscopic unevenness, microscopic unevenness, and friction, is difficult to consider a sensible image; alternative onomatopoeias such as smooth, rough, and moist are considered effective. The samples to be placed should not be limited to existing products but should also include prototypes and natural materials so that human perception can be systematically measured. Kansei communication tool is different from conventional catalogs based on physical properties. Material manufacturers can use this tool by adding physical properties e.g., specific gravity, thermal conductivity, heat flux, surface roughness, friction coefficient, viscoelastic behavior related to sensibility, and conventional physical properties.

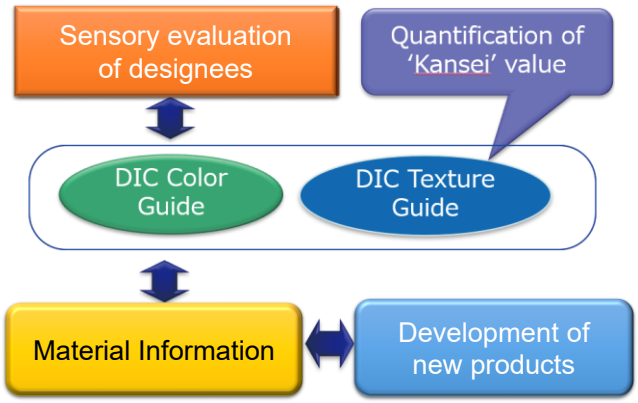

Fig. 4-7. Concept of communication tool.

4.4 Creating a Texture Guide

As a first step in developing a communication tool, we created a "texture guide" that combines the two axes of "color" and "touch." This study aimed to investigate the necessity of a Kansei communication tool and the value of adding texture to an exhibition. This study aims to investigate the need for Kansei communication tools and the value of adding texture to exhibits. For this reason, the texture guide was designed to be something that designers and product development departments could touch. In addition, to make the concept easier to understand, we considered a combination of commercially available DIC color guides and tactile printed materials using a newly developed tactile varnish.

Figure 4-8 shows the texture guide that we created. The specifications of the texture guide consist of a front cover, a back cover, seven color charts sandwiched between them, and seven PET films printed with various patterns using tactile gravure varnish. These are fixed with pigeonholes and can be easily rotated around the pigeonholes so that combinations of colors and textures can be tested. The size of the color chart is the same as that of the commercially available DIC Color Guide (200 mm x 60 mm). For the color chart section, seven green colors were selected with green tea beverages in mind. For the tactile printing part, a significant pattern was used to recognize the difference visually. The texture guide that we created for the evaluation was designed to focus on the concept of a Kansei communication tool, so we could not include specifications that would systematically capture the changes in human perception. To compensate for this, when we evaluated the tool, we also presented the systematic sample shown in **Fig. 4-2** at the same time.

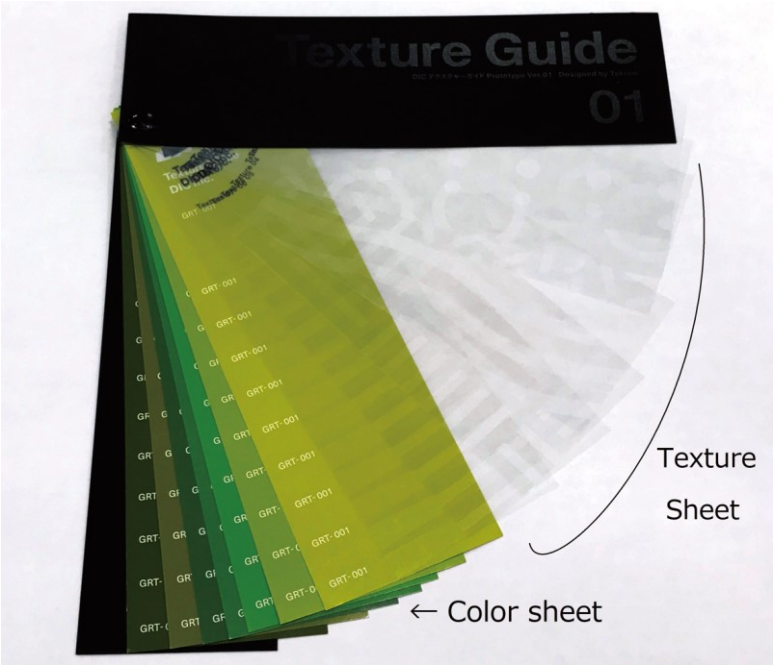

Fig. 4- 8. DIC Texture Guide（Sheet Sample).

Photo courtesy: DIC Corporation

4.5 Evaluation of the Texture Guide

At the packaging-related exhibition “TOKYOPACK2018” (10/2/2018-10/5/2018, 4 days), we evaluated the booth of “Texture Sample (Kansei Communication Tool)” in the exhibition space of DIC Corporation. The evaluation method was based on a questionnaire survey of visitors. Two staff members were stationed at the booth for all four days to explain and conduct the survey. The survey was conducted by the author

and the person whom the author instructed. The survey, which was conducted simultaneously with the explanations at the exhibition, was based on the following procedure.

1) An explanatory staff member explains that the texture guide is intended to communicate to visitors, and that the texture guide is a prototype under consideration for commercialization according to the customers' requests.

2) Present the texture guide.

3) Reiterate that the original purpose of the questionnaire was to create a systematic communication tool and provide an explanation by showing a systematic sample**, Fig. 4-2**.

The staff member filled out the questionnaire with the paper and writing utensils during the explanation to the visitors or by the staff member himself after the visitors left. The questions were: “Are you interested in the texture guide? “Do you want the prototype? Furthermore, “Do you want this prototype? As a result, 64 people responded to the questionnaire, 49 (77%) of respondents answered “I am interested”, of which and 21 (31%) answered “I want a prototype. “ The opinions and requests were as follows: “I was intrigued by the quantified samples (printing equipment-related manufacturer),” “I am interested in the quantification of sensitivity (printing company),” “It seems to be useful as a solution since we are having problems in communication with designers (confectionery manufacturer) The author's hypotheses were: “I am interested in the quantification of sensibility communication (printing company),” “I have a problem in communicating with designers, so this may be useful as a solution (confectionery manufacturer),” “This may be a good tool to communicate with designers (industry unknown),” “This is a good initiative, so I would like you to expand it to brand owners (converter),” and “I would like you to sell the guide (multiple companies). “The author hypothesizes that sensibility communication tools are necessary for material manufacturers and users and that the value of adding texture is also recognized. The survey results showed that 77% of the respondents were “interested” in the tool, and there was also a request to sell the tool, which confirmed the necessity of the tool and the value of the texture to some extent.

Some of the visitors asked for an explanation of the concept of the tool after the exhibition, so we provided individual explanations. The participants agreed with the concept and the value of the tactile sensation.

4.6 Issues and Development of Communication Tools

This study aimed to propose a Kansei communication tool at an exhibition and ascertain the tool's needs. The survey of visitors is qualitative since the survey was conducted in an exhibition environment. Many of the visitors (77%) responded that they were interested, suggesting the authors' usefulness of the systematic sample-based communication tool. Regarding the texture value, even though the samples we presented were not systematic, 31% of the visitors responded that they would like to have a prototype using texture,

suggesting that a certain proportion of people feel the value of texture. Since we were able to confirm the usefulness of the communication tool, we decided to develop a prototype, "DIC Material Box," which is a development of the texture guide. The DIC Material Box was designed to facilitate the development of products with Kansei value based on the sense of touch and facilitate the selection of materials. The concept of DIC Material Box is to provide systematic samples of surface characteristics of materials, such as warm/cold sensation, hard/soft sensation, and smoothness/roughness, which humans perceive, and to identify the preferred sensibility vectors for designers and product developers. The concept of DIC Material Box is to clarify the vector of sensitivity for designers and product developers.

Figure 4-9 shows the DIC material box, which measures W427mm x D304mm x H104mm and can hold four sample holders. Each sample holder can hold 16 samples (4 x 4). This arrangement allows the user to vectorially feel the two-dimensional tactile characteristics of the material, such as the hardness and softness of the material and the roughness of the material. Since there are 4 sample folders, various combinations of tactile sensations can be mounted. The following is a description of the two-dimensional tactile combinations. Two-dimensional combinations of material hardness/softness and surface properties (smoothness to roughness) and warm/cold sensation and surface properties are prepared. The box that can perceive the hardness/softness and surface properties (smoothness to roughness) of the material is made of urethane resin with four different hardnesses for the core part and attached with a film with four different surface roughnesses. For the hot/cold sensation and surface properties, four different surface roughnesses were created by spraying abrasives on the surfaces of four different thermal conductivity samples. The other two boxes contained samples of natural materials, unique textures, and other samples that would stimulate ideas for product development, regardless of the two axes.

Currently, designers and product developers are beginning to use this prototype as a reference for selecting materials. Designers and product developers have evaluated the tool as a promising tool for the future, as there has never been a systematic combination of tactile sensations in two dimensions. However, since the tool is being utilized with priority given to business applications, evaluation from an academic perspective, such as its usefulness, is an issue to be addressed in the future. In the future, we plan to consider the goals of this research, such as conducting sensitivity evaluation by changing the combination of two dimensions and developing products by having both parties use the tool remotely.

In our attempt to quantify tactile sensations, such as a feeling of "*shittori*," which we have focused on in the quantification of sensitivity, a study similar to our proposed method using the coefficient of kinetic friction was recently reported [54], [55], [56]. These study focused on the "moist feeling" as we did, and the evaluation objects were cosmetic powders, artificial leathers, fibers, resins, and metals. For the evaluation of dynamic friction, a finger model made of urethane resin was used as a probe, and a sinusoidal motion friction evaluation device that makes a sinusoidal motion was used to evaluate friction force

On the other hand, our proposed method uses a felt cloth as a friction probe and paper or coated metal/film as the object to be measured and measures the coefficient of friction by changing the probe's speed during the measurement of dynamic friction. The results of this research were presented at a conference in Japan in 2015 [50] and a patent application was filed in 2014-2016 [57], [58], [59].

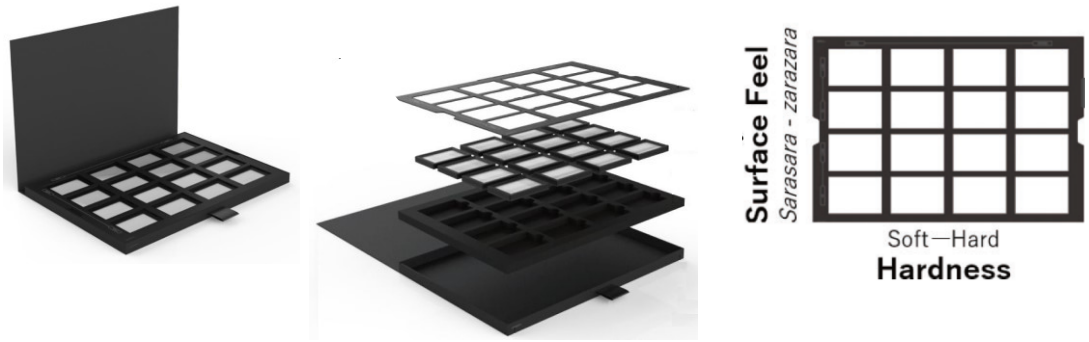

Fig. 4- 9. DIC Material BOX
Photo courtesy: DIC Corporation

4.7 Conclusion

This study describes a proposal for a tool for quantification and communication of sensibility, focusing on tactile sensation. These tools are expected to reduce the stress and efficiency of communication by reducing trial and error, since the material supplier can understand the sensibility requirements of the designer as physical property information. When a customer requests a sensibility product outside the tool's scope, the direction of improvement can be confirmed through physical property information, which clarifies the guidelines for product development and improvement. Since the texture guide is coated on a rigid base material, the physical property information is limited to surface roughness, friction, and adhesion. When using flexible materials such as artificial leather, the rheological properties of the soft base material also affect tactile sensation. The “DIC Material Box”, which is currently under development, will incorporate these elements. While the quantification of sensibility is helpful in manufacturing, a large amount of data is required in various fields. Although it is difficult to collect data from the internet for evaluations using objects, such as tactile sensation.

By acquiring tactile data using the tools we have presented, it can become high-quality data for creating products with sensory value. In the future, it will be necessary for consortiums to collaborate in the creation and standardization of general-purpose tools.

Chapter 5: Development of a camera-based remote diagnostic system focused on color reproduction using color charts

In this chapter, we will explain our development of color reproduction using color charts for telemedicine. In telemedicine, color reproduction is necessary because accurate observation of the patient's skin color is necessary for medical treatment. In remote sensory evaluation, it is also necessary to capture changes in the subject's facial expressions. This chapter describes color reproduction and automatic correction using color charts, which are necessary technologies for telemedicine and remote sensitivity evaluation.

5.1 Introduction

The telemedicine market is growing, particularly in the area of chronic illness, because conducting interviews and observations thorough a network is sufficient for an examination of such illnesses [60]. Because it is necessary to conduct a medical examination of the area of infection even during ordinary medical checkups, owing to the spread of COVID-19, the importance of telemedicine has been recognized as a means to prevent infections in healthcare workers conducting diagnosis and treatment [61], [62]. If the number of patients is significantly increased, it will become difficult to care for all patients in the hospital, and asymptomatic or mild patients will be forced to move to a hotel, home, or other unsupervised area. For the care of such patients, it is also extremely important to monitor any sudden deterioration in their condition, for which telemedicine will play an extremely important role.

To address this situation, Greenhalgh et al. published a guide for general practitioners in charge of primary care (video consultation: March 2020 BJGP Life Practice Guide) [63]. This guide notes that pulse measurements using fitness equipment may not be suitable for assessing the patient status from the perspective of reliability. Regarding the examination of color, “skin features (such as flushing, pallor, cyanosis—though note that if lighting is suboptimal this can be difficult to assess)” should be noted at the time of a medical examination. As the guide indicates, a proper color examination is important.

The importance of a color reproduction in medicine is also described in [64]. In particular, it is noted that telemedicine is affected by significant color errors incurred through the differences in the setup conditions, such as the illumination [65] . Dermatologists, dentists, and otolaryngologists observing patients based on the color of their face and tongue may make an improper diagnosis if the color is not reproduced correctly. A practical color reproduction system was standardized by the CIE [66] . In achieving a color reproduction in telemedicine, monitor correction on the doctor’s side can be performed relatively easily using a profile creation tool of a commercially available display device. However, a correction on the patient’s side is not easy to achieve, because a correction when the color of the light source and camera

characteristics may be needed. Because the light source and camera for each patient usually differ, such a correction should be performed for each patient and illumination condition.

Therefore, in this study, we created a color chart for a color examination that can be used immediately for each patient during telemedicine. We will examine whether the color examination of the patient's skin or tongue has reached a level sufficient for a diagnosis.

5.2 Methods and Results

We propose an accurate color examination approach for a telemedicine system using a color chart designed by medical doctors. The color chart can be used by following two strategies for a color examination of the patient.

1) In the first strategy, the color chart is placed next to the face of the patient, and the face and color chart are captured in the same image. The medical doctor is asked to view the difference in the color chart between the patient and doctor sides. Based on this difference, the medical doctor is expected to be able to examine the color of the patient appropriately.

2) In the second strategy, the color chart is also placed next to the face, and the face and color chart are captured in the same image. The software calculates the difference in the color chart between the patient's side and the doctor's side. The software can correct the color on the patient's side for presentation on the doctor's side by using a color transformation function. After the color transformation is obtained, it is no longer necessary to present the color chart using the same color transformation functions.

This study was conducted with the approval of the Ethics Committee of Kanazawa University School of Medicine.

5.2.1 Creation of color chart including skin and tongue colors

Skin color and tongue color are different for individual. Therefore, in selecting the skin and tongue color four Kampo doctors discussed and extracted representative colors that were considered to be effective for color judgment from the tongue image and the skin image. The difference in color between individuals is can be considered to be the deviation from this representative color, and this difference in color between individuals can be examined by the eyes of a doctor.

The proposed chart is designed to be used only for the yellow race. Since the color of the tongue is the color of the mucous membrane, it is generally said that it is not related to the race for the tongue color. However, since we have not examined this relation deeply, we need to ask the user to the color chart only for patient of yellow race.

The proposed design is shown in **Fig. 5-1.** The color chart is the size of a business card for easy handling. Because the medical doctor is asked to see the difference in the color chart between the patient's side and the doctor's side, color patches are used to make it easier to accomplish.

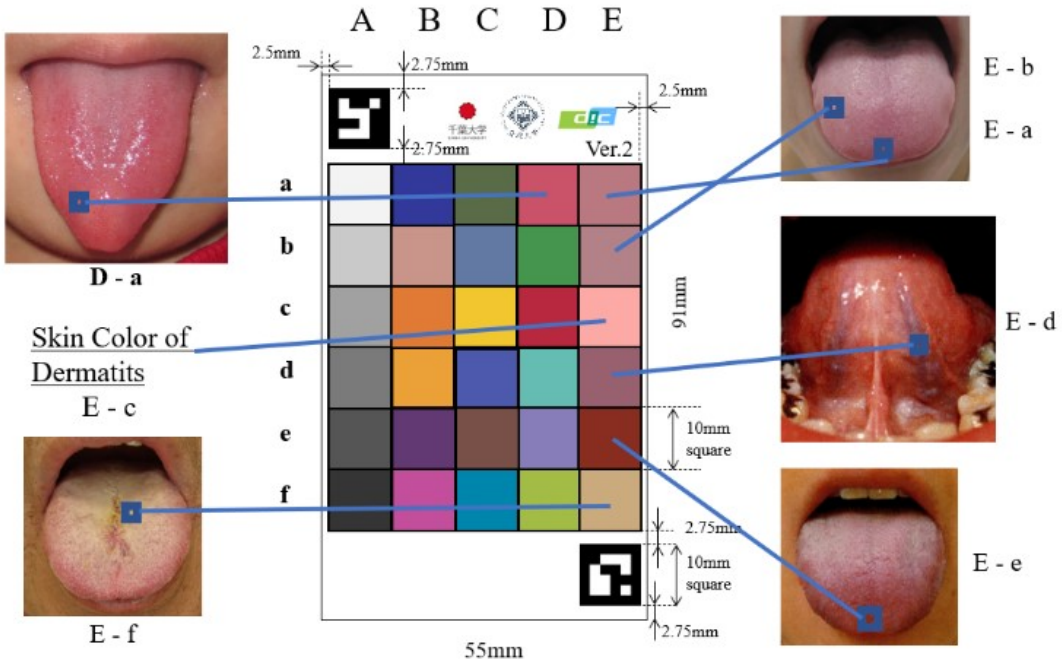

Fig. 5-1. Proposed color chart arrangement and selection of seven important colors.

Table 5-1. L* a* b* color values for the proposed color chart.

	A	B	C	D	E
	L*, a*, b*	L*, a*, b*	L*, a*, b*	L*, a*, b*	L*, a*, b*
a	97, 0, 0	28, 24, -55	43, -12, 18	52, 50, 13	58,27,7
b	87, 0, 0	67, 20, 14	51, 0, -25	56, -37, 30	60, 20, 5
c	76, 0, 0	62, 38, 55	82, 6, 74	42, 57, 24	78, 30, 15
d	64, 0, 0	72, 22, 62	40, 14, -47	70, -30, -4	48, 25, 2
e	51, 0, 0	30, 27, -26	38, 17, 12	55, 14, -30	33, 40, 30
f	36, 0, 0	50, 54, -18	51, -21, -30	73, -22, 54	72, 8,22

The L*a*b* color value is calculated by using white reference plate under D50 light source.

A grayscale is arranged in 6 steps on the left side to judge lightness and contrast, and 17 colors are arranged in the middle to see the general color change. Seven types of skin and tongue color, which are important for examination, are placed on the right side. These colors are based on the colors of the skin and tongue, which have been judged to be important by a Kampo practitioner. The L*a*b values of the colors are shown Table 5-1. Because the color changes depending on the printing conditions, the version number is given. The medical doctor and patient should use color charts of the same version. In addition,

considering an automatic color discrimination, we also placed two markers diagonally across the corner. To handle the color chart correctly, we placed a logo on the upper part and provided a blank part on the lower left. The print data were created using Adobe Illustrator and printed on a dedicated matte paper using an industrial inkjet printer.

The color quality of the products was confirmed using a colorimeter.

5.2.2 Telemedicine using only a color chart

With the cooperation of eight doctors of Kampo medicine from Kanazawa University Hospital, we examined whether the color examination of the patient's skin or tongue reaches a level that can be applied for diagnosis.

The outline of the experiment is shown in **Fig. 5-2**. First, the patient uses a smartphone to take a photograph of both the patient and the color chart in a single image, and sends the photograph to the doctor through email or SNS. The doctor compares the actual color chart on the doctor's side with the color chart in the photograph sent by the patient to determine the color change.

The doctor compares the actual color chart on the doctor's side with the color chart in the photograph sent by the patient to determine the color change.

The paper used for the chart is 243 micrometers thickness for jet ink that does not bend under normal use. Matte paper was used for this color chart. Even if the matt paper due to the positional relationship between the light source and the camera, the captured chart may be suffered by the specular component that reduces the color reproducibility. Therefore, it is necessary to ask the user of color chart to prevent the setting of light source and color chart where the specular component is appeared on the paper. We need to confirm this situation to medical doctors and patients.

For doctors who are unfamiliar with conducting a color comparison, we also prepared a specific procedural manual. The contents of the manual are as follows.

1) Gray scale: Observe the transition from black to white on the left side of the chart to note the contrast in the image. Observe the brightness level and color balance to determine the lighting environment and the characteristics of the camera.

2) Consider the difference in the appearance of the color of blood by comparing the multiple red patches and observing their strengths and weaknesses.

3) Compare patches of healthy tongue and check for shades of color.

4) Compare the blue patches and check the intensity of the color. The difference between red and blue can then be seen.

5) Use a patch of tongue color to determine the patient's condition more accurately.

6) Identify any inflammation using a provided patch showing the color of skin with dermatitis.

In this section, doctors were asked to evaluate patients using their own different smartphones, computers, different lighting environments, and different applications. In this environment, medical doctors evaluated whether they could make judgments about tongue and skin color by visually referring to color patches without automatic correction.

The evaluation results of the eight doctors are shown in Table 5-2.

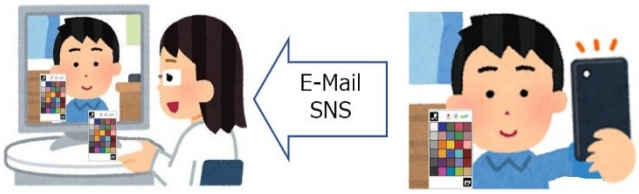

Fig. 5- 2. Usability survey by comparing color charts.

Table 5-2. Evaluation results by eight medical doctors for the proposed color chart

No.	Comments
1	I think it is very good to have a color checker because I can make corrections depending on the model and lighting. Because it is difficult to judge a moving image, it seems good to receive multiple still images to make such a judgment.
2	Once I got used to it, I was able to use it.
3	I felt that the color chart leads to an objective diagnosis.
4	I found it difficult to tell if there was a shadow or not unless the light came from the front of the tongue. If possible, images taken from three directions, the frontal, first oblique, and second oblique, would provide a more reliable diagnosis. But it would be complicated.
5	For the tongue color, if you are unfamiliar to you, there may be subjective impression of the color, so I think the proposal is good.
6	It seems to be useful for telemedicine. I hope to the patients and doctors will get used to it.
7	Until now, I was unable to understand what I was looking at, but I felt the potential of the chart.
8	Skin diseases can be diagnosed accurately by the simultaneous color checker and imaging of the affected area before and after treatment and over time.

The opinions of doctors with color knowledge evaluated the system highly, whereas doctors with little color knowledge found it useful after we explained to how it should be used. There were no negative opinions, and it was determined that the examination could be conducted better than without the color chart.

From the above results, it was found that “color correction using color charts to asked medical doctor to see the difference of the color chart between patient side and doctor side” is effective in emergency

situations, but for many doctors to use it, knowledge of color reproduction and experience in telemedicine are required.

5.2.3 Automatic color correction using color chart

Automatic color correction is required for an easier diagnosis. We therefore propose reproducing the color using a color chart. **Figure 5-3** shows color differences in images taken using commercially available smartphones under different devices and illuminations. We can see visually that the colors are different in each image. The medical doctors stated that the color differences in these images tended to give improper results for the examination.

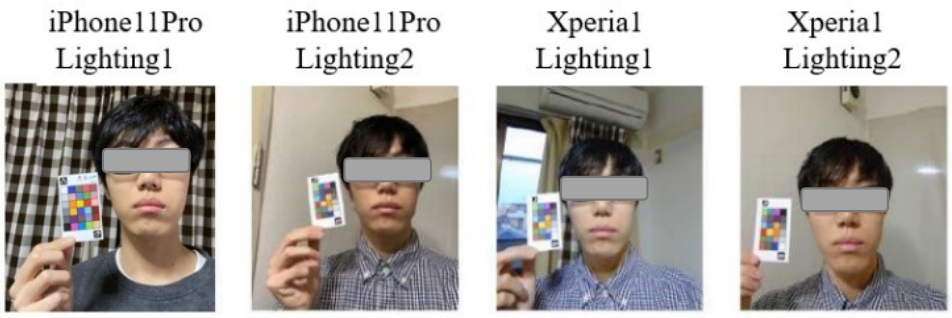

Fig. 5- 3. Selfies photo under diverse conditions.

Automatic color correction using a color chart is performed in two steps, as shown in **Fig. 5-4.**

By matching the colors of every patch on the color chart, the image taken will be displayed correctly on the doctor's monitor. The first step (offline) is to adjust every color patch (using RGB data) displayed on the monitor to match the color patch on the real color chart. The second step (online) is to adjust the RGB data of every color patch captured by the camera to match the reference RGB data.

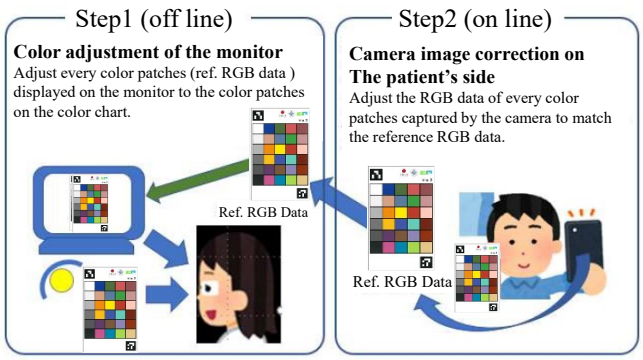

Fig. 5- 4. Overview of automatic color correction method

Matte paper was used. In this case, depending on the positional relationship between the light source and the camera, the glossiness that deteriorates the color reproducibility may be appeared on the captured chart.

Therefore, it is necessary to ask the user of color chart to prevent the setting of light source and color chart where the specular component is appeared on the paper. We need to confirm this situation for medical doctors and patients.

5.2.3.1 Display color reproduction

The colors on the color chart that the doctor sees depend on the light source in the room. This is because the spectral distribution of the light that illuminates the color chart depends on this light source. Therefore, when the light source is different, the color when observing the color chart differs. In addition, the performance of the display varies depending on the model, and the same color cannot be output even if the same RGB is input. Thus, the correction starts by adjusting the color development of the monitor using the color of the color chart observed by the doctor as the correct value.

Because people recognize color by the three stimulus values *XYZ*, the *XYZ* values of each color patch on the color chart, which are the correct values, were measured using a colorimeter under the same lighting environment as the doctor. The monitor side correction was performed with reference to [67].

The relationship between the luminance and input level is

$$\begin{aligned} L'_R &= a_0R^2 + a_1R + a_2 \\ L'_G &= b_0G^2 + b_1G + b_2 \\ L'_B &= c_0B^2 + c_1B + c_2 \end{aligned} \tag{5-1}$$

where L'_R, L'_G, L'_B are the luminance of *R, G, B* respectively, and a_i, b_i, c_i (i = 0–2) are the coefficients. The tristimulus values *X, Y, Z* on the display can be decomposed to *R, G, B* as shown in the following equation:

$$\begin{pmatrix} X' \\ Y' \\ Z' \end{pmatrix} = \begin{pmatrix} X'_R + X'_G + X'_B \\ Y'_R + Y'_G + Y'_B \\ Z'_R + Z'_G + Z'_B \end{pmatrix}, \tag{5-2}$$

where, X'_i, Y'_i, Z'_i (i = *R, G,* B) are tristimulus values for red, green, and blue luminescence, respectively. The tristimulus values corresponding to each luminescence can be calculated from *L, x, y* when the monitor is measured. The relationship between *X*-*Y* and *Y*-*Z* of each emission can be expressed through the following linear equation:

$$
\begin{aligned}
X'_R &= a_R Y'_R + b_R \\
X'_G &= a_G Y'_G + b_G \\
X'_B &= a_B Y'_B + b_B \\
Z'_R &= c_R Y'_R + d_R \\
Z'_G &= c_G Y'_G + d_G \\
Z'_B &= c_B Y'_B + d_B,
\end{aligned}
\tag{5-3}
$$

where a_i, b_i, c_i, and d_i (i = *R, G, B*) are the coefficients.

Equation (5-4) is obtained from Equations (5-2) and (5-3).

$$
\begin{aligned}
\begin{pmatrix} X' \\ Y' \\ Z' \end{pmatrix} &= \begin{pmatrix} a_R Y'_R + a_G Y'_G + a_B Y'_B + b_R + b_G + b_B \\ Y'_R + Y'_G + Y'_B \\ c_R Y'_R + c_G Y'_G + c_B Y'_B + d_R + d_G + d_B \end{pmatrix} \\
&= \boldsymbol{A} \begin{pmatrix} Y'_R \\ Y'_G \\ Y'_B \end{pmatrix} + \begin{pmatrix} b_R + b_G + b_B \\ 0 \\ d_R + d_G + d_B \end{pmatrix} \\
\boldsymbol{A} &= \begin{pmatrix} a_R & a_G & a_B \\ 1.0 & 1.0 & 1.0 \\ c_R & c_G & c_B \end{pmatrix}
\end{aligned}
\tag{5-4}
$$

From Equation (5-4), the luminance of each RGB can be calculated using Equation (5-5) when the three stimulus values *X'Y'Z'* are to be displayed on the monitor.

$$
\begin{pmatrix} L'_R \\ L'_G \\ L'_B \end{pmatrix} = \begin{pmatrix} Y'_R \\ Y'_G \\ Y'_B \end{pmatrix} = \boldsymbol{A^{-1}} \begin{pmatrix} X' - b_R - b_G - b_B \\ Y' \\ Z' - d_R - d_G - d_B \end{pmatrix}
\tag{5-5}
$$

According to Equation (5-5), *R, G, B* can be calculated by applying the luminance obtained through Equation (5-2). This allows the doctor to correct the display.

We will explain the color adjustment of the monitor on the doctor side based on the calculation formula.

First, we measure the performance of doctor's monitor. We change input RGB values by increasing the value of the input value *R* from 0 to 255 by 8 with keeping the *G* and *B* values to be 0, and measure the brightness on the monitor for each color. We execute the same operation about G, B channels. Since the relationship between the *RGB* input value and the luminance *L* is shown in Equation (5-1), the parameters of Equation (5-1) are obtained by multiple regression analysis based on the measured data. The next step is to obtain the *RGB* values to input the monitor where the *XYZ* values measured by real color patch can be

displayed. By inputting the *X'Y'Z'* values into Equation (5-5), the monitor emission brightness, the *RGB* values required for input can be obtained as follows. To determine the *RGB* value required for input, we input the *X'Y'Z'* values in Equation (5-5), and obtain monitor emission brightness. The obtained monitor emission brightness is input into the inverse function of Equation (5-1), then the *RGB* input values are calculated when the *X'Y'Z'* values of the color chart are displayed on the doctor's monitor in the doctor's environment.

5.2.3.2 Image color correction on the patient's side.

Because the *RGB* values (standard *RGB* values) of each patch of the color chart projected on the doctor's monitor are calculated, the color can be reproduced by converting each *RGB* value taken at the patient's side into a standard *RGB* value. For this purpose, we describe the correction of images taken at the patient's side.

The conversion formula is obtained by examining the correlation between the *RGB* value corresponding to each patch of the color chart displayed on the doctor's display (reference *RGB*) with the *RGB* value corresponding to each patch of the color chart taken on the patient's display.

Specifically, a gamma correction is applied using the grayscale portion of the color chart and the grayscale portion of the reference *RGB*. The *RGB* values are then corrected using all colors in the color chart.

First, we extract the color chart part of the photograph using AR markers. The portions of each square are further taken and averaged. The model is created through a multiple regression from the difference between the averaged numbers and the reference *RGB* values. Based on this, all pixels are converted to correct the color of the human face and tongue.

The details of the gamma correction are next described. First, such correction is applied based on the luminance of the grayscale portion of the color chart measured by a colorimeter against the *RGB* value when the grayscale was photographed. Similarly, this is also conducted for the grayscale portion of the reference *RGB* value. Next, a gamma correction is applied for each *RGB*. In the case of *R*, the form is as shown in Equation (5-6).

$$R_c = aY^{\gamma} + b, \tag{5-6}$$

where *Rc* is the *R*-value of the image taken, and *Y* is the luminance of the color chart's grayscale. In the grayscale of the color chart, the brightness of the grayscale is transformed to within the range of zero to 1 by normalizing with the brightness value of white such that black has a value zero and white has a value of 1. This model can be used to correct the gamma for any *RGB* value. Specifically, we compute the gamma-corrected *RGB* values by multiplying the inverse function of Equation (5-6) for each value.

Next, we construct a model using multiple regression on the color of each gamma-corrected color patch. In the case of *R*, we have Equation (5-7).

$$R'_c = aR_r + bG_r + cB_r + d, \tag{5-7}$$

where *R'c* is the *R* value of the corrected image and *Rr, Gr, Br* indicate an un-corrected *RGB* value. Each parameter is calculated by a multiple regression with every color patch.

Finally, the color correction is completed by performing a transformation on each pixel of the captured image. The above program was created in Python.

As a result, we were able to return the image to its original equivalent. The original and corrected images are shown in **Fig. 5-5**.

One medical doctor compared the correct image with the corrected image, and rated the resulting color correction as reliable.

The automatic color correction results of the seven important colors are shown in Table 5-3. The evaluation image is “iPhone 11 Pro Lighting 1” at the far left of **Fig. 5-3**. For the color comparison, we used seven important patches, one color for skin color of dermatitis and six different tongue colors. The comparison about *L*a*b** value was performed with images that were converted according to the correct values of the color chart of the paper under the doctor's illumination and the paper under the doctor's illumination. The light colors showed good matching, the dark colors had a difference of Δ5 or more, which is a problem when visually observed.

Next, we will explain the comparison method for automatic correction of the proposed color chart and a typical color chart. Our proposed method used all 30 patches on the color chart for automatic correction. A typical color chart does not have tongue color. Therefore, to compare the effectiveness of automatic correction with the case of using a general color chart, we compared with or without the tongue colors. Comparative experiments were conducted using all 30 colors of the proposed color chart and 24 colors excluding six tongue colors of the proposed color chart.

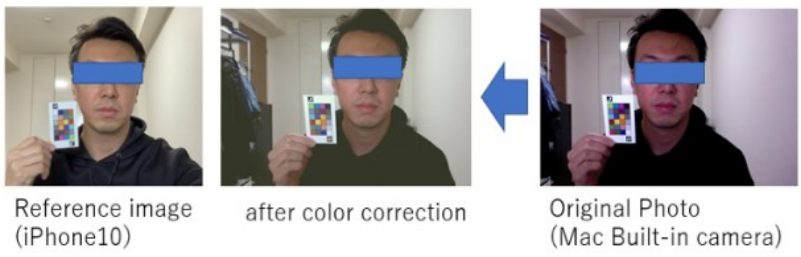

Fig. 5- 5. Automatic color correction result.

The results are shown in Table 5-3. It has been shown that the proposed method produces a better correction due to the number of patches exceeding Δ5 was smaller. From the above, the proposed color chart including tongue colors worked well with automatic color correction.

Table 5-3. Error for seven important colors in Fig. 5.1.

	*L*a*b** error (*ΔE*)	
Patch Number	Proposed method Using all 30 colors	Using general 24 colors (excluding tongue colors)
E – a (Tongue, fur)	3.4	10.0
E – b (Tongue)	0.8	4.3
E – c (Skin, dermatitis)	0.8	2.0
E – d (Tongue)	11.1	9.0
E – e (Tongue)	17.3	13.4
E – f (Tongue, fur)	1.4	3.3
D – a (Tongue)	1.2	7.1

5.3 Conclusions and Future work

The results of this study show that the use of color charts that incorporate the color of the human skin can help doctors recognize the color of patient's skin more accurately when applying telemedicine.

In this study, we created a color chart for a color reproduction that is easy to use with COVID-19, and confirmed that it is possible to reproduce the facial and tongue colors of the patient accurately. We also found that the captured image can be reproduced automatically using a color chart. If a color reproduction can be achieved easily and automatically, it can be used by numerous members of the medical staff. This study was conducted as part of an emergency response to the spread of COVID-19. Therefore, only a few cases were considered, and there remains room for improvement in the proposed automated color correction method.

In the future, we plan to improve the colors applied and the layout of the color chart for color correction (which relies on human perception) based on the opinions of numerous medical personnel. For the color used, it may be possible to select a color corresponding to the clinical department, such as dentistry, or in consideration of the differences in the color of natural skin. We also plan to proceed with an automatic color correction method that can easily handle changes in the lighting environment and display devices, in addition to its application to moving images.

Chapter 6: Development of telemedicine tools with an emphasis on visual observation

This chapter describes the results of the evaluation of the telemedicine tool implemented in iOS, based on the results of the telemedicine tool development conducted in the previous chapter. The telemedicine tools include features such as patient color reproduction and non-contact vitals measurement of the patient. Non-contact vital measurements have the potential to be deployed for detecting others' emotions and sensory evaluation in mobile work.

6.1 Introduction

The demand for telemedicine services is increasing, and their value in the global market is expected to expand from US$ 2.68 billion in 2016 to US$ 22.71 billion in 2025 [68]. Telemedicine services include online medical care and doctor-to-doctor communication, specialist advice to doctors, home monitoring of chronic diseases, and physical therapy guidance. With the spread of Covid-19, infection control in healthcare is also an essential factor. To prevent the spread of infections, face-to-face encounters between patients in medical facilities and between clinicians and patients need to be alleviated. Telemedicine is used because it helps avoid face-to-face encounters [69], [70], [71]. Smartphones are used to monitor human health to detect biometric information such as heart rate, respiration rate, sleep patterns, and activity levels. However, a few of these health apps are reported to lack sufficient quality [72]. Meanwhile, smartphones are used for telemedicine in ophthalmology and otorhinolaryngology [73], [74].

The development of video communication systems has been remarkable, and they are being used for conferences, classes, and academic conferences. However, color management in videoconferencing systems emphasizes the reproduction of preferable colors, which leads to incorrect judgements regarding the color of a person's skin or tongue in telemedicine. The importance of color reproduction in medical care has already been highlighted [64].

In Japan, the spread of Covid-19 has led to a rapid increase in the need for telemedicine from the perspective of infection prevention, and the Japanese government has implemented measures to promote online medical care, such as revising medical fees and allowing utilization from the first visit [75]. The revised “Guidelines for the Appropriate Implementation of Online Medical Treatment” issued by the Ministry of Health, Labor and Welfare in Japan in July 2019 [76] also states that, “…before implementing online medical care, it is desirable to actually conduct tests using information and communication devices to confirm the color and operability of images obtained through the devices”. However, no specific color management method has been proposed thus far. The following processes need to be managed for accurate color reproduction: image input, processing, transmission, and image output. The input section needs to consider the characteristics of the ambient light, lighting, and camera; the processing and transmission

section needs to correct color and prevent degradation; and the output section needs to adjust for the luminous characteristics of the monitor and ambient light. Such color management techniques require specialized knowledge and corrective equipment to be performed accurately. Therefore, doctors who practice vision-oriented medicine have been demanding simple and accurate color reproduction systems. In particular, Kampo doctors need to observe the color of a patient's face and tongue.

Kampo doctors use all five senses in their practice. The five senses are categorized as follows: “inspection” by sight, “listening and smelling examination” by hearing and smell, “inquiry” by listening to the patient's condition and subjective symptoms, and “palpation” by touching the patient. In “inspection,” the doctor observes the patient's movements, skin color, and tongue signs [77]. We have been developing a telemedicine system using color charts and RGB cameras to address the needs of Kampo doctors who emphasize visual observation [78].

This report describes the implementation of the system on ISO devices such as iPhone and iPad, and the verification results for practical application.

6.2 Methods and Results

This section provides an overview of the developed telemedicine system, improvement of the color chart, evaluation of the automatic color correction module using the color chart, and evaluation of the pulse wave measurement module.

6.2.1 Overview of Telemedicine Tools

Figure 6-1 shows an overview of the developed telemedicine tool. The system has two main functions: color correction to correctly grasp the color of the face and tongue; and pulse wave measurement, which is necessary for auscultation. The system also helps import images of questionnaires written by patients. These functions were selected based on the requests of Kampo doctors. The color chart is used for color correction; the patient uses an iOS device such as an iPhone or iPad, and the doctor uses a personal computer. The color correction function was based on the method we proposed in a previous paper [78]. The pulse wave is obtained from the hemoglobin value, by signal processing the video captured by the RGB camera [45], [79].

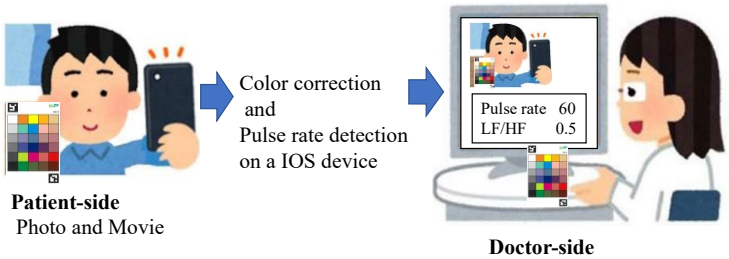

Fig. 6-1. Overview of telemedicine Systems.

Figure 6-2 shows the screen of the patient's iPad in Japanese. The initial screen shows the items to be executed by the patient. The upper left side of the screen is the face image; the center is the tongue image; and the right side is the logbook image. The lower left side of the screen shows the vital information obtained from the video. The patient performs four types of input operations. The patient executes the input operations in sequence, and the input information will be displayed. Vital information is shown as

a) Screenshot of the initial menu screen

b) Screenshot of all acquired data

Fig. 6-2. Screenshot of the telemedicine system using an iPad on the patient's side.

numerical values analyzed from the video. When the patient finishes all the input operations, the doctor will send the information via SNS. Currently, the information is sent via SNS called LINE. A series of operations are executed daily, and the data are accumulated sequentially. Next, we explain the system on sent from the patient through the SNS on the PC screen. The accumulated data can be used to observe the

Fig. 6-3. Screenshot of the telemedicine system using a Windows PC on the doctor's side.

patients over time. The system is currently designed in Japanese; however, for explanation. When the doctor selects the list in the upper row on the PC screen, the patient's information is displayed. The bottom-right corner of the screen allows the doctor to add comments. The patient's image displayed on the screen is automatically color-corrected. Clicking on a patient's image increases the size of the image.

6.2.2 Color chart improvements

Improved color chart for the Ver.3 is shown in **Fig.6-4**. The color chart is a modified version of Ver.2, which was used in a previous study [78], and modified based on feedback from doctors to improve ease of use. The specifications are the same as in Ver.2, and the chart was printed on matte paper using an industrial inkjet printer. The improvements were only in the arrangement of color patches. The color-related data of the color charts are listed in Table 6-1.

The color chart was improved through trial and error by consulting with Kampo doctors. We finally concluded that it would be better to arrange similar colors together, which led to the color chart Ver.3. In the revision process, we gathered similar colors, respecting the doctors' opinion that it would be easier to use if similar colors were placed side by side.

The color chart was established for use in the Asian race and needs to be improved for application to the global population. However, the tongue color is of a mucous membrane, it can be adaptable to all humans.

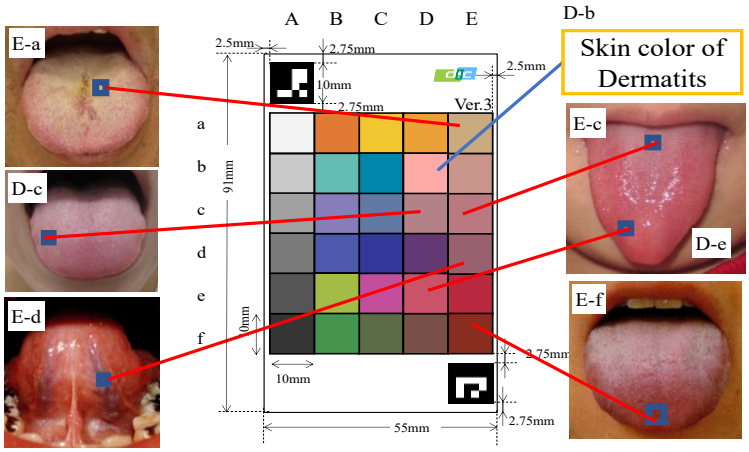

Fig. 6-4. Proposed color chart Ver.3 arrangement and selection of seven important colors.

Table 6-1. *L*a*b** color values for the proposed color chart Ver.3

	A	B	C	D	E
	L,a*,b**	*L*,a*,b**	*L*,a*,b**	*L*,a*,b**	*L*,a*,b**
a	97, 0, 0	62, 38, 55	82, 6, 74	72, 22, 62	72, 8,22
b	87, 0, 0	70, -30, -4	51, -21, -30	78, 30, 15	67, 20, 14
c	76, 0, 0	55, 14, -30	51, 0, -25	60, 20, 5	58,27,7
d	64, 0, 0	40, 14, -47	28, 24, -55	30, 27, -26	48, 25, 2
e	51, 0, 0	73, -22, 54	50, 54, -18	52, 50, 13	42, 57, 24
f	36, 0, 0	56, -37, 30	43, -12, 18	38, 17, 12	33, 40, 30

The L*a*b* color value is calculated by using white reference plate under D50 light source.

6.2.2.1 Evaluate the usability of the color chart

To evaluate whether the color charts were easier to see, we interviewed three Chinese medicine doctors and presented them with Ver.2 and Ver.3. **Fig. 6-5** shows the color chart presented for the evaluation. Three of the subjects used color chart Ver.2. The results showed that all three doctors agreed that the improved Ver.3 color chart was easier to read than the Ver.2 color chart. Two comments were included on the color chart, which have been listed in Table 6-2.

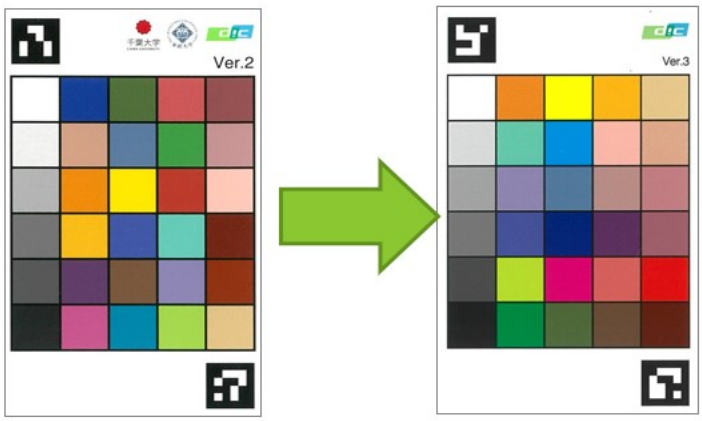

a) Ver.2 Previous version b) Ver.3 Improved version

Fig. 6-5. Comparison of the color chart before and after the improvement.

Table 6-2. Evaluation of the easier to see improved color chart

No	Comments
1	The colors are close to actual living organisms, making it easier to compare and contrast.
2	The patches are arranged in a similar color gradient, which makes it easier to compare them.

6.2.3 Accuracy evaluation of the automatic color correction module using the color chart

6.2.3.1 Automatic color correction using the color chart

Automatic color correction using a color chart was performed in two steps, as shown in **Fig. 6-6**. By matching the colors of every patch on the color chart, the image taken will be displayed correctly on the doctor's monitor. The first step (offline) is to adjust every color patch (using RGB data) displayed on the monitor to match the color patch on the actual color chart. The second step (online) is to adjust the RGB data of every color patch captured by the camera to match the reference RGB data.

6.2.3.2 Accuracy evaluation of the automatic color correction module

Automatic correction was verified in the second step (online) part of **Fig. 6-6**. The correct value of the color chart data was measured with a color difference meter (Konica Minolta CS-150) under a D50 light source, referring to the lighting environment of the doctor's office. For evaluation, ten types of color chart images were taken, using two smartphones (iPhone 8 and iPhone 12), each at five indoor locations.

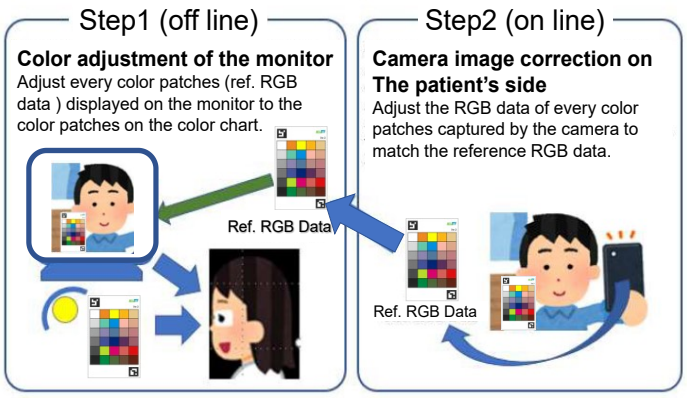

Fig. 6- 6. Overview of automatic color correction method

We used our software written in Python to compare the auto-corrected color patches with the correct values. **Figure 6-7** shows the contents of the software procedure. The software extracted part of the color chart from the corrected image, using AR markers as a guide and obtained data for seven patches. Each of the seven patches was averaged and converted to *L*a*b** values using OpenCV's cvtColor. The obtained data were used as test data.

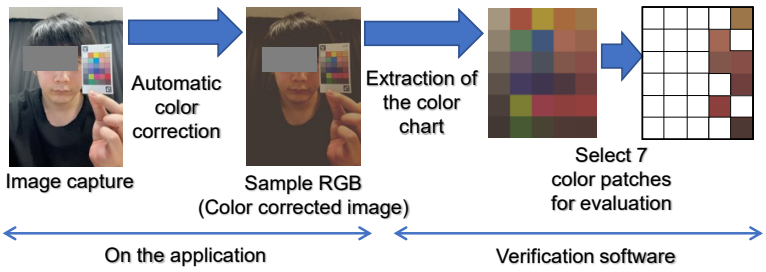

Fig. 6-7. Procedure for extracting the seven color patches for comparison.

The corrected values and test data were compared using Equation (6-1), and the color difference ΔE in the $L^*a^*b^*$ space.

$$\Delta E = \sqrt{(L_1^* - L_2^*)^2 + (a_1^* - a_2^*)^2 + (b_1^* - b_2^*)^2} \qquad (6-1)$$

where $L_1^*\ a_1^*\ b_1^*$ is the reference RGB data, and $L_2^*\ a_2^*\ b_2^*$ is the test data value.

Table 6-3 summarizes the experimental results of automatic color correction. The data before the correction showed a significant color difference, whereas the data after correction showed that ΔE was within 8.0.

When ΔE was less than 5.0, the data could be considered identical, but two patches had a ΔE greater than 5.0. These patches were darker in color.

Table 6-3. Comparison of color difference before and after color correction

	Average ΔE	
Patch number	Original	Correction
E-a Tongue	44.5	4.9
D-d Tongue	35.4	3.2
E-d Tongue	23.7	5.5
E-c Tongue	30.9	4.3
E-e Tongue	29.2	3.0
E-e Tongue	24.8	7.5
D-b Skin	42.8	3.8

Table 6-4 summarizes the data after automatic color correction, including the maximum error value, to examine its practical use. Even in the data where the average value of ΔE was below 5.0, some cases with a maximum value of ΔE exceeding 5.0 were observed.

Table 6-4. Correction results including the maximum error value of ΔE

Patch number	ΔE			
	Average	Min	Max	SD
E-a Tongue	4.9	1.7	13.2	3.3
D-d Tongue	3.2	1.0	7.0	2.0
E-d Tongue	5.5	1.0	9.5	2.7
E-c Tongue	4.3	1.4	10.2	2.6
E-e Tongue	3.0	1.0	5.9	1.5
E-e Tongue	7.5	5.1	11.5	1.9
D-b Skin	3.8	2.4	9.4	2.0

6.2.4 Accuracy evaluation of the pulse wave measurement module.

Several methods for pulse wave acquisition using RGB cameras have been proposed. Green (G) signals have been reported to result in an extremely high AC/DC ratio of the PPG waveform [80], [81]. Accordingly, an accuracy evaluation was performed by comparing the implemented hemoglobin signal with the G signal.

6.2.4.1 Pulse Wave Measurement Method

The method we implemented is based on Tsumura et al.'s method [45], [79], which converts RGB signals into three signals (hemoglobin, melanin, and shading) and utilizes the changes in the hemoglobin signal to acquire a stable pulse wave without the influence of luminance changes. In this method, the shading

components are separated, resulting in higher accuracy than methods that are affected by motion and light sources.

6.2.4.2 Acquisition of RGB signals

The pulse wave signal is detected by capturing the change in the weak signal from the living body. In the iOS normal video recording mode, weak signals are challenging to capture because of the automatic correction and compression of the video. The implemented software directly controls the camera system to acquire uncompressed RGB signals

6.2.4.3 Acquisition of vital information from the RGB Signals

Figure 6-8 shows a method for obtaining vital information from a video image. First, the region of interest (ROI) that is applicable for pulse wave detection is selected from the total pixels and separated into temporal images. Then, each image is separated into hemoglobin, melanin, and shadow component images using independent component analysis. The average value of the pixel values was calculated from the separated hemoglobin component pixels. Because the change in hemoglobin quantity is correlated with the pulse wave, the pulse wave can be calculated from the time variation of the mean hemoglobin value. To obtain a pulse wave signal with high accuracy, a band-pass filter was used. A pulse wave peak was detected from the obtained signal. The pulse rate was calculated from the average value of the R-R interval.

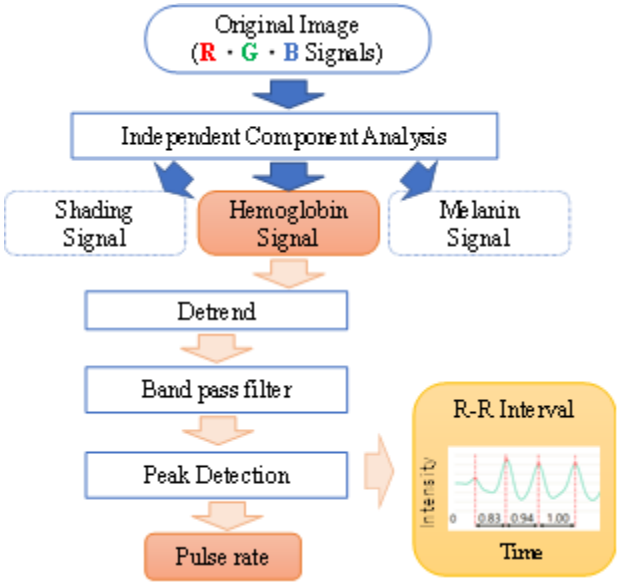

Fig. 6-8. Overview of Signal Detection Algorithm.

6.2.4.4 Separation of hemoglobin components

An overview of the hemoglobin component separation is shown in **Fig. 6-9**. Independent component analysis (ICA) is a method for finding hidden factors and components in multidimensional data. The difference between ICA and other methods is that the components to be searched are statistically independent and non-Gaussian [82]. Assuming that t is the time and the RGB signal (observed value) is generated by a linear mixture of hemoglobin, melanin, and shade components, which are independent of each other, the signal can be expressed as in Equation (6-2).

$$\begin{pmatrix} R(t) \\ G(t) \\ B(t) \end{pmatrix} = \mathbf{A} \begin{pmatrix} H(t) \\ M(t) \\ S(t) \end{pmatrix} \qquad (6-2)$$

where $R(t)$, $G(t)$, and $B(t)$ are the RGB signals, and $H(t)$, $M(t)$, and S(t) are the hemoglobin, melanin, and shade signals, respectively. Once transformation matrix **A** can be calculated, the signals can be separated. For the RGB signals, a logarithm was used. Since the three separated components are orthonormal, the hemoglobin component is separated from the shadow component, and it is robust to illumination variations. In addition, the melanin component does not change in the range of measurement time; therefore, the variation in hemoglobin can be extracted.

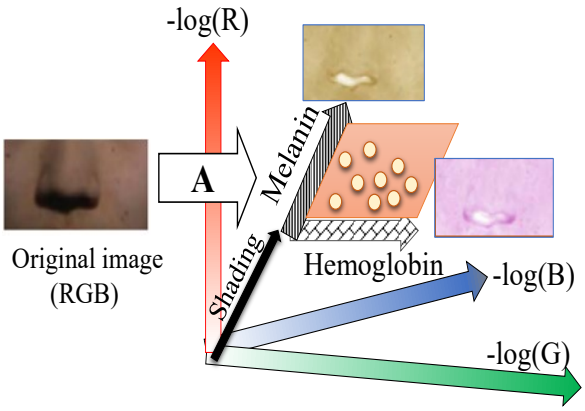

Fig. 6-9. Overview of the separation of hemoglobin components using ICA.

The pulse wave signal is detected by capturing the change in the weak signal from the living body. In the iOS normal video recording mode, weak signals are challenging to capture because of the automatic correction and compression of the video. The implemented software directly controls the camera system to acquire uncompressed RGB signals. In addition, the power spectrum was calculated from the time variation

of the R-R interval, and the LF/HF ratio of the high-frequency component (HF 0.15-4 Hz) and the low-frequency component (LF 0.05-0.15 Hz) was calculated for use in emotion detection. The LF/HF data were not used for the validation of the evaluation because the data are currently undergoing improvements to improve the accuracy.

6.2.4.5 Verification of the accuracy of the pulse waveform data

The iPhone 8 was used as a video recording device for accuracy verification. Because the developed application can obtain both RGB signals and hemoglobin signals calculated from the RGB signals in the CSV format, we used these two signals as the dataset for comparison. We used two types of shooting environments: a stationary state under LED illumination without flicker, and the other was a moving state under 3-wavelength fluorescent light, a typical shooting environment. The video was taken without a chin rest and with a smartphone fixed in place.

The accuracy verification results are shown in **Fig. 6-10**. The plotted signal was obtained before denoising. The hemoglobin intensity was plotted as the reciprocal of the G signal because the absorption of the G signal increases when the hemoglobin content is high. Both signals were normalized.

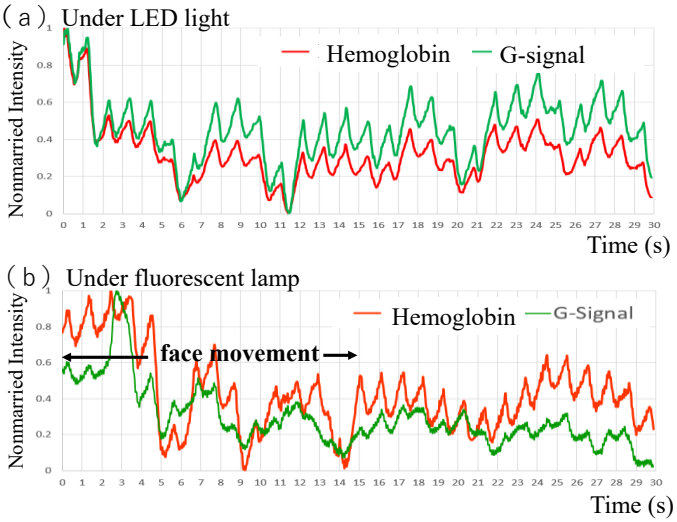

Fig. 6- 10. Verification results of pulse wave extraction accuracy. (a) Under LED light (b) Under fluorescent lamp.

Figure 6-10 b is the signal obtained from a movie taken in a fluorescent light environment. During the first 15 s of the measurement, the face was slowly moved up and down, left and right. In the next 15 s, the face was kept still.

Under LED illumination and stationary conditions, the hemoglobin and G signals were almost the same. However, under fluorescent illumination and motion, the hemoglobin waveform was more robust to motion than the G signal, as can be observed from the waveform.

6.2.5 Verifying the Accuracy of Pulse Rate Detection

The experiments were conducted in conjunction with a clinical trial to verify the accuracy of pulse rate detection at Kanazawa University to investigate the effects of needle treatment. [Medical Ethics Committee of Kanazawa University (2018-154)].

The experiment was conducted in the Kampo consultation room of Shinseikai Toyama Hospital, and the subjects were 39 nurses who gave their consent. Measurements were taken before and after needle treatment. We conducted two types of lighting, one with a fluorescent lamp and the other with an LED lamp, and the measurement time for each was 30 s. The setup of the system was the same as that used in the preliminary experiment conducted at the Chiba University campus (**Fig. 6-11**). A VILTROX L116T RA CRI 95+ Super Slim LED Light Panel was used as the LED light, and the color temperature was set to 5600 K. The fluorescent light was a 3-wavelength fluorescent light for room lighting in the examination room. The frame rate of the iPhone XR was set to 60 fps.

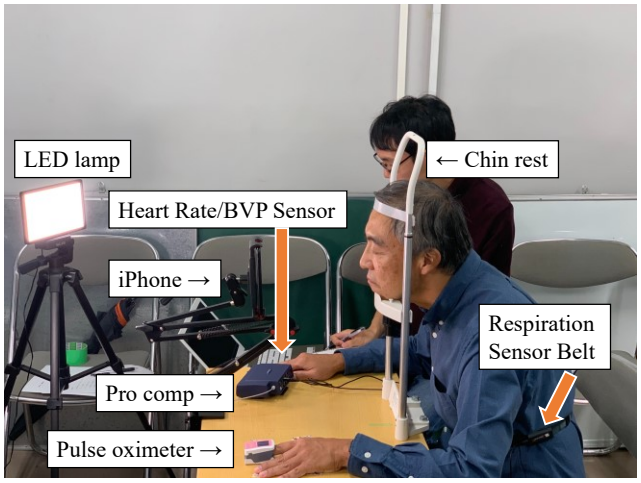

Fig. 6-11. Setting for preliminary experiments.

The correct values were obtained using the ProComp system (Thought Technology, Canada). ProComp was controlled by a laptop computer running Windows 10 with ProComp-specific software to capture the data. The pulse rate measurement device connected to ProComp was a fingertip photoplethysmograph (PPG) sensor (Thought Technology Heart Rate/BVP Sensor) using infrared rays, and data sampling was performed at 2048 Hz. The pulse rate was calculated from the pulse wave signal obtained, using a program written in Python.

We also used a two-wavelength blood absorption pulse oximeter (PO) (Pulsfit BO-650 NISSEI) for pulse rate measurements as a comparison target. As the PO cannot acquire continuous pulse wave signals, the values 15 and 30 s after the start of the experiment were read visually, and the average value was used.

The heart rate measurement results under fluorescent light before and after treatment are shown in **Fig. 6-12**. The results of three subjects showing evident abnormal values were removed from the experimental

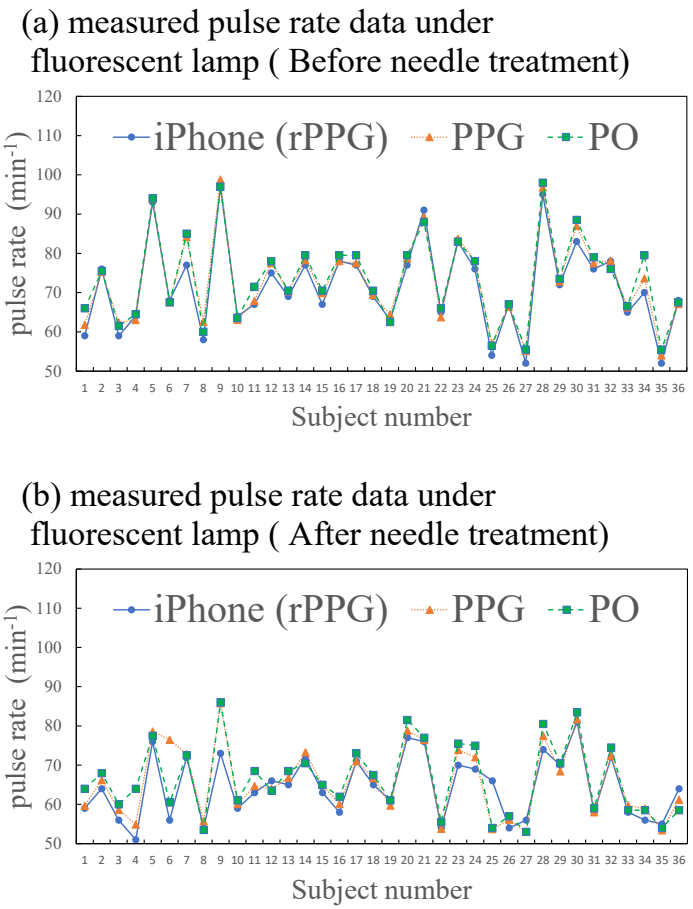

Fig. 6-12. Accuracy Verification Results for the Pulse Rate.

results, and the data of 36 subjects were used. In **Fig. 6-12**, the vertical axis of

the heart rate is shown for the 36 subjects. The experimental data before needle treatment showed that the accuracy was within the range where the differences between subjects could be discerned. The post-treatment data showed a decrease in the heart rate compared with the pre-treatment data. The accuracy of the data showed good consistency, except for subject 6. All four types of experimental data are presented in **Fig. 6-12**. The graphs show the iPhone and PO data plotted in a scatter plot against the heart rate obtained from PPG. The upper and lower auxiliary lines indicate an error rate (*Er*) of 10%, which was calculated using Equation (6-3).

$$Er = \frac{measured\_data - PPG\ Data}{PPG\ Data} \times 100 \quad (6-3)$$

where *measured data* were calculated from iPhone and PPO.

The case data of fluorescent and LED lamps before needle treatment showed that the Er of the iPhone was almost within 10%, and the correlation coefficient was 0.99. This indicates that the accuracy was almost equal to that of the PO.

Figure 6-13 shows the experimental data after the needle treatment, where the pulse rate was relatively low. The accuracy of the data under fluorescent light immediately after needle treatment was lower than

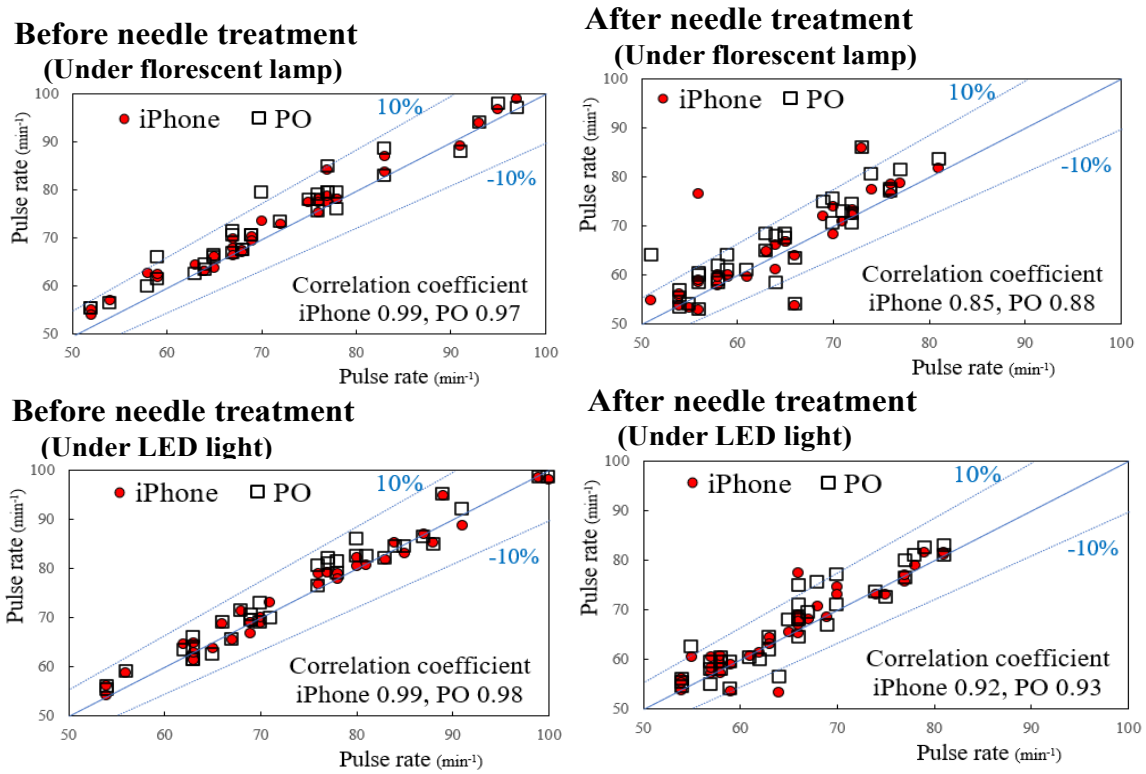

Fig. 6- 13. Accuracy verification results for the pulse rate.

that under the other three conditions.

The error rates and correlation coefficients were almost the same for iPhone and PO.

Next, we will discuss the comparison results between the G signal and the hemoglobin signal obtained using ICA. Since the system used in this experiment records each RGB signal separately, which is the original data during video recording, the recorded G signal was used for analysis. The process for counting pulse rate from the G signal, i.e., smoothing, bandpass filtering, pulse wave peak detection, and pulse rate

counting, used the same algorithm as the process for counting pulse rate from hemoglobin signals. However, the processing of the G signal was analyzed using Python on a PC. The processing of the hemoglobin signal, on the other hand, was conducted in an iOS, with a different module for the Fourier transform.

The true value is PPG, and the correlation of pulse rate counts was performed under the same four conditions as in the previous chapter. The experiments results are shown in Table 6-5. The correlation factor was almost the same for both the G and the hemoglobin signals. In this case, since we use a chin rest, we can assume that there is no effect of shading caused by movement.

Table 6-5. Correlation of heart rate obtained from G signals and hemoglobin signals to the true value.

	Fluorescent lamp		LED light	
	G signal	Hemoglobin signal	G signal	Hemoglobin signal
Before treatment	1.00	0.99	0.99	0.99
After treatment	0.90	0.85	0.99	0.92

6.2.6 Comprehensive evaluation of iOS-based telemedicine tool

In this section, we present the results of Survey results for application improvement on doctors to evaluate the tool. The evaluation was conducted in August 2021 for doctors, mainly in Hiroshima and Shizuoka prefectures. The doctors used this telemedicine tool for multiple days and submitted questionnaires after completion. Submissions were accepted either anonymously or unnamed. The evaluation items were operability, rated in three levels (easy to understand, normal, and difficult to understand). In addition, a free entry column was provided.

The results are shown in Table 6-6. A total of three questions were asked and responses were rated at three different sensitivity levels. More than 80% of the respondents answered normal or above.

The following summarizes the comments made in the free comments section. Regarding face and tongue photo shooting, there was a comment that “it was difficult to shoot while holding the color chart.”

Regarding the operation of the application, several comments mentioned that “it was difficult to install the application.” However, there were no negative comments about the telemedicine tool itself, and the participants agreed that the accumulation of such data is important.

Table 6-6. Survey results for application improvement

	Easy to understand (%)	Normal (%)	Difficult to Understand (%)
Face and tongue photo shooting (n = 33)	55	30	15
Vital measurement (n = 34)	62	38	0
Operation of the application (n = 34)	26	62	12

6.3. Discussion

Telemedicine increased after the COVID-19 pandemic, where "forward triage," the sorting of patients before they arrive in the emergency department (ED), is the most important and emerging medical need. For example, respiratory symptoms that may be early signs of COVID-19 are among the most evaluated with this approach. Telemedicine may be a virtually perfect solution. Telemedicine with high quality can allow physicians and patients to communicate 24 hours a day, using smartphones or webcam-enabled computers. At the same time, physicians can observe the color of the face, lips, or tongues.

It is reported that telephone consultations typically convey less information than video consultations and are reimbursed at a fraction of a comparative video telehealth consultation [83].

Natural face color is one of the most important physical examination points.

Our previous studies demonstrated that tongue color reflects the diagnosis in Kampo medicine [84], and evaluation of Kampo Disease State is possible with images of the face and tongue [85], [86]. Facial color diagnosis is also an important diagnostic method in Kampo medicine and traditional Chinese medicine (TCM). Another study showed that face color diagnosis can properly identify patients with hepatitis into three groups (healthy, severe hepatitis with jaundice, and severe hepatitis without jaundice) with accuracy higher than 73% [87]. We believe that the usefulness of the color chart-based telemedicine tool will increase, and we will continue to improve it further.

The automatic color correction of the color chart was evaluated by determining the difference between Ref. RGB and the corrected samples. Sample images with a significant error ΔE were considered to have inaccurate interpolation because of the narrow of ΔE between the white and black patches of that image. To examine the relationship between the magnitude of the error and the color difference between the white patch (A-a) and the black patch (A-f), all ten conditions, which are the test data, are described in **Fig. 6-14**. The horizontal axis shows the color difference ΔE between the white patch (A-a) and the black patch (A-f), and the vertical axis shows the number of patches with the correct error difference ΔE greater than 6. Because we evaluated seven different patches for one test data sample, the maximum number of patches on the vertical axis was seven. The smaller the ΔE of the black and white patches, the larger the error. The

difference between the models used for photography was that the iPhone 8 had a smaller ΔE than the iPhone 12, but the number of errors was not significantly different. In the future, we would like to conduct additional experiments to reduce the ΔE.

It is necessary to calibrate the monitor for accurate color reproduction. By using a calibration tool for commercially available monitors, accurate color reproduction can be achieved.

Automatic color correction helps to compare images between patients, even if the monitor is not calibrated. In this system, doctors use color charts, so they can recognize the differences in colors. We believe that this system will work effectively as long as the physician understands the characteristics of the proposed method. In a future study, we will address the simplification of the calibration of the monitor. We are currently developing a simple correction method using a mirror. We examined the possibility of performing color correction by simultaneously photographing the color chart and the doctor's monitor.

The accuracy of the pulse wave signal obtained from the captured images, the comparison of the hemoglobin signal, and the G signal showed that the hemoglobin signal was robust against motion.

As a result of verifying the accuracy of the implemented system with 36 subjects, the correlation

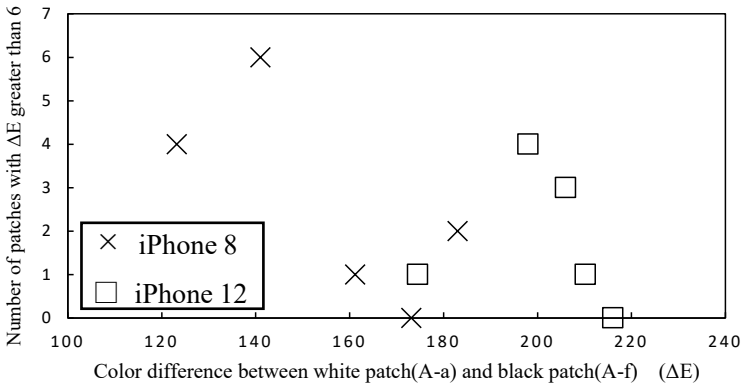

Fig. 6-14. Relationship between the number of errors and the color difference between white and black patches.

coefficient with the correct answer values was equivalent to that of the PO, confirming the effectiveness of this system. The accuracy of the data under fluorescent light after acupuncture was poor compared with the other conditions. This result may have been due to the effect of needle treatment. Needle treatment was performed for approximately 30 min. After the needle treatment, the patient was fitted with a sensing device for approximately 2 min, and the tongue and face were photographed under fluorescent light. Next, video recording for vitals was performed under fluorescent light for 30 s, followed by measurements under LED light, for tongue and face. The pulse wave was obtained from the changes in the hemoglobin signal. The decrease in the detection accuracy may be due to the decrease in blood pressure resulting from the

drowsiness owing to the needle treatment, which reduces the range of change in the hemoglobin signal. The measurement time under LED illumination after needle treatment was a few minutes after the measurement under fluorescent illumination. The error may have decreased as blood pressure returned to normal over time.

In this verification, there were some data where the true value, PPG, was not certain. That is the case where the iPhone and PO data were the same but only the PPG data was different. To detect biological signals, methods for isolating weak signals are essential. Since many signal processing methods have been proposed [88], in the future, we plan to utilize signal processing methods to find a way to obtain a more reliable pulse wave.

6.4 Conclusion

We implemented a non-contact telemedicine tool for infection prevention in iOS and conducted an accuracy verification experiment. As a result, the doctors who participated in this study evaluated the tool as being at a level where they would like to try it out in the medical field. Because the tool can be used with commercially available iPhones, the range of use will expand. In the future, we plan to test and improve the tool by using it in conjunction with clinical trials.

Chapter 7: Non-invasive measurement of pulse wave in soles of rats using an RGB camera

In this chapter, we describe a non-contact method we have developed to obtain heart rate from rats. This research is useful as a technique for conducting experiments in animals that would be ethically problematic in humans.

7.1 Introduction

Animal studies are essential for investigating biological mechanisms of an entire living system that would be too difficult to perform in human subjects [89], [90], [91]. However, from the perspective of animal welfare, the 3Rs (replacement, reduction, and refinement) are essential issues in animal experiments [92], [93]. In animal experiments, heart rate (HR) measurement is widely used to observe vitals, and electrocardiography (ECG) is the gold standard [94], [95], [96].

Non-contact measuring of pulse waves without attaching a device, such as using microwaves and cameras, have been proposed [37], [38], [97]. A vital signal measurement method using cameras including RGB, infrared, and Time-of-Flight (TOF), has been proposed. Among them, RGB cameras are easy to use because they are general purpose. An RGB camera-based method has been proposed to measure rats and wild animals' HR and respiration rate (RR) by capturing their skin movements using a camera [40], [41], [42], [43]. The same methods are affected by ambient light and require observation in a sedation state. In human HR measurement, a photoplethysmography (PPG) method that directly utilizes the color channels of an RGB camera has been proposed [80], [98], [99]. Use of the green (G) channel signal of an RGB camera has the advantage in that it can be quickly realized by spatially averaging the G signals, and it can be processed in real-time [100], [101].

This paper proposes to use the G channel of the camera to measure the HR of rodents. This is a non-invasive method for measuring pulse waves corresponding to HR by capturing the color change on the soles of rats' feet using a high-speed RGB camera. These results and discussion of the paper give a new analysis compared to the conference proceedings SPIE-BIOS [102]. We used the same video datasets as in the conference proceeding. There are two challenges in adapting the remote PPG (rPPG) to rats. The first challenge is that the human pulse rate is 60–150 beats per minute (bpm), whereas the rat pulse rate is 350–450 bpm [103]. Therefore, the image and signal processing should be improved. The second challenge is that rPPG captures skin color changes; thus, rats covered with body hair need to be depilated. To solve these problems, we decided to capture images at a faster frame rate than that for humans and focus on the rat soles, where the skin is directly visible, to capture changes in skin color. As a result, pulse waves could

be detected from videos of the sole captured at a frame rate of 250 fps. Furthermore, we were able to detect arrhythmia that occurred when fear was inflicted.

7.2 Material and methods

7.2.1 Creating the dataset for analysis

The dataset used in this study is common to the dataset described in the SPIE-BIOS manuscript. In this section, the dataset is briefly described.

7.2.1.1 Animals

Sixteen eight-week-old male Wistar rats (Japan SLC, Hamamatsu, Japan) were used. The rats were housed under 12 h light/12 h dark cycles at 21 °C with unrestricted access to food and water. All images were captured in the afternoon. The Committee of Animal Research at the International University of Health and Welfare approved our experiments (no. 19021).

7.2.1.2 Experimental set up for creating the data set

Figure 7-1 and **Fig. 7-2** show an overview of the experimental setup for video and ECG acquisition. The experiment was conducted in the laboratory of the International University of Health and Welfare, Ohtawara.

Figure 7-1 shows the experimental setup used to acquire data from rats under sedation. To observe color change, we removed the hair from the head, back, and abdomen areas using a hair removal cream (Hair Removing Body Cream “epilat”, Kracie Holdings, Tokyo, Japan) 3 h before the experiment. The intravenous anesthetic propofol (500 µL/kg body weight, Wako Pure Chemical Industries, Tokyo, Japan), which was used for sedation, was injected intraperitoneally 30 min before the experiment. The camera was set up on a tripod 60 cm above the rat skin, and two LED lights were placed on either side of the camera. We used a Memrecam-Q1m high-speed RGB camera (NAC Image Technology Inc., Tokyo, Japan) with a

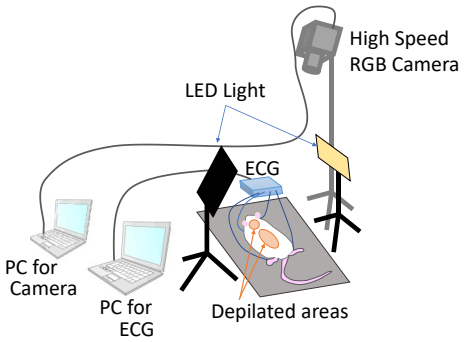

Fig. 7- 1. Experimental setup for creating the dataset of rats under sedation.

frame size of 1024 × 768 pixels. The lens (FL-CC1614A-2M, RICHO, Tokyo, Japan) had a focal length of

16 mm (f = 1.4), and only LED (ViltroxL116T, 810LX/0.5m) lighting was used with 100% output at a color temperature of 5600 K. The camera-specific software HXLink64 was installed on a laptop computer for camera control and data acquisition. The frame rate was set at 250 fps, which is approximately eight times higher than the human experiment considering to measure heart rate variability (HRV) [79] in our future work, to account for the temporal resolution because the pulse rate of rats is 350-450 bpm [103], while that of humans is 60-150 bpm. The true value was determined using a gold standard 3-point ECG system (SP-2000, EP95U, Softron Co., Ltd., Tokyo, Japan). The ECG was measured simultaneously with a video recording. The sampling rate for converting the ECG analog signals to digital signals was 1000 Hz.

Figure 7-2 shows the experimental setup used to acquire data from the sole of normal rats. The rat was placed in a rectangular box with a partition and was illuminated from below using LED lights. The distance between the floor and the tip of the camera lens is 10 cm. The floor is made of transparent plastic, and the partition allows indirect placement of odorous substances. The lighting and camera apparatus are the same ones used in under sedation state. The lens (FL-CC0814A-2M, RICHO, Tokyo, Japan) with focal length of 8 mm (f = 1.4) was used. The HR was determined using an implant ECG system (ATR-1001, ATE-02s, EP95U, Softron Co., Ltd, Tokyo, Japan).

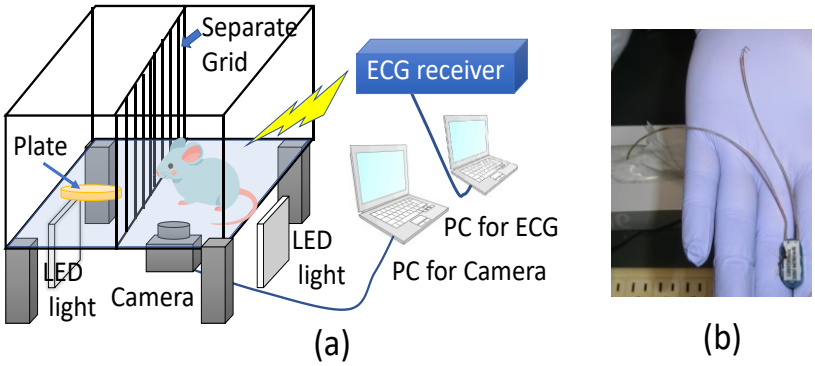

Fig. 7- 2. Experimental setup for creating the dataset of a normal rat sole;
(a) video recording setup for rat's sole; (b) implanted ECG sensor.

Three different states were set up to determine the detection sensitivity: normal, fox smell-induced, and sedentary. The fox smell was included in the experiment because the smell of foxes, which are natural predators of rats, causes stress. We used 2-methylthiazoline (2-MT, Tokyo Chemical Industries, Tokyo, Japan), which creates a unique stress-like pattern of dynamic and endocrine activation in rats [104]. For the sedation experiment, intravenous anesthetic propofol (500 µL/kg body weight, Wako Pure Chemical Industries, Tokyo, Japan) was injected into the abdominal cavity 10 min before the experiment.

7.2.2 Pulse rate detection procedure

The data processing procedure used in this experiment is illustrated in **Fig. 7- 3**. To extract the video of the regions of interest (ROIs) for the experiment, we used the camera-specific software HXLink64. First, the video dataset was visually checked to identify the locations of the ROIs to be extracted. Next, the ROIs were selected, and the videos were converted to uncompressed AVI files. MATLAB2019b was used for the subsequent data processing. The G signal was obtained by extracting the pixel values of the G channel from a file in the AVI format and averaging the pixel values. The obtained G signal was detrended, and bandpass filtered, and its peaks were detected. The signal was passed between the 3 and 9 Hz bands, considering the HR range for the rat. The findpeaks function in MATLAB was used for peak detection. For ECG signals, we used the threshold method because the peak values were almost constant. For rPPG, because the peak values fluctuated, we used the nearest-neighbor method. The definitions of the PI in the rPPG and ECG are shown in **Fig. 7- 3 (b).**

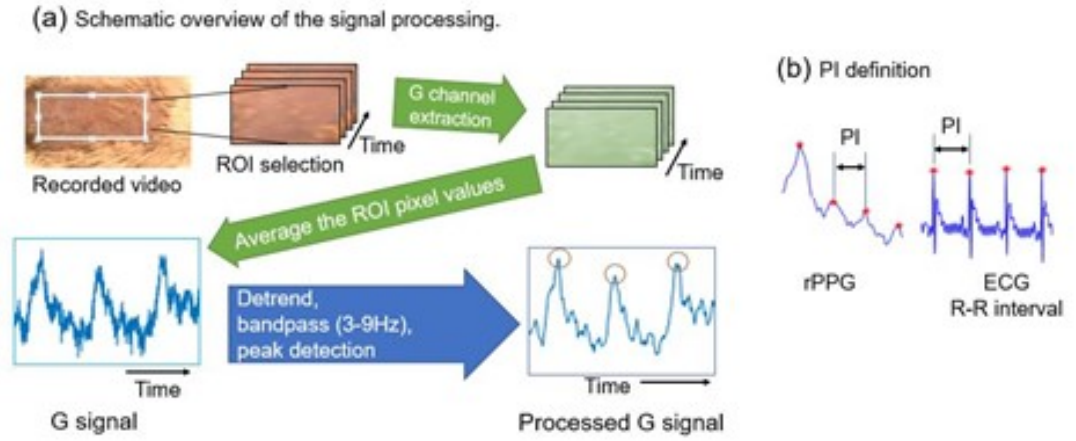

Fig. 7- 3. The schematic overview of the signal detection from the video data; (a) Schematic overview of the signal processing; (b) PI definition.

The *PI* was obtained from the extracted peak detection time *T* = [T2,..., Tk,..., TN-1]. To avoid false peak detection, *T* was set from 2 to N-1.

$$PI[k] = T_k - T_{k-1} \,. \tag{7-1}$$

HR was calculated from *PI*

$$HR = \frac{60}{mean(PI[k])} \,. \tag{7-2}$$

7.3 Results and discussion

7.3.1 Pulse wave analysis from the head and back ROIs

7.3.1.1 Signal analysis in the prone position

Table 7-1 shows the HR, relative error (RE) based on the ECG, and standard deviation (SD) for 20 s in the prone position. The HR measured from the gold standard 3-point ECG was used as the correct value and was compared with the HR calculated from the G signal. The ROIs set up for the rPPG measurements were the depilated head and back. The ROIs were set to the same size (60 × 52 pixels) to obtain the same denoising effect as the averaging process. The results showed that the values obtained from the head were in excellent agreement with the ECG signals. In comparison, the signals from the back were sometimes inconsistent with the correct ECG values. This might have been due to the noise caused by respiration, which prevented accurate peak detection.

Table 7-1. HR, RE, and SD over 20 seconds Obtained from ECG and rPPG in Prone Position.

	Experiment #1			Experiment #2		
	HR (bpm)	RE (%)	SD	HR (bpm)	RE (%)	SD
ECG	270	---	3	220	---	3
rPPG: Head (ROI-3)	271	0.4	21	220	0.0	19
rPPG: Back 1 (ROI-4)	271	0.4	35	214	-2.7	38
rPPG: Back 2 (ROI-5)	267	-1.1	41	221	0.5	30

Figure 7-4 shows the ECG signal compared with the unprocessed G signals from the ROIs on the rat skin removal area in experiment 2. The ROIs were positioned in four different areas: the depilated head, depilated back, back of the hair, and paper as a dummy. Every ROI was set to the same size. No well-defined waveforms corresponding to RR and HR were observed in the paper area (ROI-1). The signal from the hair-removed head showed peaks at intervals similar to those of the HR, and the signals from the hair-removed areas (ROI-4, 5) showed the same periodic signal. In comparing the signals of ROI-2 and ROI-5, we also observed a periodic peak of about 0.8 Hz, which was different from that of the HR. To investigate the origin of this periodic signal, we observed the original video. We found that the periodic signal corresponds to the body movement caused by the respiration of the rat.

These results showed that the pulse wave signal could be obtained from the unprocessed G signal at a frame rate of 250 fps. The respiratory signal could also be obtained by analyzing the G signal in the ROI of the area with large movements due to respiration. This result is similar to the results of several studies [41], [42] that obtained the RR from the luminance change in rPPG.

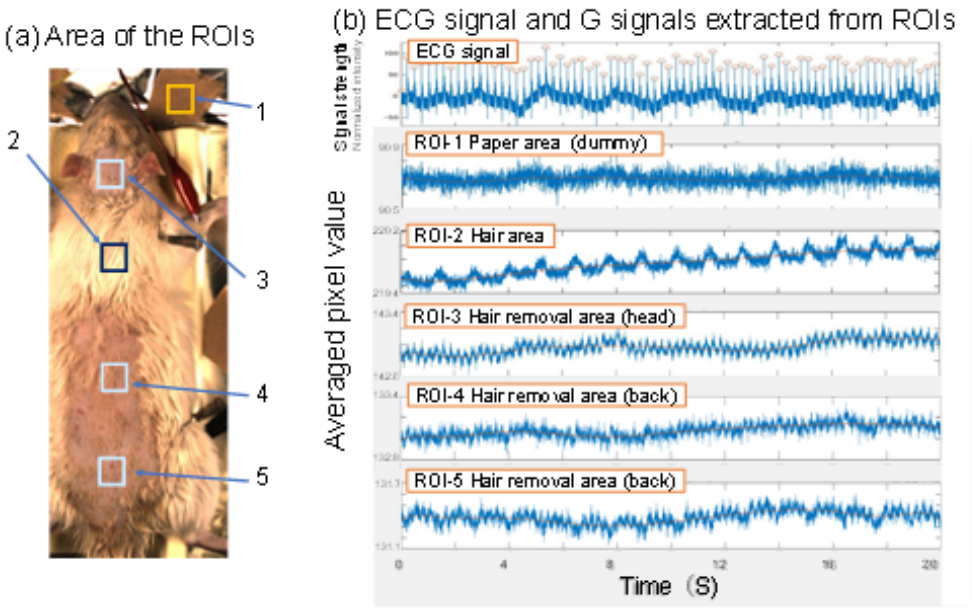

Fig. 7-4. ECG signals compared with unprocessed G signals from ROIs in the prone position in experiment 2. a) Area of ROIs; b) ECG signal and G signals extracted from ROIs; paper as a dummy ROI-1, non-hair-removal ROI-2, hair-removal ROIs (ROI-3, 4, 5).

Figure 7-5 shows the results of comparing the ECG and pulse wave signal from the hair-removed area of the head in experiment 2. A graph comparing the temporal changes in the pulse wave PI is also presented. The pulse wave peaks in ECG and rPPG are almost identical, and the pulse wave interval graph supports this. Since the ECG and rPPG devices are manually synchronized, it is not easy to compare the ECG and rPPG data accurately against the time axis. The rPPG shows more significant variation in the pulse wave interval than the ECG in PI variation. The rPPG shows an amplitude variation that is within 0.04 s. From the above results, it can be concluded that the signal processing worked well in the head area where respiratory noise was low. The rPPG had a more comprehensive range of variability than the ECG. The accuracy of peak detection needs to be improved to support applications that measure HRV. The G signal peak for calculating the HRV, the same as PI, was not sharp, as shown in **Fig. 7-4.** In order to reliably capture the peak, higher frame rate is necessary in the imaging system.

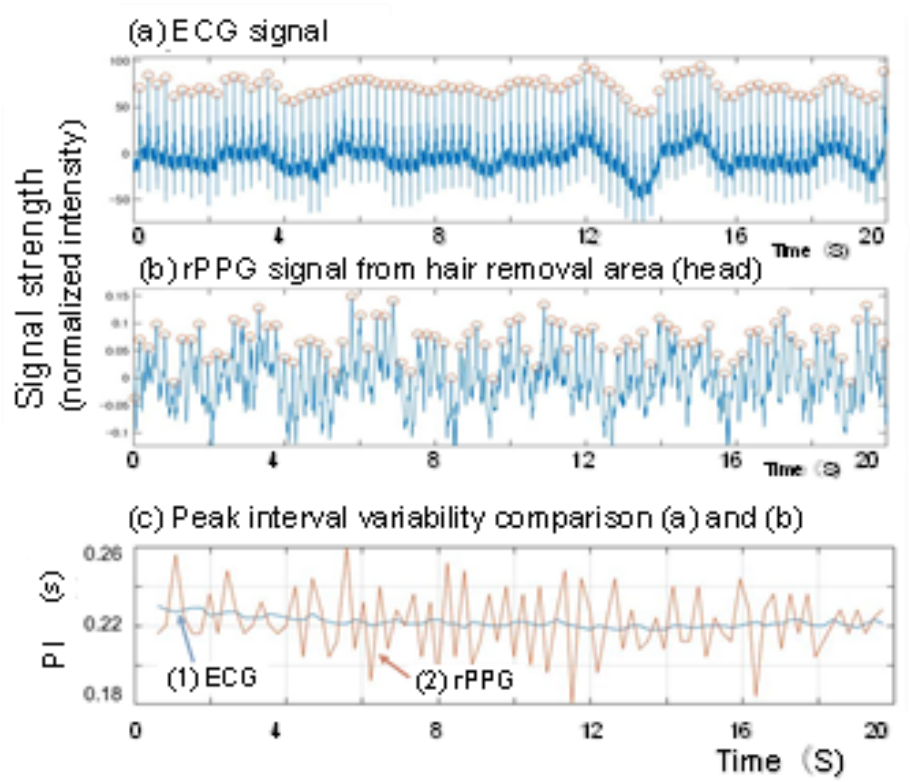

Fig. 7- 5. Comparison of the ECG and pulse wave signal from the hair-removal area of the head in experiment 1. (a) ECG signal, (b) rPPG processed signal, (c) HRV comparison with ECG (a) and rPPG (b).

7.3.1.2 Signal analysis in the supine position.

Table 7-2 shows the result in the supine position. The measurement conditions were the same as those described in the previous section. The ROIs set up for rPPG measurements were the hair-removed abdomens. The results showed that the values obtained from the abdomen were in good agreement with the ECG signals. The accuracy was not as good as that of the signal from the head, as shown in Table 7-1.

Table 7-2. HR, RE, and SD over 20 seconds obtained from ECG and rPPG in Supine Position.

	Experiment #3			Experiment #4		
	HR (bpm)	RE (%)	SD	HR (bpm)	RE (%)	SD
ECG	199	---	2	195	---	1
rPPG: Abdomen1 (ROI-4)	201	1.0	40	212	3.6	41
rPPG: Abdomen2 (ROI-5)	206	3.5	39	212	3.6	51

Figure 7-6 shows the locations of the ROIs taken from the abdomen and their respective unprocessed G signals. From the ROIs set on the rat, low-frequency signals different from the ECG signals were observed from the graphs. The ROI-4 and ROI-5 had reversed phases. The periodic signal set on the rat's body fluctuated in the same cycle as the respiratory rate, as seen in the video. As for the HR signal, the unprocessed G signal obtained from the video taken from the ventral side did not show a clear HR signal, similar to the signal obtained from the head in the prone position. However, in the skin area, pulse waves could be observed from the signal processing, as in the prone position.

The correlation between heart rate and the mean value of rPPG for experiment number 1-4 was 0.70 to show the correlation over time. From the above results, the pulse wave signal could be extracted from the abdomen ROI by processing the G signal at a frame rate of 250 fps, but the noise due to the influence of respiration was larger than that of the head ROI.

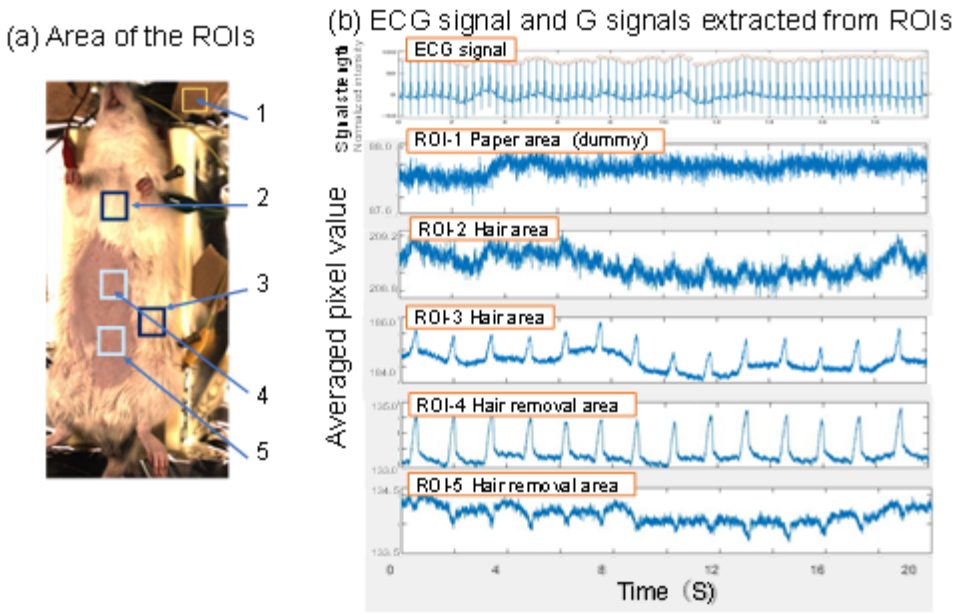

Fig. 7- 6. ECG signals compared with unprocessed G signals from ROIs in the supine position in experiment 3. a) Area of ROIs; b) ECG signal and G signals extracted from ROIs; paper as a dummy ROI-1, non-hair removal ROIs (ROI-2,3), hair removal ROIs (ROI-4,5).

7.3.2 Pulse wave detection from different body locations

This section describes the results of pulse wave detection from different body locations of a rat under three conditions: normal, stress-added, and under sedation. The time events of the experiments are sequenced by experiment number. ROIs were set at two locations on the soles and two locations on the abdomen. The size of the ROI varies due to the rat's movement and the camera's viewing angle. In experiments 5 and 10, only one sole was visible in the camera's field of view, so ROIs were set to two different locations on the

same sole. Table 3 lists the HR, ECG-based RE, and SD obtained from data measured for 20 s under three different conditions and at different body parts. The standard deviation of the pulse wave was calculated using the pulse wave interval time converted to pulse rate per minute. The correlation between heart rate and the mean value of rPPG for experiment number 5-10 was 0.86 to show the correlation over changing heart rates.

Table 7-3a. Results of pulse wave detection from different body locations under different conditions

	Normal (Experiment #5)			Normal (Experiment #6)		
	HR (bpm)	RE (%)	SD	HR (bpm)	RE (%)	SD
ECG	346	---	10	336	---	6
rPPG Average	346	-0.1	---	328	-2.5%	---
Sole1	346	0.0	41	323	-3.9%	55
Sole2	344	-0.6	44	332	-1.2%	60
Abdomen1	346	0.0	41	329	-2.1%	39
Abdomen2	346	0.0	260	327	-2.7%	64

Table 7-3b. Results of pulse wave detection from different body locations under different conditions

	Stressed (Exp. #7); 2MT (Fox smell)			Stressed (Exp. #8); 2MT (Fox smell)		
	HR (bpm)	RE (%)	SD	HR (bpm)	RE (%)	SD
ECG	310	---	10	266	---	38
rPPG Average	310	-0.2	--	278	4.5	--
Sole1	311	0.3	31	274	3.0	64
Sole2	310	0.0	36	277	4.1	48
Abdomen1	307	-1.0	42	290	9.0	60
Abdomen2	310	0.0	20	271	1.9	42

Table 7-3c. Results of pulse wave detection from different body locations under different conditions

	Under Sedation (Experiment #9)			Under Sedation (Experiment #10)		
	HR (bpm)	RE (%)	SD	HR (bpm)	RE (%)	SD
ECG	411	---	3	385	--	2
rPPG Average	409	-0.5	--	385	0.0	--
Sole1	408	-0.7	36	385	0.0	22
Sole2	409	-0.5	33	385	0.0	33
Abdomen1	408	-0.7	26	385	0.0	15
Abdomen2	411	0.0	15	385	0.0	10

Except for experiments 6 and 8, rPPG obtained the exact HR in RE. The comparison of variances showed that rPPG tended to be wider than ECG, which was the same as the experimental results in the previous section.

We investigated the cause of the large errors in experiments 6 and 8. **Figure 7-7** shows the ROIs of experiment number 6 and the pulse wave data obtained from each ROI. **Fig. 7(b)** shows the G-channel source signal obtained from each ROIs. The pixel values changed significantly between 11 and 12 s. The original video showed fluctuating illumination. While the signal intensity of the pulse wave component in rPPG, which captures pulse wave fluctuations, is less than 0.5, the noise estimated to be due to lighting fluctuation is 5. Since the lighting fluctuation range was extensive, the pulse wave fluctuations were presumably undetected. The PI in **Fig. 7-7 (c)** is also longer in this area, and the pulse wave signal is not detected. From this result, although the pulse wave signal was normally captured correctly, our detection software was unable to cope with the large fluctuations in the base signal. Therefore to improve the accuracy of the obtained average pulse wave, approaches such as cutting off the large variation portion in the calculation can be considered in future.

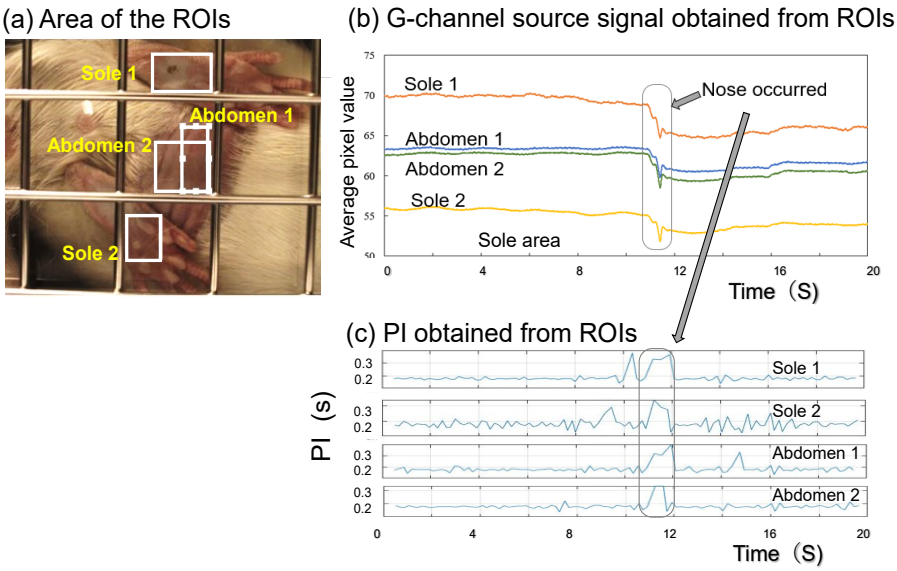

Fig. 7-7. Pulse data of experiment 6. a) Area of ORIs. b) G-channel source signal obtained from ROIs; the vertical axis represents the average pixel value of the ROI. c) PI obtained from ROIs.

In experiment 8 there was an over-detection of pulses. **Figure 7-8** shows the data for experiment number 8, i.e., for the rat that sniffed 2-MT. In this experiment, the rat experienced extreme fear and was immobile as a result. According to the ECG data in **Fig. 7-8** (b) and (d), the pulse wave was inconsistent and showed an arrhythmia-like waveform. In **Fig. 7-8** (c), the PI at approximately 8 s showed that the pulse was lost for one beat. The peak differences between the three locations shown in the ECG and rPPG PIs were all 0.33

s. The waveforms of the ECG and rPPG peaks are shifted by two factors: the origin of the signal and the coincidence of the trigger. The origin of the signal, which is the gap between the ECG and rPPG, is estimated to be around 40 msec in mice [105]. Since automatic synchronization was not available, the trigger operation in this experiment was performed manually. The deviation of the manual operation of the triggers is considered to be within 0.5 seconds. Based on this result, we concluded that the time deviation between ECG and rPPG was 0.33 s. By correcting for this time difference, the peak positions of ECG and rPPG can be correctly compared. The red asterisks on the rPPG graph in **Fig. 7-8 (d)** show the instances when peaks were recognized using peak detection. Comparison of rPPG and ECG peak detection showed that rPPG incorrectly detected peaks in the area indicated by the red arrows at around 12 seconds. We used the findpeaks function for peak extraction. In this experiment, we adjusted the parameters for optimality. It is noted that various methods have been proposed for peak extraction. In the future, we will continue to conduct and test the various state-of-the-art methods.

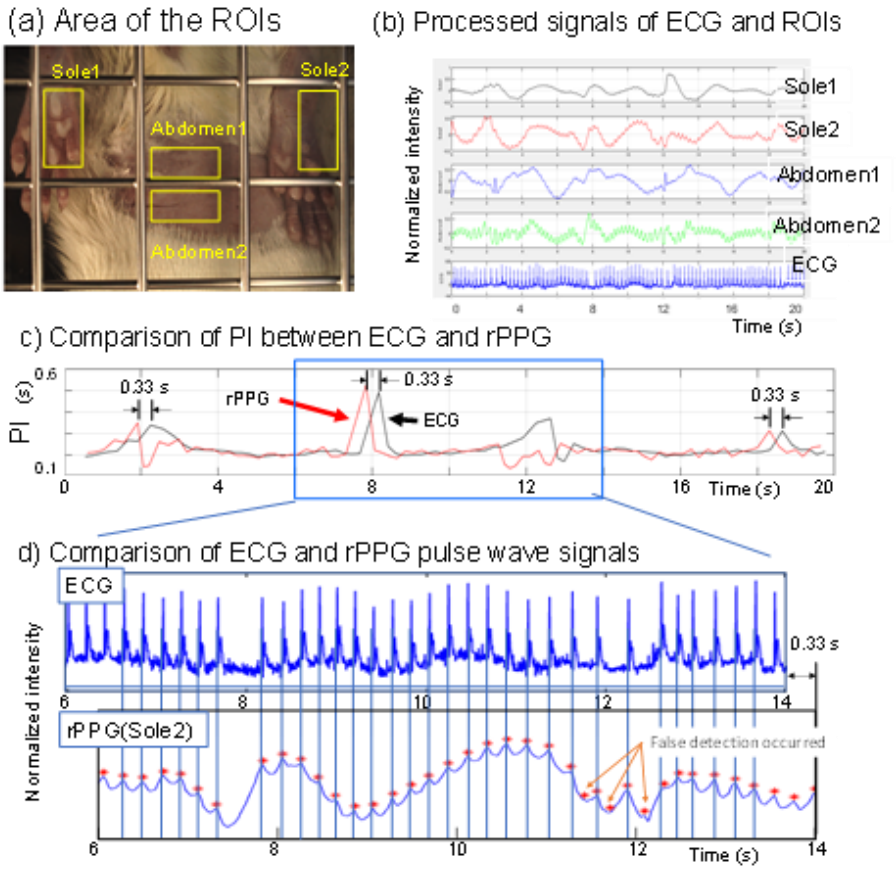

Fig. 7- 8. Pulse data of experiment 6. a) Area of ORIs. b) G-channel source signal obtained from ROIs; the vertical axis represents the average pixel value of the ROI. c) PI obtained from ROIs.

7.3.3 Comparison of pulse waves obtained from different areas of the body

The differences in the pulse waves obtained from the four different parts of the body were compared. **Figure 7-9** shows the ROIs of experiment number 9 and the G signals obtained from each ROI in 4 s after detrending. Similar signals were observed at all four ROIs. Then, to investigate the possibility of detecting the pulse wave propagation velocity, we analyzed the signal shift for the four ROIs of rPPG. The calculation was performed for experiment numbers 6–9, where both feet could be measured. The xcorr function in MATLAB was used to detect the signal shift. The maximum value of the shift width was set to 0.1 s. The 20-s detrended signal was divided into time regions of every 4 s, i.e., 0-4, 4-8, 8-12, 12-16, and 16-20 s, and the signal in each region was calculated. Table 7-4 Calculation result of signal time delay of three conditions. Table 4 summarizes the results of the signal shift from xcorr function for 4 s. According to this result, the signals obtained from the four ROIs set at different body locations showed no time deviation. The delay due to pulse wave propagation between the ROIs is estimated to be less than 1/250 s. In experiment 6-8, the SD values were larger than in experiment 9, whereby rats were under sedation. We plan to investigate this issue of large SD values in future studies.

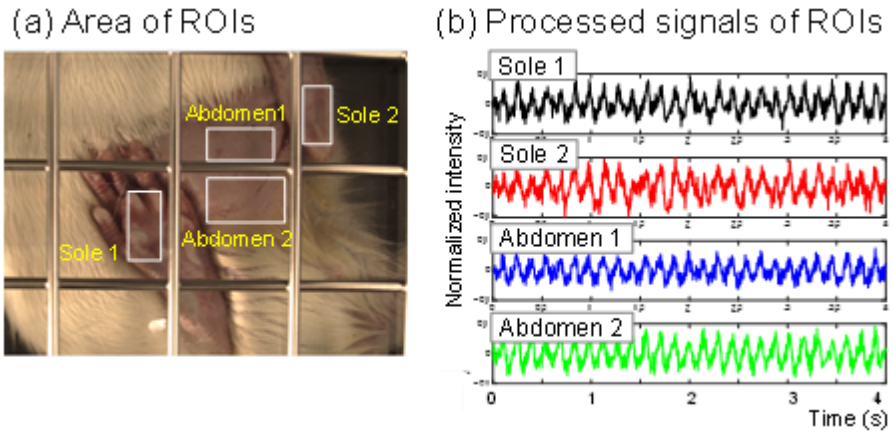

Fig. 7-9. Pulse wave signals from experiment number 9. a) Area of ROIs of experimental number 9; b) Detrended signals obtained from each ROI in 4 s.

Table 7-4. Calculation result of signal time delay of three conditions

Pair of xcorr function		Sole1 Sole2		Abdomen1 Abdomen2		Sole1 Abdomen1		Sole2 Abdomen2	
		s	SD	s	SD	s	SD	s	SD
Normal	Ex. 6	-0.03	0.04	-0.0	0.05	-0.04	0.04	0.03	0.04
Stressed 2-MT (Fox smell)	Ex. 7	0.00	0.00	0.02	0.00	0.01	0.02	-0.02	0.00
	Ex. 8	0.00	0.00	0.02	0.01	0.00	0.06	-0.01	0.00
Under sedation	Ex. 9	0.00	0.00	-0.00	0.00	-0.01	0.00	0.01	0.00
ALL data	Ex. 6-9	-0.01	0.02	0.01	0.03	-0.01	0.04	0.00	0.05

7.4 Conclusion and outlook

We developed a non-invasive pulse wave measurement method for rats using a high-speed RGB camera to obtain rPPG signals with high accuracy from changes in skin color using only general signal processing. The feature of this method is that heart rate can be detected simply by using a high-speed camera system (250 fps) that generates high-quality pulse signals, selecting an appropriate ROI, and detecting all signal peaks in the band-pass filtered average signal of that ROI. This method yielded the same pulse rate measurement as the gold standard ECG. Furthermore, using this method, we found that pulse waves could be detected by video recording from the sole, which did not require hair removal. Our proposed method is non-contact and non-invasive, and is valuable for detecting the pulse wave of rats in a non-restrained manner. In addition, because various parts of the body can be video-recorded using a single camera, we have demonstrated the possibility of simultaneously detecting respiration from body movement.

In an experiment to measure the normal state of the rat, we detected the signals during the periods when the feet were not moving. When the feet moves a lot, blood distribution on the sole changes and noise can be expected to increase. In the future, we plan to take these into account when performing continuous measurements.

For continuous measurements, the system may need to be equipped with a program that tracks the location of the sole and also automatically excludes areas of the foot that frequently move. Rats perform grooming behaviors such as scratching their heads with their hands and standing up, even when their feet are not moving. Collecting measurements from a hair-removed area is challenging when rats are standing because the position of their hair changes. Therefore, imaging of the sole is considered to be superior to imaging of depilated skin.

In this study, we were able to obtain the same HR from the G signal in the video as from the ECG, which represents the true value of our research. Because the rats used in this study did not have melanin, the G signal was used, but for mice with melanin or under fluctuations in illumination, the signal processing would need to be modified. In a previous study, Fukunishi et al. used a method to separate shade, hemoglobin, and melanin components from RGB signals using independent component analysis (ICA) [79]. This component separation method may be useful for future studies involving animals with melanin. Wang et al. used RGB channels to improve the robustness of the method [44]. In the future, we plan to apply these findings to improve the accuracy in rats.

Because we were able to measure PI in rats under normal conditions, we were able to find a way to measure stress using PI fluctuations. The measurement of stress in animals is currently conducted by observation, which is time-consuming and costly. Our proposed method has the potential to reduce the labor of researchers. In human stress research, blood samples are taken to measure biomarkers such as

inflammatory cytokines. However, animal blood collection is sometimes difficult. Our method has the potential to solve these problems.

In the future, we plan to improve the signal processing to achieve more accurate measurements.

Chapter 8: Conclusion and Future Work

In the industrial product sector, there has been competition among companies to increase the functional value of their products. With the advancement of technology, it is becoming increasingly difficult to differentiate products based on their functions. The Kansei value has a different axis from the functional value and has attracted attention. Developing products with functional value is relatively easy in a mobile environment if the physical property values are determined based on the required functions. However, developing products with Kansei value requires face-to-face discussion and sensory evaluation.

Under the COVID-19 epidemic that began in 2019, face-to-face discussions and sensory evaluations could not be easily conducted due to prevention of infection. Hence, I selected the theme of developing Kansei value products in mobile work because I want to realize product development and sensibility evaluation through remote communication.

8.1 Review of results and future work

1. Tactile sense: mutual conversion of sensory and physical property information (Chapter 4)

Prototypes of tool creators and material providers, which can used to develop products with Kansei value, were devised and presented at an exhibition. At the exhibition, we displayed concept materials for the Kansei Communication Tool, samples to experience surface roughness changes, and a Kansei Communication Tool prototype. The prototype has the same specifications as the DIC Color Guide, a color swatch widely used in Japan, and combines a tactile film in addition to the color swatch. We investigated the Kansei communication tool at the exhibition by asking questionnaire-style questions to visitors. As a result, 64 people responded to the questionnaire; 49 (77%) of respondents answered “I am interested,” of which 21 (31%) answered, “I want a prototype.”

Based on the results of the exhibition, we created the "DIC Material box," which allows users to experience systematic tactile sensations in two dimensions. This tool allows the user to arrange samples of material surface characteristics such as warmth/coldness, hardness/softness, and smoothness/roughness. This sample arrangement allows designers and product developers to identify their preferred sensory vectors.

Table 8.1 shows the differences between this tool and the commonly used sample book. The "Kansei communication tool" that we developed enables each participant in mobile work to communicate tactile

sensations. In order to improve the usefulness of the Kansei communication tool, it is necessary to diversify the samples to be mounted on the tool. Furthermore, it is necessary to optimize the evaluation axes of sensibility and physical properties. Currently, there are two evaluation axes: one for warm/cold sensation and surface sensation, and the other for hard/soft sensation and surface sensation. In the future, while using the prototype created in our research, we will make improvements and develop a more helpful tool.

Table 8.1 Features of a tactile material box

Item	Conventional method (Sample Book)	Proposed method (Material Box)
Purpose of Sample Book	Tools for material promotion	Tools for material selection
Sample Type	Rough sorting (e.g., stone, paper, plastic, glass) Grooving on samples	A systematic sample designed for industrial manufacturing
Sample shape	Uncontrolled	Same shape
How to touch the samples	Controlled by experiment	Touching with fingers, pinching with fingers
Sample placement	Controlled by experiment	Physical features arranged in two dimensions.

The "Kansei communication tool" that we developed enables each participant in mobile work to communicate tactile sensations. In order to improve the usefulness of the Kansei communication tool, it is necessary to diversify the samples to be mounted on the tool. Furthermore, it is necessary to optimize the evaluation axes of sensibility and physical properties. Currently, there are two evaluation axes: one for warm/cold sensation and surface sensation, and the other for hard/soft sensation and surface sensation. In the future, while using the prototype created in our research, we will make improvements and develop a more helpful tool.

2. Color Reproduction (Chapter 5, 6)

We developed a new color chart and a telemedicine tool that can use the color chart to communicate the patient's complexion and tongue color correctly. The contribution of this study is the development of a color chart including human tongue and skin colors that can reproduce the colors required for medical diagnosis and its implementation in iOS. Development was performed in collaboration with Kampo medical doctor with expertise in color; since this was an urgent task under the COVID-19 epidemic, priority was given to actual use, so the tool's usability was mainly evaluated qualitatively.

Two types of evaluation were conducted: correction based on human color perception and automatic color correction. The results showed that color correction based on human color perception was more beneficial than without correction. The onboard telemedicine tool evaluated the automatic color correction function for qualitative usability and quantitative color difference. The results confirmed the usefulness of this method.

Our research on color correction is currently undergoing continuous evaluation in the medical field. While using the telemedicine application, quantitative evaluation has not been fully completed due to the priority of improvements for medical support under COVID-19. In the future, we will conduct quantitative evaluation. We will then use the color chart that we developed to evaluate whether it can be used for material development and sensitivity evaluation, which was our project's original purpose.

Future work will require the development of a simple method for color correction of displays. In our research, we have developed a simplified method (**Fig. 8-1**) using a mirror [106]. In this system, a monitor (smartphone screen) is used and the color chart is simultaneously photographed to obtain color correction parameters. We intend to verify and utilize this system in the future.

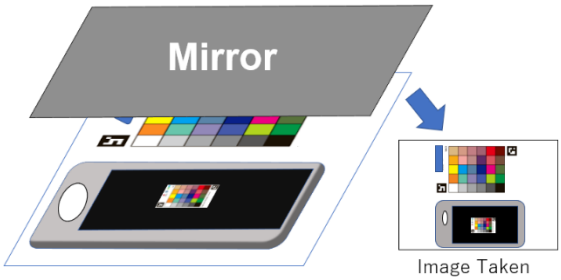

Fig. 8- 1 Color correction using 'selfie' camera of smartphone [96].

Color reproduction technology is used in product development, telemedicine, and online shopping. In the future, we will examine whether the color chart created can be applied to the development of products that impart sensitivity, which was the original purpose of the project. In addition, we would like to study other areas of application.

3. Measurement of emotional state: non-contact pulse wave measurement (Chapter 6,7)

Biometric signals, such as heartbeat, reflect the movement of the emotion. We created and validated a heart rate measurement tool using an RGB camera. There are two main contributions of this study.

The first was implementing the telemedicine tool described in Chapter 6 on iOS to verify the accuracy of heart rate detection. The pulse wave detection technique utilizes a technology that separates signals from an RGB camera into hemoglobin signals using independent component analysis and captures changes in

the hemoglobin signals. Accuracy validation was performed by 39 subjects using a clinical trial setting. The results showed that the accuracy was similar to that of commercially available pulse oximeters. Since the pulse oximeter is a contact type, we believe our method is effective for patients who need a non-contact approach. Currently, we are improving the software while considering opinions from members of the clinical field.

The second is the pulse rate measurement from the sole of rats, as described in Chapter 7. This study was conducted considering emotional experiments in model animals that are otherwise difficult to conduct in humans. The challenge is that the pulse rate of rats is approximately eight times higher than in human experiments, and their skin cannot be observed due to body hair covering the skin. Therefore, we devised an approach for measurement from the sole, which was captured using a high-speed video camera. As a result, we acquired pulse waves from the sole. This method allowed for unrestrained pulse wave measurements and observations in a more normal state, since it does not require the depilation process or electrocardiogram implantation.

The accuracy of our heart rate measurement from pulse waves using the RGB camera was comparable to that of commercially available pulse oximeters. In the future, we plan to verify the accuracy of the R-R interval, which is useful for measuring emotions.

In the rat pulse wave measurement, we were able to measure the pulse waves of rats in normal state and in an unrestrained and non-invasive manner. Using this technique, we may be able to detect pulse waves in other states such as courtship and fighting. Furthermore, the measuring of pulse waves from the sole can also be applied to humans. In nursing, there are related issues such as preventive care for foot lesions caused by poor blood flow and lymphedema caused by the removal of lymph nodes during cancer surgery. The developed technology could also be adapted to visualize blood flow in the feet, which is necessary for nursing.

8.2 Conclusion

Social issues across the world are expected to become increasingly complex and sophisticated. In order to solve such issues, we need a high level of expertise and a broad perspective to address the issues from a bird's eye view. Under these circumstances, I challenge the field of multifaceted research to address the objectives I have highlighted in my research through a broad perspective.

I set three goals for developing elemental technologies necessary to develop Kansei value products remotely and was able to achieve them. Kansei communication tools and medical tools are currently being examined in the field, and through this, issues and needs that require resolution will become apparent.

Further development is expected by making improvements based on such issues and needs, and conducting further research in response.

The road to remotely developing products with sensitivity is a long trek. However, we are moving forward step by step, boldly going where no one has gone before.

References

[1] S. Stoppe, “Getting Immersed in Star Trek. Storytelling Between "True" and False on the Holodeck,” Science Fiction Research Association Review, 4 (15) p. 316 (2016).

[2] M. Farshid, J. Paschen, T. Eriksson , J. Kietzmann, “Go boldly!: Explore augmented reality (AR), virtual reality (VR), and mixed reality (MR) for business,” Business Horizons, 61 (5) pp. 657-663 (2018).

[3] D. Probst , J.-L. Reymond, “Exploring DrugBank in Virtual Reality Chemical Space,” Journal of chemical information and modeling,58(9) pp. 1731-1735 (2018).

[4] S. Alina, “Can Multisensory Cues in VR Help Train Pattern Recognition to Citizen Scientists?,” https://arxiv.org/abs/1804.00229, (2018).

[5] 荒木 潤, “感性価値創造イニシアティブ--第 4 の価値軸の提案,” *感性工学*, 7 (3) pp. 417-419, 3 (2008).

[6] 延岡 健太郎, “意味的価値の創造: コモディティ化を回避するものづくり, “ *國民經濟雜誌,* 194 (6), pp. 1-14 (2006).

[7] D. A. Norman, “Emotional design: Why we love (or hate) everyday things,” in *Basic Civitas Book*, New York: Basic Books (2004).

[8] M. Eisenman, “Understanding aesthetic innovation in the context of technological evolution,” *Academy of Management Review,* 38 (3), pp. 332-351 (2013).

[9] Y. Shigemoto, “Designing emotional product design: when design management combines engineering and marketing,” in *International Conference on Applied Human Factors and Ergonomics* (2019).

[10] “Brain and information science on SHITSUKAN,” 2010 [Online] Available: http://shitsukan.jp/ [Accessed April 25, 2022].

[11] S. Nishida, “Innovative “SHITSUKAN” Science and Technology,” 2015 [Online] Available: http://shitsukan.jp/ISST/en/outline/index.html [Accessed April 25, 2022].

[12] JST, “COI,” 2013 [Online] Available: https://www.jst.go.jp/coi/ [Accessed April 25, 2022].

[13] Takram, [Online] Available: https://www.takram.com/ [Accessed April 25, 2022].

[14] Mitsui Chemicals, Inc., “Molp,” [Online] Available: https://jp.mitsuichemicals.com/en/molp/ [Accessed April 25, 2022].

[15] DIC Color Design Corporation, “Asia-color-trend Book,” [Online] Available: http://asia-color-trend.com/ [Accessed April 25, 2022].

[16] DIC, “DIC Colorial,” 2018. [Online] Available: https://www.dic-global.com/ja/contents/colorial/ [Accessed April 25, 2022].

[17] 館 暲, “バーチャルリアリティと人間の認知機構,” バーチャルリアリティ学, pp. 7-8 (2010).

[18] 前野 隆, “ヒト指腹部と触覚受容器の構造と機能,” *日本ロボット学会誌,* 18 (6), pp. 914-919, (2002).

[19] H. Shirado and T. Maeno, “Modeling of Texture Perception Mechanism for Tactile Display and Sensor,” *Journal of VR Society of Japan,* 9 (3), pp. 235-240 (2004).

[20] S. Okamoto, H. Nagano and Y. Yamada, “Dimensions of Tactile Perception of Textures,” *in IEEE Transactions on Haptics,* 6 (1) pp. 81-93 (2013).

[21] 永野 光, 岡本 正吾, 山田 陽滋, “触感的テクスチャの材質感次元構成に関する研究動向,” *TVRSJ,* 16 (3), pp. 343-353 (2011).

[22] D. Picard, C. Dacremont, D. Valentin and A. Giboreau, “Perceptual dimensions of tactile

textures," *Acta psychologica,* 114 (2), pp. 165-184 (2003).

[23] S. Okamoto, H. Kojima, A. Yamagishi, K. Kato and A. Tamada, "Layered-modeling of Affective and Sensory Experiences using Structural Equation Modeling: Touch experiences of plastic surfaces," *IEEE transaction of affective computing,* 12 (2), pp. 429-438 (2021).

[24] M. Sakamoto, J. Yoshino and J. Watanabe, "Development of tactile materials representing human basic tactile sensations," *In Proceedings of the fifth International Congress of International Association of Societies of Design Research,* pp. 1068-1074 (2013).

[25] S. Kawabata and M. Niwa, "Fabric performance in clothing and clothing manufacture," *Journal of the Textile Institute,* 80 (1), pp. 19-50 (1989).

[26] M. Shitara, H. Yoshida, M. Kamijo, G. Fujimaki and H. Yamaguchi, "Hand Movements Used to Assess the Comfortability and Likability of Wood," *nternational Journal of Affective Engineering,* IJAE-D (2017).

[27] S. Okamoto, K. Wakamatsu, S. Nakauchi, J. Kwon and M. Skamato, "Computation of Computation of sensory-affective relationships depending on material categories of pictorial stimuli," *IEEE Transactions on Affective Computing* (2020).

[28] T. Iwamoto, M. Tatezono and H. Shinoda, "Non-contact Method for Producing Tactile Sensation Using Airborne Ultrasound," in *Haptics: Perception, Devices and Scenarios: 6th International Conference, Eurohaptics 2008 Proceedings (Lecture Notes in C* (2008).

[29] T. Hoshi, M. Takahashi, T. Iwamoto and H. Shinoda, "Noncontact Tactile Display Based on Radiation Pressure of Airborne Ultrasound," *IEEE Trans. on Haptics,* 3 (3), pp. 155-165 (2010).

[30] 田島 優輝, 加藤 史洋, 井上 康之, 舘 暲, "力・振動・温度を触原色とする触感提示デバイスにおける触感再現手法," *日本バーチャルリアリティ学会論文誌,* 24 (1), pp. 125-135 (2019).

[31] V. Yem and H. Kajimoto, "Wearable tactile device using mechanical and electrical stimulation for fingertip interaction with virtual world. In 2017 IEEE Virtual Reality (VR) (pp. 99-104). IEEE.," in *In 2017 IEEE Virtual Reality (VR)* (2017).

[32] B. Wandell and L. D. Silverstein, Digital color reproduction, vol. 2, The Science of Color, 2003, pp. 281-316 (2003)

[33] R. W. G. Hunt, "A model of colour vision for predicting colour appearance in various viewing conditions," *Color.Res. Appl.,* 12, p. 297 (1987).

[34] K. Suehara, I. Isoda, H. Mizutani and A. Hshimoto, "Color calibration for the pressure ulcer image acquired under different illumination: a key step for simple, rapid and quantitative color evaluation of the human skin diseases using a digital camera," *Journal of Light & Visual Environment,* 40, pp. 10-19 (2016).

[35] T. Aoyagi, "Pulse oximetry: its invention, theory, and future," *Journal of Anesthesia,* . 17 pp. 259-266 (2003).

[36] J. A. Dawson, C. O. F. Kamlin, C. Wang, A. B. Te Pas, M. Vento, T. J. Cole and C. J. Morley, "Changes in heart rate in the first minutes after birth," *Archives of Disease in Childhood-Fetal and Neonatal Edition,*" 95 (3), pp. F177-F181 (2010).

[37] C. Li, Z. Peng, T. Y. Huang, T. Fan, F. K. Wang, T. S. Horng and J. Lin, "A review on recent progress of portable short-range noncontact microwave radar systems," *IEEE Trans. Microw. Theory Tech.,* 65 (5), pp. 1692-1706 (2017).

[38] S. H. Oh, S. Lee, S. M. Kim and J. H. Jeong, "Development of a heart rate detection algorithm using a non-contact doppler radar via signal elimination," *Biomedical Signal Processing and Control,* 64, p. 102314 (2021).

[39] P. V. Rouast, M. T. Adam, R. Chiong, D. Cornforth and E. Lux, "Remote heart rate measurement using low-cost RGB face video: a technical literature review," *Front. Comput. Sci.,* 12 (5), pp. 858-872 (2018).

[40] A. Al-Naji, Y. Tao, I. Smith and J. Chahl, "A pilot study for estimating the cardiopulmonary

signals of diverse exotic animals using a digital camera," *Sensors*, 19 (24), p. 5445 (2019).

[41] C. Barbosa Pereira, J. Kunczik, L. Zieglowski, R. Tolba, A. Abdelrahman, D. Zechner and M. Czaplik, "Remote welfare monitoring of rodents using thermal imaging," *Sensors,* 18 (11), p. 3653 (2018).

[42] J. Kunczik, C. B. Pereira, L. Zieglowski, R. Tolba, L. Wassermann, C. Häger and M. Czaplik, "Remote vitals monitoring in rodents using video recordings," *Biomed. Opt. Express* 10 (9), pp. 4422-4436 (2019).

[43] M. Froesel, Q. Goudard, M. Hauser, M. Gacoin and S. B. Hamed, "Automated video-based heart rate tracking for the anesthetized and behaving monkey," *Sci. Rep.,* 10 (1), pp. 1-11 (2020).

[44] W. Wang, S. Stuijk and G. D. Haan, "Exploiting spatial redundancy of image sensor for motion robust rPPG," *IEEE transactions on Biomedical Engineering,* 62 (2), pp. 415-425 (2014).

[45] M. Fukunishi, D. Mcduff and N. Tsumura, "Improvements in remote video-based estimation of heart rate variability using the Welch FFT method," *Artif Life Robot,* 23 (1), pp. 15-22 (2018).

[46] A. A. Kamshilin, S. Miridonov, V. Teplov, R. Saarenheimo and E. Nippolainen, "Photoplethysmographic imaging of high spatial resolution," *Biomedical optics express,* 2 (4), pp. 996-1006 (2011).

[47] A. A. Kamshilin, V. V. Zaytsev and O. V. Mamontov, "Novel contactless approach for assessment of venous occlusion plethysmography by video recordings at the green illumination, *Scientific reports* , 7(1)1, pp. 1-9 (2017).

[48] N. B. Margaryants, I. S. Sidorov, M. V. Volkov, I. P. Gurov, O. V. Mamontov and A. A. Kamshilin, "Visualization of skin capillaries with moving red blood cells in arbitrary area of the body, *Biomedical optics express,* 10 (9), pp. 4896-4906 (2019).

[49] S. Okamoto, "Perceptual Mechanism," [Online]. Available:http://www.mech.nagoya-u.ac.jp/asi/ja/member/shogo_okamoto/papers/PerceptualMechanism.pdf [Accessed April 25, 2022].

[50] 小林健作, 関野吉厚 , 高橋雅人, "アンカー塗布による水性 UV ニスはじき効果の実用事例," *日本印刷学会,* 第 134 回 研究発表会 プログラム, P.A06 (2015).

[51] M. Ohkura, Kawaii Engineering, Measurements, Evaluations, and Applications of Attractiveness, Springer, pp. 49-75 (2019).

[52] Y. Kurita, I. Ikeda, J. Ueda and T. Ogasawara, "A fingerprint pointing device utilizing the deformation of the fingertip during the incipient slip," *IEEE Transactions on Robotics,* 21 (5), pp. 801-811 (2005).

[53] T. Arakawa, K. Nakahara, M. Takahashi, T. Ohkura, T. Tsuji and Y. Kurita, "Investigation of human subjective feelings for differentsurface textures of slipping obhects based on the analysis of contact conditions," in *Haptics: Perceptin, Devices, Control, and Application-10th International Conference, Euro Haptics* (2016).

[54] K. Kikegawa, R. Kuhara, J. Kwon, M. Sakamoto, R. Tsuchiya, N. Nagatani, Y. Nonomura, "Physical origin of a complicated tactile sensation:'shittori feel'," Royal Society open science, 6 (7) p. 190039 (2019).

[55] Y. Aita, N. Asanuma, A. Takahashi, H. Mayama, Y. Nonomura, "Nonlinear friction dynamics on polymer surface under accelerated movement," AIP Advances, p. 045005 (2017).

[56] Y. Aita, N. Asanuma, H. Mayama, Y. Nonomura, "Sliding profile and energy at static friction between polymer surfaces," Chem. Lett., 47, p. 767–769 (2018).

[57] 小林 健作, 関 吉厚 , 高橋 雅人, "水性紫外線硬化型オーバープリントワニス組成物". 特許番号: WO2015/029878.

[58] 鑓水 清隆, 中原 昭 , 高橋 雅人, “金属容器用溶剤系熱硬化型上塗りニス”. 特許番号: 特願 2015-040162.

[59] 高橋 雅人, “手触り感の評価方法および当該方法を実行する測定装置”. 特許番号: 特願 2015-40161.

[60] BCC Research , “Global markets for telemedicine technologies,” (2018).

[61] A. C. Smith, E. Thomas and C. Snoswell, “Telehealth for global emergencies: Implications for coronavirus disease 2019 (COVID-19),” *Journal of telemedicine and telecare,* 26(5), pp. 309-313 (2020).

[62] L. Tindale, M. Coombe, J. Stockdale and C. Caroline, “Transmission interval estimates suggest pre-symptomatic spread of COVID-19,” *MedRxiv* (2020).

[63] T. Greenhalgh, G. C. H. Koh and J. Car, “Covid-19: a remote assessment in primary care,” *bmj,* p. 368 (2020).

[64] M. Nishibori, “Problems and solutions in medical color imaging,” *Proceedings of the Second International Symposium on Multi-Spectral Imaging and High Accurate Color Reproduction,* pp. 9-17 (2000).

[65] J. Penczek, P. A. Boynton and J. D. Splett, “Color error in the digital camera image capture process,” *Journal of digital imaging,* vol. 27, no. 2, pp. 182-191 (2014).

[66] Schanda, J (Ed);, Colorimetry: understanding the CIE system, John Wiley & Sons (2007).

[67] F. Imai, N. Tsumura, H. Haneishi and Y. Miyake, “Principal component analysis of skin color and its application to colorimetric color reproduction on CRT display and hardcopy,” *J. Imaging Sci,* 40 (5), pp. 422-430 (1996).

[68] BCC Research, “Global telehelth market.,” 2020. [Online]. Available: https://www.bccre search. com/partners/verified-market-research/global-telehealth-market-vmr235a.html [Accessed April 25, 2022].

[69] T. Greenhalgh, J. Wherton, S. Shaw and C. Morrison, “Video consultations for Covid-19,” p. 368:m998 (2020).

[70] J. Hollander and B. Carr, “Virtually perfect? Telemedicine for COVID-19,” *New England J Med,* 382 (18), pp. 1679-1681 (2020).

[71] A. Baum, P. Kaboli and M. Schwartz, “Reduced in-person and increased telehealth outpatient visits during the COVID-19 pandemic,” *Annal Internal Med,* 174 (1), pp. 129-131 (2021).

[72] S. Majumder and M. Deen, “Smartphone sensors for health monitoring and diagnosis,” *Sensors,* 19 (9), p. 2164 (2019).

[73] J. Hollander and B. Carr, “Virtually perfect? Telemedicine for COVID-19,” *New England J Med,* 382 (18), pp. 1679-1681 (2020).

[74] A. Baum, P. Kaboli and M. Schwartz, “Reduced in-person and increased telehealth outpatient visits during the COVID-19 pandemic,” *Annal Internal Med,* 174 (1), pp. 129-131 (2021).

[75] S. Majumder and M. Deen, “Smartphone sensors for health monitoring and diagnosis,” *Sensors,* 19 (9), p. 2164 (2019).

[76] J. Hollander and B. Carr, “Virtually perfect? Telemedicine for COVID-19,” *New England J Med,* 382 (18), pp. 1679-1681 (2020).

[77] 小川 恵子, 経方理論への第一歩, 全日本病院出版会 (2020).

[78] M. Takahashi, R. Takahashi, I. Kin, K. Ogawa-Ochiai and N. Tsumura, “Development of a camera-based remote diagnostic system focused on color reproduction using color charts,” *Artif Life Robot,* 25 (3) , pp. 370-377 (2020).

[79] M. Fukunishi, K. Kurita, S. Yamamoto and N. Tsumura, “Non-contact video-based estimation of heart rate variability spectrogram from hemoglobin composition,” *Artif Life Robot,* 22 (4), pp. 457-463 (2017).

[80] W. Verkruysse, L. Svaasand and J. Nelson, “Remote plethysmographic imaging using

ambient light," *OpticsExpress,* 16 (26), pp. 21434-21445 (2008).

[81] Y. Maeda, S. Masaki and T. Toshiyo, "The advantages of wearable green reflected photoplethysmography," *Journal of medical systems,* 35 (5), pp. 829-834 (2011).

[82] A. Hyvärinen and O. Erkki, "Independent component analysis.algorithms and applications," *Neural Netw,* 4-5, pp. 411-430 (2000).

[83] C. Contreras, G. Metzger, J. Beane, P. Dedhia, A. Ejaz and T. Pawlik, "Telemedicine: patient-provider clinical engagement during the Covid-19 pandemic and beyond," *J. Gastrointestinal Surgery,* 24 (7), pp. 1692-1697 (2020).

[84] S. Amamoto, Y. Ishikawa, T. Nakaguchi, K. Ogawa-Ochiai, N. Tsumura, Y. Kasahara, T. Namiki and Y. Miyake, "Temporal changes in tongue color as criterion for tongue diagnosis in Kampo medicine," *Complementary medicine research,* 19 (2), pp. 80-85 (2012).

[85] F. Matsushita, K. Kiyomitsu, K. Ogawa and N. Tsumura, "Evaluation of Kampo disease state using facial images," *Artif Life Robotics,* 24 (1), pp. 44-51 (2019).

[86] R. Koike, K. Ogawa-Ochiai, A. Shirai, K. Hayashi, J. Arimitsu, H. Li and N. Tsumura, "reating a diagnostic assistance system for diseases in Kampo medicine," *Applied sciences,* 11(21), p. 9716 (2021).

[87] M. Liu and Z. Guo, "Hepatitis diagnosis using facial color image," in *International conference on medical biometrics* (2008).

[88] P. V. Rouast, T. A. Marc, C. Raymond, C. David and E. Lux, "Remote heart rate measurement using low-cost RGB face video: a technical literature review," *Frontiers of Computer Science,* 12 (5), pp. 858-872 (2018).

[89] S. Festing and R. Wilkinson, "he ethics of animal research: talking point on the use of animals in scientific research," *MBO reports,* 8 (6), pp. 526-530 (2007).

[90] P. Camacho, H. Fan, Z. Liu and J. Q. He, "Small mammalian animal models of heart disease," *AJCD,* 60 (3), p. 70 (2016).

[91] M. R. Fernandes and R. P. Pedroso, "Animal experimentation: A look into ethics, welfare and alternative methods," *Revista da Associacao Medica Brasileira,* 63, pp. 923-928 (2017).

[92] E. O. Kehinde, "They see a rat, we seek a cure for diseases: the current status of animal experimentation in medical practice," *Med. Princ. Pract.,* 22(Suppl. 1), pp. 52-61, (2013).

[93] N. Levy, "The use of animal as models: ethical considerations," *Int. J. Stroke,* 7 (5), pp. 440-442 (2012).

[94] D. Ho, X. Zhao, S. Gao, C. Hong, D. E. Vatner and S. F. Vatner, "Heart rate and electrocardiography monitoring in mice," *Curr. Protoc. Mouse Biol.,* 1, pp. 123-139 (2011).

[95] D. Park, M. Lee, S. E. Park, J. K. Seong and I. Young, "Determination of optimal heart rate variability features based on SVM-recursive feature elimination for cumulative stress monitoring using ECG sensor," *Sensors,* 18 (7) p. 2387 (2018).

[96] Y. Shikano, T. Sasaki and Y. Ikegaya, "Simultaneous recordings of cortical local field potentials, electrocardiogram, electromyogram, and respiration rhythm from a freely moving rat," *JoVE,* 134 (2018).

[97] C. González-Sánchez, L. C. Fraile, J. Pérez-Turiel, E. Damm, J. G. Schneider, H. Zimmermann, S. Daniel and F. R. Ihmig, "Capacitive sensing for non-invasive respiration and heart monitoring in non-restrained, non-sedated laboratory mice," *Sensors,* 16 (7), p. 1052 (2016).

[98] K. Alghoul, S. Alharthi, H. A. Osman and A. E. Saddik, "Heart rate variability extraction from videos signals: ICA vs. EVM comparison," *IEEE Access 5,* pp. 4711-9, (2017).

[99] R. Mitsuhashi, K. Iuchi, T. Goto, A. Matsubara, T. Hirayama, H. Hshizume and N. Tsumura, "Video-based stress level measurement using imaging photoplethysmography," *In: 2019 IEEE International Conference on Multimedia & Expo Workshops (ICMEW),* pp. 90-95 (2019).

[100] Y. Maeda, M. Sekine and T. Tamura, "Relationship between measurement site and motion artifacts in wearable reflected photoplethysmography," *J. Med. Syst.,* 35, pp. 969-976 (2011).

[101] B. A. Fallow, T. Tarumi and H. Tanaka, “Influence of skin type and wavelength on light wave reflectance,” *J. Clin. Monit. Comput.,* 27, pp. 313-317 (2013).

[102] M. Takahashi, T. Yamaguchi, R. Takahashi, N. Tsumura and N. Iijima, “Non-contact measurement of pulse wave in rats using an RGB camera,” *Optical Diagnostics and Sensing XXI: Toward Point-of-Care Diagnostics,* p. 116510E (2021).

[103] M. Kuwahara, M. D. Hue, H. Hirose and S. Sugano, “Alteration of the intrinsic heart rate and autonomic nervous tone during the growing process of rats and pigs,” *Jpn. J. Vet.,* 48 (4), pp. 703-709 (1986).

[104] T. Isosaka, T. Matsuo, T. Yamaguchi, K. Funabiki, S. Nakanishi, D. Kobayakawa and obayakawa, “Htr2a-expressing cells in the central amygdala control the hierarchy between innate and learned fear,” *Cell,* 163.5, pp. 1153-1164 (2015).

[105] H. Zakaria and P. Hasimun, “Non-invasive pulse wave velocity measurement in mice,” in *2017 International Seminar on Sensors, Instrumentation, Measurement and Metrology (ISSIMM)* (2017).

[106] 高橋 雅人, 高橋 凌, 森原 康博, 金 一石, 小川 恵子, 津村, 徳道, “質の高い遠隔医療用カラーチャートの開発と自動補正,” *光技術コンタクト*, 59 (1) pp. 22-28 (2021)

Publication List

1. Journal Papers

1.1 M. Takahashi, "Development of Texture communication tools, "*The imaging society of Japan*, 59 (5), pp. 474-479 (2020) **(in Japanese).**

1.2 M. Takahashi., R. Takahashi, Y. Morihara, I. Kin, K. Ogawa-Ochiai, & N. Tsumura, "Development of a camera-based remote diagnostic system focused on color reproduction using color charts," *Artificial life and robotics*, 25 (3), pp. 370-376 (2020).

1.3 M. Takahashi, T. Yamaguchi, R, Takahashi, K. Ogawa-Ochiai, N. Tsumura, & N. Iijima, "Non-invasive measurement of pulse wave in sole of rats using an RGB camera," *OSA Continuum*, 4(12), pp. 3014-3025 (2021).

1.4 M. Takahashi, K. Nagasawa, R, Koike, Y. Manabe, M. Takamura, T. Hongwa, I. Kimoto, K. Ogawa-Ochiai, & N. Tsumura, "Development of telemedicine tools with an emphasis on visual observation," *Artificial life and robotics*, 27, pp. 38-47 (2022).

2. International Conference

2.1 M. Takahashi, T. Yamaguchi, R. Takahashi, N. Tsumura, & N. Iijima, "Non-contact measurement of pulse wave in rats using an RGB camera," Optical Diagnostics and Sensing XXI: Toward Point-of-Care Diagnostics 11651 (2021). https://doi.org/10.1117/12.2577481

2.2 M. Takahashi, T. Yamaguchi, K. Ogawa-Ochiai, N, Tsumura, & N. Iijima, "Accuracy of pulse wave measurement from the sole of rodents using RGB camera," Optical Diagnostics and Sensing XXII: Toward Point-of-Care Diagnostics 11968, 69-74(2022). https://doi.org/10.1117/12.2607919

3. Domestic Conference (in Japanese)

3.1 高橋 雅人, 金 一石, "非接触での色再現とバイタルデータをスマホで取得," 第 1 回 高品質遠隔医療シンポジウム バイオカラー研究会, （招待講演 Web 開催 2020/10/18）.

3.2 高橋 雅人, 高橋 凌, 森原 康博, 金 一石, 小川 恵子, 津村 徳道, "質の高い診察（望診）のための遠隔医療用カラーチャートの開発," 2020 年度色材研究発表会, （Web 開催 2020/10/23）.

3.3 高橋 雅人, "RGB カメラを用いた生体計測/遠隔医療、実験動物の非侵襲脈波測定," 日本オプトメカトロニクス協会　デジタル・イメージング技術部会（依頼講演 2021/7/14, Web 開催）.

3.4 高橋 雅人, “魅力ある触感を探るコミュニケーションツールの開発,” 魅力工学研究会シンポジウム 2021 電子情報通信学会 魅力工学研究会 (招待講演, Web 開催,2021/9/16).

3.5 高橋 雅人, “感性マテリアル開発に役立つ評価技術,” 色材インクジェット部会講演会, 色材協会（招待講演, Web 開催,2021/10/21）.

3.6 高橋 雅人, “介護に応用可能な、非接触バイタル測定と正確に色を伝える技術,” (公財)千葉市産業振興財団 ビジネス交流会 (Web 配信,2022/3/15～4/28).

4. Review papers

4.1 高橋 雅人, “感性マテリアル開発に役立つ, 評価技術とコミュニケーションツールの開発,” *感性工学* 19 (1), 16-19 (2020).

4.2 高橋 雅人, 高橋 凌, 小川 恵子, 津村 徳道, “RGB カメラを用いた質の高い遠隔診療システムのための色補正技術とバイタル情報の取得,” *レーザー研究,* 49 (9), 496-500 (2021).

4.3 高橋 雅人, 高橋 凌, 森原 康博, 金 一石, 小川 恵子, 津村 徳道, “独自のカラーチャートを用いた質の高い遠隔診療システムの開発,” *3D 映像* 33 (4), pp 4-10 (2021).

4.4 高橋 雅人, 高橋 凌, 金 一石, 小川 恵子, 津村 徳道, “質の高い遠隔診療用カラーチャートの開発と自動補正,” *光技術コンタクト*, 59 (1), (2021).

4.5 高橋 雅人, 中村 健二, “感性（質感）コミュニケーションツールの開発とテクスチャー評価”, *ソフトドリンク技術資料*, 195, (3) 43-58 (2021).

4.6 高橋 雅人, 中村 健二, “感性マテリアル開発に役立つ評価技術とコミュニケーションツール,” *化学と教育*, 70 (4) 200-203 (2022).

4.7 高橋 雅人, “カラーチャートを利用した、質の高い遠隔診療用ツールの開発,” *色材協会誌*, 95, (6) 14-155 (2022).

5. Other related works

5.1 T. Arakawa, A. Nakahara, K. Yarimizu, M. Takahashi, M. Ohkura, T. Tsuji, & Y. Kurita, “Investigation of human subjective feelings for different surface textures of slipping objects based on the analysis of contact conditions,” In International Conference on Human Haptic Sensing and Touch Enabled Computer Applications (pp. 131-138). Springer, Cham. (2016).

5.2 W. Morishita, R. Miyazaki, M. Ohkura, M. Takahashi, H. Sakurai, K. Yarimizu, & A. Nakahara, “Affective Evaluation for Material Perception of Bead-Coated Resin Surfaces Using Visual and Tactile Sensations: Preparation of Adjective Pairs to Clarify the Color Effect,” Advances in Intelligent Systems and Computing 251-258 (2017).
https://doi.org/10.1007/978-3-319-41661-8_25

5.3 M. Ohkura, W. Morishita, R, Miyazaki, M. Takahashi, H. Sakurai, K. Yarimizu, & A. Nakahara, “Analysis of Affective Evaluation for Material Perception of Resin Surfaces: Combined Effect of Tactile Sensation and Hue,” Advances in Intelligent Systems and Computing 190-198 (2018). https://doi.org/10.1007/978-3-319-60495-4_20

5.4 M. Ohkura, W. Morishita, K. Inoue, R. Miyazaki, R. Horie, M. Takahashi, H. Sakurai, T. Kojima, K. Yarimizu, & A. Nakahara, “Affective Evaluation for Material Perception of Bead-Coated Resin Surfaces Using Visual and Tactile Sensations—Focusing on Kawaii,” In: M. Ohkura(eds). Kawaii Engineering. Springer Series on Cultural Computing. Springer, Singapore, P49-75(2019). https://doi.org/10.1007/978-981-13-7964-2_3

5.5 N. Iijima, M. Takahashi, R. Takahashi, R. Koike, T. Yamaguchi, & N. Tsumura, “Development of non-contact measuring system of pulse wave of rodents using RGB camera to monitor the activities of autonomic nervous system,” 第 126 回日本解剖学会総会・全国学術集会 / 第 98 回日本生理学会大会合同大会 (WEB 2021.3.28)

6. Other related works (in Japanese)

6.1 大倉 典子, 井上 和音, 堀江 亮太, 高橋 雅人, 桜井 宏子, 小島 隆, 鑓水 清隆, 中原 昭, “ビーズを塗布した樹脂表面の質感の感性評価-40・50 代による評価,” 日本感性工学会大会予稿集 (CD-ROM) 16th (501(HIP2013 78-105)) 23-27 2014 年 3 月 (2014).

6.2 荒川 剛, 中原 昭, 鑓水 清隆, 高橋 雅人, 大倉 典子, 辻 敏夫, 栗田 雄一, “指先力ならびに接触面変化が表面質感の感性評価へ与える影響,” 計測自動制御学会システムインテグレーション部門講演会 (CD-ROM) 16th (2015).

6.3 大倉 典子, 黒田 侑樹, 高橋 雅人, 桜井 宏子, 鑓水 清隆, 中原 昭, 長澤 俊一, “樹脂表面の質感の感性評価の分析,” 人間工学, 51,184-185(2015).

6.4 荒川 剛, 中原 昭, 鑓水 清隆, 高橋 雅人, 辻 敏夫, 栗田 雄一, “物体の表面特性の違いによる弾性体接触面の変化に関する考察,” 研究報告グラフィクスと CAD (CG) 2015(9) 1-3 2015 年 6 月（2015）.

6.5 森下 和, 宮崎 隆次, 大倉 典子, 高橋 雅人, 桜井 宏子, 鑓水 清隆, 中原 昭, “樹脂表面の質感の感性評価の分析 -触感と色相の複合効果-, “日本感性工学会大会予稿集 (CD-ROM) 18th (2016).

6.6 小林健作, 関野吉厚, 高橋雅人, “アンカー塗布による水性 UV ニスはじき効果の実用事例 -, “日本印刷学会 第 134 回 研究発表会 プログラム A-06 (2016).

6.7 荒川 剛, 中原 昭, 鑓水 清隆, 高橋 雅人, 大倉 典子, 辻 敏夫, 栗田雄一, “指先接触面変化が触感性に与える影響の考察,” 日本機械学会ロボティクス・メカトロニクス講演会講演論

文集 (CD-ROM) (2016).

6.8 森下 和樹, 宮崎 隆次, 大倉 典子, 高橋 雅人, 桜井 宏子, 鑓水 清隆, 中原 昭, “樹脂表面の質感の感性評価の分析-感性評価による色相の分類,” 日本感性工学会春季大会予稿集 (CD-ROM) 11th (2016).

6.9 小林 健作, 関野 吉厚, 高橋 雅人, 石井 融, 浅田 匡彦, “触り心地の良いコーティング材とその定量化技術,” 色材研究発表会講演要旨集 (2016).

6.10 荒川 剛, 中原 昭, 鑓水 清隆, 高橋 雅人, 辻 敏夫, 栗田 雄一, “指先接触面の変化による感性評価への影響の考察,” 計測自動制御学会システムインテグレーション部門講演会 (CD-ROM) 17th (2016).

6.11 鯉沼 佳希, 森下 和, 宮崎 隆次, 伊藤 弘大, 大倉 典子, 高橋 雅人, 桜井 宏子, 鑓水 清隆, 中原 昭, “樹脂表面の質感の感性評価の分析-色相に着目した重回帰式の比較-樹脂表面の質感の感性評価の分析-色相に着目した重回帰式の比較-,” 日本バーチャルリアリティ学会大会論文集 (CD-ROM) 22nd (2017).

6.12 設楽 稔那子, 加我 直人, 吉田 宏昭, 上條 正義, 高橋 雅人, 浅田 匡彦, 江原涼子, “木材のしっとり感についての基礎検討,” 繊維学会年次大会、3A02（2018）

6.13 設楽 稔那子, 加我 直人, 吉田 宏昭, 上條 正義, 高橋 雅人, 浅田 匡彦, 江原 涼子, “人工木材と天然木材の “しっとり” の違いとは?,”日本感性工学会大会, D3-07（2018）

6.14 深田 雅裕, 静野 大樹, 中原 昭, 鑓水 清隆, 高橋 雅人, 田中 由浩, 辻 敏夫, 栗田 雄一, “指先振動計測に基づく触感テクスチャ感性の予測,” 日本機械学会ロボティクス・メカトロニクス講演会講演論文集 (CD-ROM) (2018)

7. Awards related to this work

7.1 2016 年・日本印刷学会技術奨励賞

小林 健作, 関野 吉厚, 高橋 雅人, “ソフトな手触りを付与する水性 UV ハイブリッド型ニス（UV ピーチフィールニス）の開発とそれを用いたはじき加工（オーストリッチ加工）について,”（2016）

8. Patents related to this work

8.1 発明者：小林 健作, 関野 吉厚, 高橋 雅人, “水性紫外線硬化型オーバープリントワニス組成物,” 特許第 5712338 号（出願日 2014/8/21）

8.2 発明者：鑓水 清隆, 中原 昭, 高橋 雅人, “金属容器用溶剤系熱硬化型上塗りニス,” 特許第 6514525 号（出願日 2015/3/2）

8.3 発明者：高橋 雅人, “手触り感の評価方法および当該方法を実行する測定装置,” 公開番号

2016-161389（出願日 2016/9/5）

8.4 発明者：高橋 雅人, “触感見本システム及び触感評価方法,” 公開番号 2020-056878（出願日 2018/10/1）

8.5 発明者：高橋 雅人, 鳥井美帆, “触感見本及び触感見本システム,” 公開番号 2020-098315（出願日 2018/12/19）

8.6 発明者：高橋 雅人, 森原 康博, 津村 徳道, 高橋 凌, 小川 恵子, 金 一石, “カラーチャート,” 特許第 6981561 号（出願日 2021/3/11)

8.7 発明者：高橋 雅人, 森原 康博, 津村 徳道, 高橋 凌, 小川 恵子, 金 一石, “画像表示システム、及び画像表示方法,” 特開 2022-000686（出願日 2021/3/11）

Acknowledgements

With the support of many persons, I was able to complete my doctoral thesis.

First, I would like to express my deepest gratitude to Professor Norimichi Tsumura of Chiba University, who invited me to participate in his doctoral research and continued supervising my research and dissertation. I am also grateful to the rest of my committee. Professor Takahiko Horiuchi (Chiba University), Professor Yoko Mizokami (Chiba University), Professor Hideaki Haneishi (Chiba University), Dr. Ayumi Amemiya (Chiba University), Professor Norio Iijima (International University of Health and Welfare), Professor Yuichi Kurita (Hiroshima University).

The *Kansei* evaluation in Chapter 4 describes what I did during my tenure at DIC Corporation. This work also incorporates the results of collaborative research with several universities. I would like to thank Professor Noriko Okura (Shibaura Institute of Technology), Professor Shogo Okamoto (Nagoya University), and Professor Shigeki Nakauchi (Toyohashi University of Technology), Professor Hiroaki Yoshida (Shinshu University), and others for their guidance and support. And I would like to thank Mr. Kiyotaka Yarimizu, Mr. Hideyasu Machida, Mr. Masafumi Nishigaki, and other people at DIC corporation for their great help in creating the Kansei Communication Tool.

For the telemedicine-related work in Chapters 5 and 6, we are grateful to Professor Keiko Ogawa-Ochiai (Hiroshima University), Dr. Yasuhiro Manabe, Dr. Hirofumi Hirana, Dr. Mitsuyuki Takamura, Dr. Tetsuya Hongawa, Dr. Izumi Kimoto, and other medical doctors for their guidance and cooperation, and to the students of Chiba University, including Mr. Ryo Takahashi, Mr. Reimei Koike, and Mr. Kazuki Nagasawa, for their help in the experiments. I would like to express my gratitude to all of them. We are grateful to Mr. Morihara Yasuhiro (DIC Graphics Corporation) and others involved in the creation of the color chart and to Mr. Isseki Kin for his help with implementation. For the Chapter 7 rat heart rate measurement, I would like to thank Dr. Takeshi Yamaguchi (International University of Health and Welfare) for their guidance on animal experiments and physiology.

In the doctoral course at Chiba University, I was taught by the late Dr. Keita Hirai and others. Dr. Hirai passed away just as I was thinking of collaborating with him. I pray for his soul rest in peace.

Finally, I would like to thank my wife, Kumi, for her understanding of my decision to enter the doctoral program.

This work was supported by JST SPRING, Grant Number JPMJSP2109.